Institute for Condensed Matter Physics of the National Academy of Sciences of Ukraine

Coventry University

Institute for Condensed Matter Physics of the National Academy of Sciences of Ukraine

Qualification research
on the rights of the manuscript

HONCHAR Yulian Ivan Mykhailo Nazarovych

UDC 537.9, 538.9, 539.2

DISSERTATION

SCALING PROPERTIES OF PHASE TRANSITIONS ABOVE THE UPPER CRITICAL DIMENSION AND IN THE DESCRIPTION OF DNA DENATURATION

104 — physics and astronomy

10 — natural sciences

Applied for the Doctor of Philisophy degree

The dissertation contains the results of my own research.
The use of other authors' ideas, results and texts have references to the relevant source _____ Y. Honchar

Scientific advisors: Yurij Holovatch, Dr. Sci., professor, full member of the National Acad. Sci. of Ukraine
Ralph Kenna, Dr. rer. nat., professor, Coventry University (United Kingdom)

Lviv — 2023

АНОТАЦІЯ

Гончар Ю.-І.-М.Н. Особливості скейлінгу при фазових переходах вище критичної вимірності та описі денатурації ДНК.— Кваліфікаційна наукова праця на правах рукопису.

Дисертація на здобуття ступеня доктора філософії за спеціальністю 104 — Фізика та астрономія. — Інститут фізики конденсованих систем НАН України, Львів, 2023.

Дисертація присвячена вивченню принципів скейлінгу та універсальності в критичних явищах, які є фундаментальними концепціями в багатьох ділянках науки. В теорії критичних явищ гіпотеза скейлінґу стверджує, що термодинамічні потенціали є узагальненими однорідними функціями відповідних змінних поблизу критичної точки, а універсальність означає, що поведінка системи не залежить від деталей і мікроскопічної структури системи. Незважаючи на те, що ці ідеї виявилися ефективними для вирішення різноманітних завдань, їх застосування та розуміння залишається неповним. Ця дисертація досліджує явища скейлінґу вище верхньої критичної вимірності та заглиблюється в масштабування складних полімерних мереж.

При дослідженні скейлінґу над верхньою критичною вимірністю основна увага приділяється скінченновимірному скейлінґу з вільними граничними умовами. Звичайні методи недостатньо точні, що перешкоджає всебічному розумінню скейлінґової поведінки в різних явищах. Крім того, це дослідження стосується масштабування кополімерних мереж, зокрема в рамках моделі Поланди-Шераги, що описує термічну денатурацію ДНК. Для опису розщеплення ланцюга ДНК використовуються нові показники для кополімерних мереж. Структура дисертації наступна: чотири основні розділи (огляд літератури, комп'ютерне моделювання п'ятивимірної моделі Ізінга, аналіз Фур'є мод намагнічення та аналіз нулів Лі Янга, а також комплексне дослідження скейлінгових показників полімерних мереж), заключний розділ з ключовими висновками.

У другому розділі ми підтверджуємо запропонований скейлінг для п'ятивимірної моделі Ізінга з вільними граничними умовами при псевдокритичній температурі. Ми використали алгоритм Вольфа для моделювання $d = 5$ моделі Ізінга з вільними граничними умовами, щоб отримати скейлінгову картину таких величин, як намагнічення, ізотермічна сприйнятливість, енергія та теплоємність при нульовому магнітному полі та критичній, а також псевдокритичній температурах вище за верхню критичну вимірність $d_c = 4$. У дослідженні моделі Ізінга над верхньою критичною вимірністю за допомогою комп'ютерного моделювання, головний акцент поставлено на скінченновимірному скейлінгу. Коли розмір ґратки малий, вплив поверхні стає надто сильним, що ускладнює спостереження за очікуваними змінами при псевдокритичній температурі T_L. По суті, чим менша система, тим більше ці поверхневі ефекти перешкоджають скейлінгу, і чим вищу вимірність ми розглядаємо, тим менші розміри ґраток можна обчислити. Ми помітили, що для намагнічення виключення найменших розмірів ґратки допомогло обмежити поверхневі ефекти та точніше спостерігати за скейлінговою поведінкою. Однак, для сприйнятливості усі наші розміри ґраток доводиться вважати «малими». Це означає, що покращення розуміння скейлінгу намагнічення при нехтуванні ґратками малого розміру не застосовне універсально до всіх величин. Хоча у магнітному секторі загалом спостерігаються узгоджені результати, підтверджуючи G-скейлінг (тривіальна фіксована точка Гауса, де всі поля прийняті за нуль) при критичній температурі T_c та Q-скейлінг (спеціальний скейлінг, у якому кореляції перевищують розмір системи, і введено новий показник ϙ, який виправляє співвідношення гіперскейлінгу) при псевдокритичній температурі T_L для намагніченості, у енергетичному секторі скінченновимірний скейлінг не можна приписати жодному із відомих скейлінгових режимів.

У третьому розділі застосовано нові підходи, зокрема дослідження Фур'є мод намагнічення, а також аналіз нулів статистичної суми (нулів Л-Янга) в комплексній площині, що підвищують точність спостережуваного скейлінгу.

Хоча для періодичних граничних умов лише нульова мода намагнічення має внесок у скейлінг, для вільних граничних умов усі непарні моди впливають на скінченновимірний скелінг, а всі парні моди зануляються. Ми показуємо, що Фур'є моди намагнічення повторюють поведінку намагнічення, спостережувану в розділі 2, і підтверджуємо Q-скейлінг, але не покращуємо кардинально скейлінгову картину. Аналіз на основі скінченновимірного скейлінгу нулів статистичної суми в комплексній площині призводить до поведінки першого нуля Лі-Янга як функції розміру системи L: $h_1 \sim L^{-3{,}16\pm0{,}48}$ при T_c, що вказує на G-масштабування ($h_1 \sim L^{-3}$), а $h_1 \sim L^{-3.75}$ на T_L, що вказує на Q-скейлінг. Крім того, при дослідженні ізотермічної сприйнятливості в термінах нулів Лі-Янга з вищою точністю ліпше спостерігається скейлінгова поведінка у псевдокритичній точці T_L. Зауважимо, що цей скейлінг є набагато ближчим до Q-скейлінг, ніж до G-скейлінгу. Це вказує на те, що скейлінгова поведінка при вільних граничних умовах проявляється у спосіб, який більше узгоджується з Q-скейлінгом, ніж із попередніми суперечливими висновками в літературі, що дає цінну інформацію про динаміку цієї властивості.

У четвертому розділі ми розглянули показники скейлінгу складної кополімерної мережі, яка виникає при термічній денатурації ДНК в межах моделі Поланда-Шераги. Ми отримали нові скейлінгові співвідношення для показника замикання петлі c, який контролює порядок фазового переходу з упорядкованої до невпорядкованої фази з урахуванням можливої неоднорідності між денатурованою петлею та зв'язаними ланцюгами. У дисертації досягнуто найвищої на сьогодні точності під час обчислення показників скейлінгу для полімерних мереж, обчислення їх значень у тривимірному та двовимірному випадках, а також врахування впливу середовища та неоднорідності. Вплив можливої неоднорідності в показниках скейлінгу денатурованих ланцюгів ДНК на показник закриття петлі c проявляється через взаємодію двох факторів. З одного боку, кількість конфігурацій денатурованої петлі більша для петлі випадкових блукань (random walks, RW) і менша для блукань із самоуникненням (self-avoiding

walks, SAW). З іншого боку, кількість конфігурацій петлі обмежена бічними ланцюгами. Розрахунки, представлені в цьому розділі, дають надійний спосіб судити про значення показників c для різних умов неоднорідності, а отже і про порядок фазового переходу термічної денатурації ДНК. Наш аналіз ґрунтується на польовій теорії кополімерних мереж. Завдяки співвідношенням скейлінгу, ми зв'язуємо показники замикання петлі c зі скейлінговими показниками $\eta_{f_1 f_2}$, які визначають ентропійні властивості кополімерних зірок, створених взаємно взаємодіючими наборами f_1 SAW і f_2 RW. Використовуючи потужну техніку пересумовування, ми досліджуємо асимптотичні розклади для цих показників і оцінюємо їх при вимірності простору $d = 3$. Ми показуємо, що ефекти неоднорідності істотно впливають на силу переходу першого роду (показник c зростає в порівнянні зі звичайним однорідним випадком, коли всі ланцюги є SAW). Ми підтримуємо результати цього спостереження точними результатами для $d = 2$. Крім того, ми показуємо, що таке загострення різкості фазового переходу стає ще суттєвішим у так званому зайнятому середовищі з далекосяжними корельованими неоднорідностями.

У підсумку, це дослідження покращує наше розуміння явища скейлінгу і дає цінні висновки, які модуть бути застосовані до широкого класу наукових проблем. Результатами цієї роботи є три статті, дві з яких опубліковані, одна прийнята до друку, три препринти та одинадцять тез конференцій.

Ключові слова: скейлінґ, універсальність, критичні явища, фазові переходи, модель Ізінга, модель Поланда-Шераги, критичні показники, моделювання Монте-Карло, нулі Лі-Янга, асимптотичні ряди.

ABSTRACT

Honchar Y.I.M.N. Scaling properties of phase transitions above the upper critical dimension and in the description of DNA denaturation. — Qualifying scientific work on the rights of the manuscript.

Thesis for the Degree of Doctor of Philosophy on the speciality 104 — Physics and Astronomy. — Institute for Condensed Matter Physics of the National Academy of Sciences of Ukraine, Lviv, 2023.

The thesis is devoted to the study of scaling and universality in critical phenomena that constitute foundational concepts in various scientific domains. In the theory of critical phenomena scaling hypothesis states that thermodynamic potentials are generalized homogeneous functions of their respective variables in vicinity of critical point, while universality in criticality means that the system's behaviour does not depend on the details and microscopic structure of the system. Despite their proven efficacy in diverse applications, the application and understanding of these fundamental concepts remain incomplete. In particular, this dissertation explores scaling phenomena above the upper critical dimension and delves into the scaling of complex polymer networks.

In investigating scaling above the upper critical dimension, a focus is placed on finite-size scaling for systems with free boundary conditions. Conventional methods fall short in accuracy, hindering a comprehensive understanding of phenomena in physics and beyond. Additionally, this research addresses the scaling of copolymer networks, in particular within the Polanda-Scheraga model describing the thermal denaturation of DNA. Novel exponents for copolymer networks are employed to describe DNA chain unzipping. The thesis structure encompasses four chapters: a literature review, numerical simulations of the five-dimensional Ising model, Fourier analysis of magnetization modes and Lee Yang zeros analysis, and a comprehensive examination of scaling parameters in polymer networks. The concluding chapter consolidates key findings.

In the second chapter, the study validates proposed scaling for the five-

dimensional Ising model with free boundary conditions at the pseudocritical temperature. We used Wolff algorithm to simulate $d = 5$ Ising model with free boundary conditions to get a scaling picture of the quantitities like magnetisation, isothermal susceptibility, energy, and heat capacity at zero magnetic field and critical as well as pseudocritical temperatures above the upper critical dimension $d_c = 4$. In studying the Ising model above its critical dimension with numerical simulations, we focused on the finite-size scaling. When the lattice size is small, the impact of the boundaries becomes too significant, making it difficult to see the expected changes at the pseudocritical temperature T_L. Essentially, the smaller the system, the more these boundary effects overshadow the scaling picture, and the larger dimensionality we consider, the smaller lattice sizes are possible to compute. We noticed that for magnetisation, excluding the smallest lattice sizes helped to supress the boundary efects and observe the scaling behaviour more accurately. However, for susceptibility, all our lattice sizes can only be considered "small". This means that the improvement in understanding magnetisation scaling doesn't apply universally to all properties. Though, magnetic sector, in general showed consistent results proving G-scaling (Gaussian trivial fixed point, where all fields are set to zero) at the critical temperature T_c, and Q-scaling (special scaling, where correlations exceed system size, and a new exponen ϙ is introduced to fix the hyperscaling) at the pseudocritical temperature T_L for magnetisation, unlike the thermal sector, where the finite-size scaling could not be fit into any of the scaling regimes.

In the third chapter, innovative approaches involving study of magnetisation Fourier modes as well as analysis of partition function zeros in complex plane enhance the accuracy of observed scaling. While for the periodic boundary conditions only the zero magnetisation mode contributes to scaling, for the free boundary conditions all odd modes collectively contribute to the FSS, and all even modes vanish. We show that the magnetisation Fourier modes repeat the behaviour of magnetisation observed in Chapter 2, and confirm Q-scaling, but do not improve the scaling picture drastically. Analysis based on the FSS of partition function zeros in complex plane results in the following behaviour of the first Lee-Yang zero as function

of system size L: $h_1 \sim L^{-3.16\pm0.48}$ at T_c, that hints towards G-scaling ($h_1 \sim L^{-3}$), and $h_1 \sim L^{-3.75}$ at T_L, which hints towards Q-scaling. Moreover, when examining the isothermal susceptibility in terms of Lee-Yang zeros, a scaling behavior was observed at the pseudocrtitcal point T_L with better accuracy. Notably, this scaling is found to be much closer to Q-scaling than to G-scaling. This indicates that the scaling behaviour at FBC exhibits in a manner that is more consistent with Q-scaling than with the conflicting conclusions in the literature, providing valuable insights into the dynamics of this property.

In the fourth chapter we have considered the scaling exponents of a complex copolymer network that occurs in the thermal denaturation of DNA within the Poland Scheraga model. We have derived new scaling relations for the loop closure exponent c that controls the order of the phase transition from ordered to disordered phase with the account of pssible heterogeeity between the denaturated loop and bound chains. Our analysis achieves heightened accuracy in calculating scaling exponents for polymer networks, determining their values in three-dimensional and two-dimensional cases, and considering the impact of environment and heterogeneity. Influence of possible heterogeneity in entropic scaling exponents of bound and denaturated DNA strands on the loop closure exponent c is manifest by an interplay of two factors. On the one hand, the number of configurations of a denaturated loop is influenced by the loop self-avoidance interactions (the number is larger for the RW loop and smaller of the SAW one). On the other hand, the number of loop configurations is restricted by the side chains. Calculations presented in this chapter give a reliable way to judge about the values of exponents c for different heterogeneity conditions and hence to judge about the order of DNA thermal denaturation transition. Our analysis is grounded on the field theory of co-polymer networks. By scaling relations we connect loop closure exponents c to scaling exponents $\eta_{f_1 f_2}$ that govern entropic properties of co-polymer stars made by mutually interacting sets of f_1 SAWs and f_2 RWs. Using powerful resummation technique, we resum asymptotic expansions for these exponents and evaluate them at space dimension $d = 3$. As one can see, the effects of heterogeneity significantly influence the strength of the first

order transition (the exponent c increases in comparison to the usual homogeneous SAW case). We support this observation providing exact results at $d = \mathbf{2}$. Moreover, we show that the effect of strengthening is further enhanced by the so-called crowded environment with the long-range correlated inhomogeneities.

In summary, this research advances our understanding of scaling phenomena, providing valuable insights applicable to diverse scientific challenges.The outcomes of this work have yielded three articles, two published, one accepted for publication, three preprints and eleven conference reports.

Keywords: scaling, universality, critical phenomena, phase transitions, Ising model, Poland-Scheraga model, critical exponents, Monte-Carlo simulations, Lee-Yang zeros, asymptotic series.

PhD publications

1. *Honchar Yu., von Ferber C., Holovatch Yu.* Variety of scaling laws for DNA thermal denaturation. // *Physica A: Statistical Mechanics and its Applications.* — 2021. — Vol. 573. — P. 125917. Scopus (Q1), DOI: 10.1016/j.physa.2021.125917
2. *Holovatch Yu., von Ferber C., Honchar Yu.* DNA thermal denaturation by polymer field theory approach: effects of the environment. // *Condensed Matter Physics.* — 2021. — Vol. 24. — P. 33603. Scopus (Q3), DOI: 10.5488/CMP.24.33603
3. *Honchar Yu., Berche B., Holovatch Yu., Kenna R.* When correlations exceed system size: finite-size scaling in free boundary conditions above the upper critical dimension. // preprint ArXiv:. — 2023. — arXiv:2311.11721. (*to appear in Condens.Matter Phys 2024, 1*) DOI:10.48550/arXiv.2311.11721
4. *Honchar Yu., von Ferber C., Holovatch Yu.*, Variety of scaling laws for DNA thermal denaturation. // preprint ArXiv:. — 2021. — arXiv:2103.08725. DOI:10.48550/arXiv.2103.08725
5. *Holovatch Yu., von Ferber C., Honchar Yu.* DNA thermal denaturation by polymer field theory approach: effects of the environment.// preprint ArXiv:. — 2021. — arXiv:2107.11812. DOI:10.48550/arXiv.2107.11812
6. *Гончар Ю.* Закони скейлінгу в термічній денатурації ДНК. *19-та Всеукраїнська школа-семінар та Конкурс молодих вчених зі статистичної фізики та теорії конденсованої речовини.* Збірка тез. с. 22. Львів, 13-14 червня 2019.
7. *Honchar Yu., von Ferber C., Holovatch Yu.* Resummation of ε-expansion for co-polymer star exponents reveals the order of the phase transition in thermal denaturation of DNA. *5-th Conference on Statistical Physics: Modern Trends and Applications.* Book of abstracts. p. 113. Lviv, 3-6 липня 2019.
8. *Honchar Yu., von Ferber C., Holovatch Yu.* On the Order of DNA Ther-

mal Denaturation Phase Transition. *"Різдвяні дискусії 2020"*. ЛНУ ім. І.Франка. J. Phys. Stud. 24(1), p. 1998:4-5, Львів, 11-12 січня 2020.

9. *Гончар Ю., Головач Ю., фон Фербер К.* Ефекти середовища у термічній Денатурації ДНК. *XXI Всеукраїнська школа-семінар та Конкурс молодих вчених зі статистичної фізики та теорії конденсованої речовини.* Збірка тез. с. 23. Львів, Україна, 11-12 жовтня, 2021.

10. *Honchar Yu.* DNA thermal denaturation by polymer field theory approach. *46th Middle European Cooperation in Statistical Physics MECO 41.* Book of Abstracts. p. 71. Riga, Latvia, May 11-13, 2021.

11. *Honchar Yu., C. Von Ferber C., Holovatch Yu.* DNA thermal denaturation viewed as a phase transition: scaling laws and beyond. *Різдвяні дискусії 2022.* ЛНУ ім. І.Франка. J. Phys. Stud. 26. p. 1998-1. Львів, 11-12 січня 2022.

12. *Гончар Ю.* Скейлінґ для моделі Ізінґа на п'ятивимірній ґратці з вільними граничними умовами. *XXII Всеукраїнська Школа-семінар зі статистичної фізики і теорії конденсованої речовини.* Збірка тез. с. 21. Львів, 24-25 листопада 2022.

13. *Honchar Yu., Berche B., Holovatch Yu., Kenna R.* Finite-size scaling for the Ising model above the upper critical dimension. *"Різдвяні дискусії 2022/2023"*. ЛНУ ім. І.Франка. J. Phys. Stud. 27. p. 1998-3. Львів, 22-23 грудня 2022

14. *Honchar Yu., Berche B., Holovatch Yu., Kenna R.* Finite-size scaling for 5D Ising model with free boundary conditions. *DPG-Verhandlungen, Condensed Matter Section 2023*, MA 23.47. Dresden. March 26-31, 2023.

15. *Honchar Yu., Berche B., Holovatch Yu., Kenna R.* Numerical exploration of finite-size scaling above the upper critical dimension. *48th Middle European Cooperation in Statistical Physics MECO 48.* Book of Abstracts. p. 58 Stará Lesná, Slovakia. May 22-26, 2023.

16. *Гончар Ю.* Модель Ізінґа над верхньою критичною вимірністю. *XXIII Всеукраїнська Школа-семінар зі статистичної фізики і теорії конденсованої речовини.* Збірка тез. с. 20. Львів, 26-27 жовтня 2023.

CONTENTS

ABBREVIATIONS

MF	—	mean-field
FSS	—	finite-size scaling
GFP	—	Gaussian fixed point
PBC	—	periodic boundary conditions
FBC	—	free boundary conditions
L & M	—	Lundow and Markström
LRIM	—	Long-range Ising model
MC	—	Monte-Carlo
RG	—	renormalization group
LY	—	Lee-Yang
FT	—	field theory
DNA	—	deoxyribonucleic acid
PS	—	Poland-Scheraga

INTRODUCTION

Justification of the choice of research topic. Concepts of scaling and universality in critical phenomena have been very effective for a wide area of systems. Scaling hypothesis states that thermodynamic potentials are generalized homogeneous functions of their respective variables in vicinity of critical point, while universality in criticality means that the system's behaviour does not depend on the details and microscopic structure of the system. In particular, some observables are characterized by the power laws. The exponents in these power laws, as well as the amplitude ratios, exhibit universality and remain the same over a wide class of systems united in the universality classes. They do not depend on microscopic details of the system, such as parameters of interaction potentials, lattice type etc.. Universality classes are defined by so-called global variables, that include space dimensionality d, number of order parameter components n, system symmetry, type of interaction. However, there still remain unsettled problems. Among them, the problems considered in this thesis are (i) scaling above the upper critical dimension and (ii) scaling of complex polymer networks. (i) Above the upper critical dimension scaling of infinite systems becomes mean-field. For finite size systems scaling picture offers new challenges as the scaling is no longer mean-field. First of all, the boundary conditions need to be applied. For periodic boundary conditions new scaling exponent describes the finite-size scaling. Finite-size scaling of lattices with free boundary conditions above the upper critical dimension at the pseudocritical point is unsettled. We will perform high accuracy computer simulations and use complementary techniques such as Fourier modes analysis and partition function zeros analysis to obtain the finite-size scaling behaviour above the upper critical dimension. (ii) Scaling properties of mutually interacting random walks and self-

avoiding walks are in the core of many phenomena occuring in physics and beyond. In particular, they are useful within the Poland-Scheraga model in description of DNA thermal denaturation. We will use recently suggested theory of scaling of co-polymer networks to explain the unzipping transition of DNA strands, as well as the effects of crowded environment on the process of DNA denaturation.

Relationship with academic programs, plans, themes. Dissertation research was conducted in the Institute for Condensed Matter Physics of the National Academy of Sciences of Ukraine and in Coventry University, Coventry, United Kingdom. It has been supported by Institute for Condensed Matter Physics of the National Academy of Sciences of Ukraine (state funded research themes: Methods and models of statistical physics for the new structure emergence description and explanation of scaling in complex systems, 2018-2022, 0118U003012; Analytic and numeric approaches for analysis of the cooperative behaviour in complex systems, 2023-2027, 0123U100238), International doctoral college "Statistical Physics of Complex Systems" $\mathbb{L}^4$, Presidential Scholarship for young scientists (2022-2024), IEEE "Magnetism for Ukraine" programme (2023-2024).

The purpose and objectives of the study.

Object of study. Study of the $d = 5$ Ising model on the generalised hypercubic lattice, that will aid finding the finite-size scaling properties at space dimensions above the upper critical dimension $d_c = 4$. Poland-Scheraga model as a description of DNA thermal denaturation in terms of conformational properties of complex polymer networks.

Subject of study. Finite-size scaling phenomenon in a many-particle system in the vicinity of critical and pseudocritical points at the space dimension higher than the upper critical dimension d_c. Thermal denaturation of DNA – unzipping of DNA double chain with an increase of temperature. Analysis of such phenomena in scope of phase transition theory, account of the effects of possible heterogeneity of the chain on the phase transition order.

Research methods. Computer simulations of high-dimensional spin lattices, resampling of large datasets, Fourier modes analysis, partition function zeros

analysis, ε-expansion, resummation of asymptotically divergent series.

Scientific novelty of the obtained results. (i) It has been shown that the correlation length of the $d = 5$ Ising model with free boundary conditions at pseudocritical point is a non-linear function of the system size L. Its change is governed by a new critical exponent ♀. This phenomenon is known as Q-scaling and its validity has been confirmed in our simulations. Partition function zeros analysis has been used for the first time to improve the accuracy for the scaling picture on the entire lattice. (ii) New scaling relations for the loop closure exponent c_i were derived with the account of the possible heterogenity of a polymer network in DNA thermal denaturation. We demonstrate, that the number of denaturated loop configurations increases the sharpness of the phase transition from bound to unzipped state. In particular, when the entropy of the loop is higher, the first order phase transition is starker. The exponents governing the DNA denaturation transition have been calculated with the record accuracy in $\varepsilon = 4 - d$ expansio and evaluated at $d = 3$. At $d = 2$ their respective values have been obtained exactly. The impact of a structurally disordered environment has been considered and the numerical estimates for loop closure exponents for DNA chains in the environment with impurities were given.

The practical significance of the results. This research is of fundamental character, as it considers the scaling concept for the theoretical physics models of high absraction levels. For example, the Ising model (Chapters 2, 3) that describes the phase transition in magnets, is also used to study criticality of simple fluids, as well as ordering in physical systems and beyond, where the individual agents are characterized by binary opposition (are two-state variables). Finite-size scaling used for its analysis is a standard tool to get access to the properties of a many-particle system by Monte-Carlo simulations. Therefore, new results about FSS of the Ising model are also of practical use. In Chapter 4 we have considered Poland-Scheraga model. Even though this model is a simplified, "cartoon" picture of DNA, it is widely agreed that the model is perfect for studying the intricacies of interplay between the entropy and energy, and the influence it has on the universal properties

of transition from the bound double chain to the denaturated (unzipped) state. Our account of possible heterogeneity as well as the crowded environment effects makes this model one step closer to real biological objects. The results are also used in a curriculum for the theoretical physics students.

Personal contribution of PhD. PhD personally:

- performed multiple Monte-Carlo simulations of the Ising model above the upper critical dimension;
- numerically calculated the scaling exponents and located the pseudocritical points;
- performed a Fourier modes analysis of magnetisation;
- performed a Lee-Yang zero analysis above the upper critical dimension;
- applied conformal mapping resummation techniques to the ε-expansions of different polymer scaling exponents;
- visualised the abovementioned models and results in figures.

The results were discussed and interpreted together with the co-authors of the published works.

Approbation of obtained results. Key results of this research were presented at the conferences: 5-th Conference on Statistical Physics: Modern Trends and Applications, Lviv (July 3-6 2019) [5], School of statistical physics and condensed matter physics for young scientists, Institute for Condensed Matter Physics of the National Academy of Sciences of Ukraine, Lviv (June 13-14, 2019, October 11-12, 2021, November 24-25, 2022, October 26-27, 2023)[4, 6–8], Christmas Discussions, Ivan Franko University of Lviv (January 11-12, 2020, January 11-12, 2021, December 22-23, 2022) [9–11], The Conferences of the Middle European Cooperation in Statistical Physics (MECO) (Riga, May 11-13, 2021, Stara Lesna, May 22-26, 2023) [12, 13], Deutsche Physikalische Gesellschaft 2023 Spring Meeting, Dresden (March 26-31, 2023) [14], as well as seminars of the ICMP, seminars "Statistical physics of complex systems" at the Laboratory of statistical physics of complex

systems at ICMP, post-graduate seminars in Fluids and complex systems centre at Coventry University.

Publications. Results of research were published in: 2 articles in journals, included in the international scientometric citation databases Scopus and WoS [2, 3]; 1 article accepted for publication [1]; 3 preprints [1, 15, 16]; 11 conference abstracts [4–14].

Structure and scope of the thesis. Dissertation consists of the introduction, literature review chapter and three chapters with main results, that contain the research work, as well as final conclusions, bibliography, 3 appendices, 24 figures, and 5 tables. It is 94 pages long (full length 109 pages). The bibliography consists of 136 scientific publications.

In the introduction the motivation of this work is presented, as well as the purpose and the goals of the study, research novelty and the practical significance of the results. Brief contents of the dissertation is presented.

Chapter 1 is a Literature Review of the research topic. The ideas of universality, scaling, criticality are considered, especially for the cases of finite-size scaling above the upper critical dimension, and the scaling picture for complex polymer networks.

Chapter 2 is devoted to the numeric studies of the finite-size scaling above the upper critical dimension. In particular, the Wolff algorithm simulations of $d = 5$ Ising model on the hypercubic lattice with free boundary conditions were performed. The results are presented in form of scaling behaviour of magnetisation and isothermal susceptibility.

In **Chapter 3** the additional techinques for the improvement of the accuracy of finite-size scaling are exhibited. First, the magnetisation Fourier modes analysis is performed. Then, the partition function zeros analysis is presented. The results show better accuracy exponents of finite-size scaling above the upper critical dimension. Results of Chapter 2 & 3 are published in [1].

Chapter 4 contains the study of the complex polymer network scaling behaviour, in particular for the thermal denaturation of DNA in Poland-Scheraga

model. The possible heterogeneity of the unzipped chain is considered, as well as the effects of the environment. Results of this chapter are published in [2, 3].

Thesis ends with the **Conclusions**, **Bibliography** and **Appendices**.

CHAPTER 1

LITERATURE REVIEW

1.1. Universality, scaling hypothesis, relations between exponents

The concept of universality has long been in a core of the description of many phenomena occurring in physics and beyond. In the context of collective behaviour of a many-particle system, universality means the properties' of critical behaviour independence of a fine microscopic features of the system. In this thesis we will deal with manifestation of universality in critical phenomena. As the system forgoes the shift from one stable state to another, we are interested in the changes in thermodynamic functions of the system with the change of parameters during phase transitions. The subject of phase transitions and critical phenomena is key to unravelling how matter undergoes transformations [17, 18]. It has even become a part of history, as the formation of schools and academies influenced the cities and countries they were in [19]. The most recognizable phase transition explains the changes in the spacial structure of the matter among the basic states that is solids, liquids and gasses. In the early theories such as the molecular field theory of Van der Waals, reaching certain temperature, volume and internal pressure leads to the point, where two phases are existing simultaneously and even a slight away from this point settles the system's state to be one or another. This point is called the critical point and system's behaviour in its vicinity is providing us with the crucial information on the nature of this phenomenon. Similarly, in the classic theory of magnetism, the phase transition occurs when the magnetic ordering in from ferromagnetic to paramagnetic, when the material loses its spontaneous magnetisation

at a temperature called the Curie point. In this case, magnetisation, which serves as an order parameter in this problem, decays with certain dependence on the temperature below the critical point and is zero above. These and other theories of phase transitions use the mean-field (MF) approximation, where we assume that the interparticle interactions occur between all particles of the system. The behaviour of the system parameters with the change of internal fields such as temperature has been observed to be power law, so the set of critical exponents has been introduced and unified by Michael Fisher [20]. They are six exponents connected by four relations, so that knowing any two of these exponents is enough to know the whole critical behaviour of the system. The relations read:

$$\nu d = 2 - \alpha, \qquad \text{Josephson [21]} \tag{1.1}$$

$$2\beta + \gamma = 2 - \alpha, \qquad \text{Rushbrooke [22]} \tag{1.2}$$

$$\beta(\delta - 1) = \gamma, \qquad \text{Widom [23]} \tag{1.3}$$

$$\nu(2 - \eta) = \gamma, \qquad \text{Fisher [24]} \tag{1.4}$$

where β, δ control the scaling of magnetisation with respect to temperature and magnetic field respectively, α is the scaling exponent associated with the heat capacity scaling, γ governs the magnetic susceptibility scaling, and ν, η are the exponents of correlation length and correlation function scaling. The scaling exponents within the MF theory do not depend on any system parameters. They are the same for all systems and are commonly called super-universal. In the Table 1.1 we show the values of the MF exponents, note that they do not depend on the dimensionality or the symmetry of the system.

α_{MFT}	β_{MFT}	γ_{MFT}	δ_{MFT}	ν_{MFT}	η_{MFT}
0	$\frac{1}{2}$	1	3	$\frac{1}{2}$	0

Table 1.1. Mean-field critical exponents.

Landau theory, a foundational framework for understanding phase transitions was coined back in 1937 [25]. Landau's alterations were driven by the ambition to

capture the essential features of systems in the vicinity of critical points. His pivotal insight lay in the assertion that the thermodynamic function, specifically the free energy of a magnetic system, could be expanded into a series of the order parameter m at the absence of an external magnetic field h around the critical point $t = T_c - T$:

$$F(t, m) = a_0(t) + a_2(t)m^2 + a_4(t)m^4 + a_6(t)m^6 + \dots . \tag{1.5}$$

This expansion, crucially, incorporated only even powers of the order parameter, reflecting the inherent symmetry of the system. The coefficients accompanying these powers were treated as analytic functions, providing a flexible framework for describing the behavior of the system near criticality. The modified Landau theory offered a novel perspective, paving the way for a more nuanced understanding of phase transitions. One of the noteworthy outcomes of this modified theory was the identification of a specific case leading to a second-order phase transition. In this scenario, the coefficient a_2 took on a positive value, ushering in a continuous change in the system's state. This manifest in the non-zero magnetization values persisting below the critical temperature (T_c), while above T_c, magnetization dropped to zero. The Landau theory, in this context, not only provided an equation of state but also facilitated the derivation of solutions for spontaneous magnetization. The critical exponents, notably β and δ, were determined through this lens, offering insights into the system's behavior as it traversed the critical point. Because the real picture is more complex than this, we consider here a further modification of the Landau theory that is presented here in a form of the well-known Landau-Wilson-Ginzburg Hamiltonian, which introduces different classes of universality [17, 26]. It is a Helmholtz free energy functional in terms of the field variable ϕ:

$$F[\phi] = \int d^d x \left[\frac{1}{2} t\phi^2(x) + \frac{1}{4} u\phi^4(x) + \frac{1}{6} \upsilon\phi^6(x) - h\phi(x) + \frac{1}{2} |\nabla\phi(x)|^2 \right] . \tag{1.6}$$

For different models the powers of ϕ^n included into the expansion are different, which leads to different scaling behaviour and different classes of universality, which also means that all the models within the universality class have the same set of critical exponents. On the basis of this model, the hypothesis of homogeneity arose [27, 28],

which consists in the fact that the singular part of free energy per element of the system scales in critical region according to:

$$f_{sing}(t,h) = b^{-d} f_{sing}(b^{y_t} t, b^{y_h} h) \tag{1.7}$$

$$f_{sing}(t,h) = |t|^{d/y_t} \mathcal{F}^{\pm}(h|t|^{-y_h/y_t}), \tag{1.8}$$

where b is an arbitrary rescaling factor, d is the space dimension, and y_t, y_h are renormalization group (RG) eigenvalues of fields t, h in the scaling function $\mathcal{F}^{\pm}(y) = f_{sing}(\pm 1, y)$. Then, the expressions for magnetisation and other free energy derivatives are easily found in a form:

$$m_\infty(t,h) = b^{-d+y_h} m_\infty(b^{y_t} t, b^{y_h} h). \tag{1.9}$$

Subscript ∞ means that the value is considered in the thermodynamic limit of an infinite system. Setting $h = 0$, $b = |t|^{-1/y_t}$ we find the scaling around the critical temperature T_c in zero magnetic field, and in the same way at $T = T_c$ setting $b = |h|^{-1/y_h}$ gives scaling with respect to the changes in the external magnetic field. Hence, the critical exponents can be presented via y_t and y_h:

$$\beta = \frac{d - y_h}{y_t}, \quad \delta = \frac{y_h}{d - y_h}, \tag{1.10}$$

$$\gamma = \frac{2y_h - d}{y_t}, \quad \alpha = 2 - \frac{d}{y_t}. \tag{1.11}$$

Athough for many cases the problem is now solved and the critical behaviour is well known, we show and consider two problems where the scaling functions, universality, and homogeneity of correlation functions are not yet fully defined. The reason of interest in defining the critical exponents is caused by the fact that in the vicinity of the critical point only the leading asymptotic of thermodynamic values is essential. That is why the logarithm curves obtained experimentally have the form of straight lines and the critical exponent is determined by the slope of these lines. Thus often it is easier to measure the critical exponent than a whole function. One more reason is that there exist exact relations between critical exponents which are valid for any particular system, allowing to test the reliability of the data obtained.

The first task of this thesis is finite-size scaling above the upper critical dimension, where the scaling in the thermodynamic limit is mean-field, but firstly, the hyperscaling relation is violated, and secondly, finite-size scaling is not mean-field. In the second problem, which we will consider here the task is the scaling of new properties of complex polymers, namely, that in the thermal denaturation of DNA, the scaling of chains and split DNA is different. Both scaling and exponents in general here control what kind of phase transition we observe here. First, in this chapter we discuss the theory behind both. In chapter 2 we show our computer simulation results of the $d = 5$ Ising model with free boundary conditions. In chapter 3 we use the advanced techniques to find the finite-size scaling of the observables, namely the Fourier transform modes of magnetization and partition function zeros. The scaling laws of polymer networks are presented in chapter 4.

1.2. Scaling above the upper critical dimension

The upper critical dimension d_c is determined by the Ginzburg criterion for model of the universality class ϕ^n [29, 30]:

$$d \geq d_c = \frac{2n}{n-2}. \tag{1.12}$$

Above this dimension the number of interactions in the system is large enough so one can ignore the fluctuations and the mean field theory becomes valid.

For a second-order phase transitions in ferromagnetic systems, the specific heat, magnetisation, susceptibility and correlation length near to the transition temperature T_c, scale as $c_\infty(t) \sim |t|^{-\alpha}$, $m_\infty(t) \sim (-t)^\beta$, $m_\infty(h) \sim |h|^{\frac{1}{\delta}}$, $\chi_\infty(t) \sim |t|^{-\gamma}$, $\xi_\infty(t) \sim |t|^{-\nu}$, where t is a reduced temperature, h is a reduced magnetic field (each is omitted from functional arguments when it vanishes), and the formula for $m_\infty(t)$ holds only in the broken-symmetry phase where $t < 0$. and the subscript denotes the (infinite) size of the system. The critical diverging singularities are replaced by finite peaks when the linear extent, L, of the system is finite. These finite peaks are centered around the so-called pseudocritical points T_L. The rounding of

the susceptibility peak can be measured by its width at half-height, for example, and is governed by an exponent ρ: $\Delta T_{\text{rounding}} \sim L^{-\rho}$. The distance of the pseudocritical temperature T_L from the critical one T_c is described by the shift exponent λ: $T_L - T_c \sim L^{-\lambda}$. Usually (but not always) [31], the rounding and shifting exponents coincide and are given by

$$\rho = \lambda = \frac{1}{\nu}. \tag{1.13}$$

Below the critical dimension d_c and near to the critical point, the infinite-volume correlation length ξ_∞ can by replaced by the system size L when the latter is finite. This is sufficient to deliver appropriate FSS there. E.g., it for specific heat leads to $c \sim |t|^{-\alpha} = \xi^{\alpha/\nu}$ being replaced by $L^{\alpha/\nu}$. Similar applies to other observables so that

$$c_L \sim L^{\frac{\alpha}{\nu}}, \quad m_L \sim L^{-\frac{\beta}{\nu}}, \quad \chi_L \sim L^{\frac{\gamma}{\nu}}. \tag{1.14}$$

Eqs.(1.13) and (1.14) well describe FSS below the upper critical dimension. When the dimensionality d exceeds the upper critical d_c, our current picture is as follows [32]. The self-interacting term, which is responsible for the existence of the phase transition by spontaneous symmetry breaking (e.g., the ϕ^4 term in the field-theoretic equivalent to the Ising-model Hamiltonian), modifies thermodynamic functions above the critical dimension in such a way that the above FSS formulae no longer apply. The usual expression for the hyperscaling relation, $\nu d = 2 - \alpha$, also fails. These circumstances were argued by Fisher with the fact that the quartic term is coupled to a dangerous irrelevant variable (DIV) [33]. Since the amplitude of this term is proportional to $1/u$, it is dangerous to make u zero. Fisher's DIVs led to a set of further works, such as a paper by Binder, Nauenberg, Privman, and Young (BNPY) [34]. They arrive to a modification of the famous scaling homogeneity assumption:

$$f_\infty^{\text{sing}}(t, h, u) \overset{u \to 0}{=} b^{-d+p_1 y_u} u^{p_1} \mathscr{F}^{\pm}(b^{y_t + p_2 y_u} t u^{p_2}, b^{y_h + p_3 y_u} h u^{p_3}), \tag{1.15}$$

where b is a rescaling factor, and p_1, p_2, p_3 are some constants which are action-dependent and that need to be derived for consistency with MF exponents. BNPY

introduce the following notation, which is now widerly used,

$$d^* = d - p_1 y_u, \quad y_t^* = y_t + p_2 y_u, \quad y_h^* = y_h + p_3 y_u. \tag{1.16}$$

Same can be done for the scaling of the correlation length:

$$\xi_\infty^{\text{sing}}(t, h, u) \overset{u \to 0}{=} b^{1+q_1 y_u} u^{q_1} \mathscr{H}^{\pm}(b^{y_t + q_2 y_u} t u^{q_2}, b^{y_h + q_3 y_u} h u^{q_3}). \tag{1.17}$$

Authors in [34] argue in favour of $p_1 = 0$, $q_1 = 0$, the first one from the assumption that $d^* = d$, and the second from the belief that the finite correlation length ξ_L is "bounded by the system size L". Further excellent works by Luijten, Blöte and Binder [35] suggest a change of scaling variables that allows us to get to current theory coined by Berche and Kenna [36]. They introduce a new scaling exponent ϙ (Old Greek letter "coppa") that governs the scaling of the correlation length (so-called Q-FSS):

$$\xi \sim L \longrightarrow \xi \sim L^{\text{ϙ}} \tag{1.18}$$

This is based on a valid suggestion that there is no actual reason why q_1 from (1.17) is zero, the correlation length isn't length, but the rate of correlation, which as we know decays exponentially above the critical point but experiences a peak in the vicinity of criticality. So ϙ equals to 1 below the upper critical dimension and $\text{ϙ} = d/d_{uc}$ for $d > d_{uc}$. The physical interpretation of Q-FSS is that the ratio of correlation volume to actual volume, $\xi^{d_{uc}}/L^d$, is the relevant one. This way the broken hyperscaling relation is fixed by changing it to

$$2 - \alpha_{\text{MF}} = \frac{d\nu_{\text{MF}}}{\text{ϙ}}.$$

Following "surprising" analytical [44] and numerical [45] observations of a superlinear (wrt L) correlation length, it was shown in Refs.[40, 41, 46, 47] that, contrary to earlier expectations, these features of the model are also affected by such dangerous irrelevant variables, just like the properties related to free-energy [34]. This leads to the introduction of a pseudocritical exponent $\text{ϙ} = \max(1, d/d_c)$ for the FSS of the correlation length, which takes the value d/d_c when $d > d_c$ [38, 41, 47]. At first

sight, the exponent ϙ has a similar status to λ and ρ, above, in that it most directly refers to finite-size systems as opposed to the infinite-volume ones which are directly described by α, β, γ, δ and ν. Thus ϙ may be considered a pseudocritical exponent. The superlinear behaviour of the finite-size correlation length has been verified by Monte Carlo simulations in Refs.[38, 40, 41, 46–48] and its existence modifies the finite-size scaling relations for, instead of replacing ξ_∞ by L, one replaces it by

$$\xi_L \sim L^{\text{ϙ}}, \tag{1.19}$$

so that

$$c_L \sim L^{\frac{\text{ϙ}\alpha}{\nu}}, \quad m_L \sim L^{-\frac{\text{ϙ}\beta}{\nu}}, \quad \chi_L \sim L^{\frac{\text{ϙ}\gamma}{\nu}}. \tag{1.20}$$

To distinguish Eq.(1.14) from Eq.(1.20), we referred to the latter as Q-FSS [38] (the "Q" here and throughout referring to ϙ, a notation suggested by Fisher in Ref.[47]).

The form $\xi \sim L^{d/4}$ for the correlation length of the short-range Ising-model (for which $d_c = 4$) in the analytical study of Ref.[44] and verified numerically in Ref.[45] was for periodic boundary conditions (PBCs). That it also applies to free boundary conditions (FBCs) was suggested in Ref.[38] and verified in Refs.[40, 41, 46–48]. The existence of ϙ as a new, universal pseudocritical exponent allows one to extend the hyperscaling relation to beyond the upper critical dimension. This general form (valid in all dimensions) is

$$\frac{\nu d}{\text{ϙ}} = 2 - \alpha. \tag{1.21}$$

In contrast to what was suggested above where ϙ appeared to be a pseudocritical exponent, this formula links ϙ to critical exponents. This promotes the new exponent to the level of critical (as opposed to pseudocritical) exponent. Whether one considers ϙ to be a critical or pseudocritical exponent is perhaps a personal preference.

To understand the origins of the exponent ϙ, the Fourier modes associated with high-dimensional systems may be partitioned into two types [40]. Although both are governed by the Gaussian fixed point, so-called Q-modes are susceptible to

dangerous irrelevant variables while so-called G-modes are not. Here and throughout, following the terminology used in Ref.[40], "G" refers to the "pure" Gaussian sector (unmodified by dangerous irrelevant variables) to distinguish it from the Q-sector [40]. For systems with PBCs only the zero mode is of the Q-type; all other modes are Gaussian. There, as is common below d_c, the rounding exponent ρ has the same magnitude as the shifting exponent λ, $\rho = \lambda = \wp/\nu$, ensuring that the Q-scaling window, which is centred on the pseudocritical point, extends as far as the critical one. In other words, Q-FSS applies at T_L and T_c in the PBC case.

For systems with free boundaries, the partitioning is somewhat more subtle. The dominance of Q-modes at the pseudocritical point ensures that Q-FSS governs finite-size effects there. This is where universality resides above the upper critical dimension i.e., the Q-FSS formulae (1.20) hold both for PBCs and FBCs there. The rounding and shifting exponents are

$$\rho = \frac{\wp}{\nu}, \quad \lambda = \frac{1}{\nu}, \tag{1.22}$$

and, since $\rho > \lambda$, the shifting is bigger than the rounding so that the Q-FSS window, centred as it is around the pseudocritical point, does not extend to the critical point. FSS there is governed by G-type behaviour [40].

Another method widely used in theory of critical phenomena and will be used by us in this thesis is analysis of the partition function zeros. These lie in the complex plane of parameters entering the partition function (i.e., external field or temperature). The notion was developed by Lee and Yang [49, 50], who studied the partition function as a polynomial in a parameter related to the external magnetic field. Following a similar idea, Fisher suggested the study of the zeros for the temperature complex plane [20]. These ideas have been termed a "fundamental theory of phase transitions" [51]. We discuss these developments in more detail in Chapter 3, below.

The partition function on a finite lattice is given by

$$Z_L = \sum_{E,M} p(E,M) e^{-\beta E + hM}, \tag{1.23}$$

where the configurational energy E is conjugate to $\beta = \mathbf{1}/kT$ (k being the Boltzmann factor), the configurational magnetisation M is conjugate to the reduced external field $h = \beta H$ and $p(E, M)$ is the density of states. From the fundamental theorem of algebra, this can be expressed in terms of the set of Lee-Yang zeros $\{z_j\}$ as

$$Z_L(h) = A(z) \prod_j [z - z_j(L)], \tag{1.24}$$

where z is a suitable function of h (e.g., $z = \exp h$) and where A denotes a non-vanishing smooth functions of its arguments.

Well established standard FSS, applicable below the upper critical dimension, gives for the Lee-Yang zeros

$$h_j(L) \sim L^{-\frac{\Delta}{\nu}}, \tag{1.25}$$

in which

$$\Delta = \beta\delta = \beta + \gamma \tag{1.26}$$

is the gap exponent. These equations are the counterparts of Eq.(1.14) for the fundaments of the partition function zeros. A crucial element of Q-theory as developed in Ref.[38] is the prediction that, for $d > d_c$, Lee-Yang zeros scale in the Q-regime (i.e., at pseudocriticality universally and at criticality in the PBC case) as

$$h_j(L) \sim L^{-\frac{\wp\Delta}{\nu}}. \tag{1.27}$$

An aim of this research is to provide a numerical check of these scaling formulae. For convenience we list in Table 1.2 the various FSS predictions for the various theoretical possibilities - standard FSS from Landau theory, Gaussian theory and Q-FSS. The first Lee-Yang zeros allow us to access the G-sector, Eq.(1.25), through FBCs at criticality and the Q-sector, Eq.(1.27), through the pseudocritical points.

We will see that, as emphasised in Ref.[40] for the magnetisation, despite mean-field exponents being accurate in infinite volume, the extension of Landau theory to finite systems does not manifest physically through standard FSS. Instead FSS is either of the G- or Q-types consistent with the theory developed in Ref.[38, 40, 41, 46–48].

Quantity	Landau	G	Q
m	$L^{-\beta/\nu} = L^{-1}$	$L^{-\beta_G/\nu} = L^{-3/2}$	$L^{-\beta_Q/\nu} = L^{-\wp\beta/\nu} = L^{-5/4}$
χ	$L^{\gamma/\nu} = L^{2}$	$L^{\gamma_G/\nu} = L^{2}$	$L^{\gamma_Q/\nu} = L^{\wp\gamma/\nu} = L^{5/2}$
c	$L^{\alpha/\nu} = L^{0}$	$L^{\alpha_G/\nu} = L^{0}$	$L^{\alpha_Q/\nu} = L^{\wp\alpha/\nu} = L^{0}$
h_1	$L^{-\Delta/\nu} = L^{-3/2}$	$L^{-\Delta_G/\nu} = L^{-3/2}$	$L^{-\Delta_Q/\nu} = L^{-\wp\Delta/\nu} = L^{-15/8}$

Table 1.2. FSS (Landau and G columns) and Q-FSS (last column) for the variables measured in this work ($d = 5$). We expect (and find) Q-FSS at the pesudocritical point, standard FSS applied to Gaussian modes at the critical point and standard FSS which is of relevance for Landau values not to feature at all.

1.3. Scaling ideas in polymer physics: polymer stars and networks

Among different phenomena occurring in polymers the point of main interest for us will be theconformational properties of flexible macromolecules in good solvents. These solutions are to be taken in thermodynamic equilibrium and we will be interested in the time-independent properties, as the osmotic pressure or the space correlations between the chain segments. The structure of polymers was under controversial discussion until under the influence of the experimental work of Staudinger ([67], 1932) the idea of long chain like molecules began to be generally accepted.

The number N of repeating units (monomers) can be very high (e.g. $N > 10^5$). Normally polymer solutions are polydysperse: there are present macromolecules with different N in the solution. But there exist methods allowing to

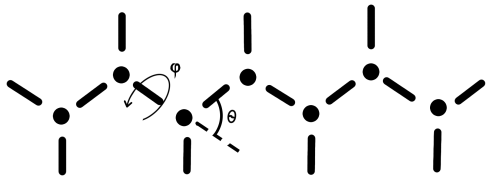

Figure 1.1. Polymer chain consists of multiple monomers (circles) connected by bonds (horizontal lines). In good solvent, the possible flexibility of the polymer chain is decided by the angles θ and ϕ.

obtain narrow enough distributions of values of N . Another important for us feature is polymer flexibility. One discriminates between static and dynamic flexibility. Consider the carbon chain (Fig. 1.1). The angle θ between two subsequent C - C bonds is fixed, but angle ϕ_n can be chosen arbitrary. There exist 3 minima corresponding to 3 main conformations (and 3 optimal angles ϕ): 1 trans- and 2 gauche-conformations. This energetic dependence is characterized by 2 main parameters: - difference between the energy levels in different minima (in our case is positive: trans-conformation is preferable in comparison with both gauche-conformations); energy barrier height E. If is smaller than thermal energy kT then the chain is called statically flexible: chain is not straight but looks like a statistical ball. The case kT corresponds to the limit of high flexibility. Passing to higher values of the relation we obtain that trans-states are preferable and the chain becomes locally rigid. But considering the chain in a larger scale again we see that it is flexible. Generally speaking if one ignores details which are smaller then certain typical length l_p one sees flexible chain. l_p is called the persistent length of the chain. So if l_p is essentially smaller than total chain length L we can choose the scale when one does not see rigid pieces l_p and state that molecule is flexible in large scales [68, 69].

Connection between polymers and critical exponents originates from the application of self-avoiding walks (SAWs) as a modeling tool for polymer molecules in good solvents [70]. This model serves as a valuable tool for understanding how polymer chains navigate without intersecting themselves. A SAW refers to a trajectory originating from one point and concluding at another without ever crossing its own path. Typically, these trajectories are examined within lattice structures, limiting steps to discrete directions and specific lengths.

The SAW model helps describe the number ways a polymer chain with N monomers can arrange itself. Represented by $\mathcal{Z}_N$, this quantity exhibits a scaling pattern:

$$\mathcal{Z}_N \sim \tilde{z}^N N^{\gamma-1} \sim R^{\eta_{\text{chain}}}, \quad N >> 1. \tag{1.28}$$

This expression illustrates the exponential growth in configuration possibilities. A related parameter, indicative of the polymer's typical size, is given by:

$$< R > \sim N^{\nu}. \tag{1.29}$$

This implies that, on average, the size of the polymer grows in a specific manner with its length. A notable proposition by De Gennes (Ref.[69]) establishes a connection between these polymer behaviors and analogous phenomena observed in magnetism at the scale of tiny particles.

In the search of critical exponents for the polymer systems within the dimension $d = \mathbf{3}$, there is a notable absence of rigorous results. The Flory values, an early proposition for the correlation length exponent ν, suggested $\nu = \frac{3}{d+2}$ for $\mathbf{1} \leq d \leq \mathbf{4}$ [104, 105]. While accurate for $d = \mathbf{1}, \mathbf{2}, \mathbf{4}$, these values fall short for $d = \mathbf{3}$, emphasizing the considerable gap between the Flory argument and a mathematically substantiated proof.

Researchers have applied three distinctive methodologies to approximate critical exponents in $d = \mathbf{3}$. The first involves non-rigorous field theory computations in theoretical physics, combining the $n \to \mathbf{0}$ limit for the $O(n)$ model with an expansion in $\epsilon = \mathbf{4} - d$ focused on $d = \mathbf{3}$, with ϵ set at 1 [68]. The second utilizes Monte Carlo studies, employing the pivot algorithm and conducting extensive walks with a length of 33,000,000 [72]. The third method employs exact enumeration coupled with series analysis, relying on the lace expansion technique for dimensions $d \geq \mathbf{3}$, with walks enumerated up to $n = \mathbf{30}$ for $d = \mathbf{3}$[87].

The findings from these diverse methodologies within the $d = \mathbf{3}$ framework provide compelling insights into critical exponents. Exact enumeration estimates for $d = \mathbf{3}$ unveil values such as $\mu = \mathbf{4.684043(12)}, \gamma = \mathbf{1.1568(8)}, \nu = \mathbf{0.5876(5)}$. Remarkably, Monte Carlo estimates closely corroborate these values, reporting $\gamma = \mathbf{1.1575(6)}$ and $\nu = \mathbf{0.587597(7)}$ [135]. This multifaceted comprehension of critical exponents in the distinctive dimensional landscape effectively bridges theoretical predictions with empirical observations.

Considering more intricate polymer structures, such as star polymers with f legs [94, 95], introduces additional nuances. The number of configurations of a star of f legs, represented by $\mathcal{Z}_f$, follows a distinct pattern:

$$\mathcal{Z}_f \sim N^{\gamma_f - 1} \sim \ell_p^{-1} R^{\eta_f - \eta_2}, \tag{1.30}$$

with γ_f and η_f reflecting a family of scaling star exponents, and ℓ_p is a microscopic scale to make R dimensionless. Notably, these exponents intricately depend on the number of legs and the space dimension, contributing to a richer understanding of the scaling behavior in complex polymer networks.

Copolymer star exponents η_G govern the scaling of a star-shaped polymer with two types of "legs" [97]:

$$Z^S_{f_1 f_2} \sim R^{\eta^S_{f_1 f_2} - (f_1 + f_2)\eta^S_{20}}. \tag{1.31}$$

Copolymer network G constitutes of F_1 chains of one type, F_2 chains of another type, scales with a mean size of a single polymer chain R:

$$\mathcal{Z}_G \sim R^{\eta_G - F_1 \eta_{20} - F_2 \eta 02}, \tag{1.32}$$

with

$$\eta_G = -d\mathcal{L} + \sum_{f_1 + f_2 \geq 1} n_{f_1 f_2} \eta_{f_1 f_2}, \tag{1.33}$$

where d is the space dimension, $\mathcal{L}$ is the number of loops in network, and the sum $\sum_{f_1+f_2\geq 1}$ goes over all posible $n_{f_1 f_2}$ nodes with f_1 legs of one type and f_2 legs of different type.

Here we will consider a copolymer network that occurs during the DNA thermal denaturation within the Poland-Scheraga model. This is a simplified model that disregards the chemical details of the deoxyribonucleic acid. It considers the monomers to be point-like, and the nodes on the double chain can be in two possible states: either the monomers on two sides of the chain are bound, then the state on the node is ordered, or the bond is "unzipped", and the state is disordered.

One of the first models to explain the DNA denaturation as the first order transition was coined in middle-sixties by Poland and Scheraga [76, 77]. Two observations lay at the core of the model: (i) the breaking of hydrogen bonds between nucleobases is an energy-demanding process, therefore the low-T bounded state is energetically favoured, and (ii) a high-T unbound state has more configurations and hence it is favoured by entropy. Being simple enough to allow analytic and numerical treatments and at the same time capturing main peculiarities of the phenomena involved, the model gave rise to a whole direction of studies, see e.g. [79–84].

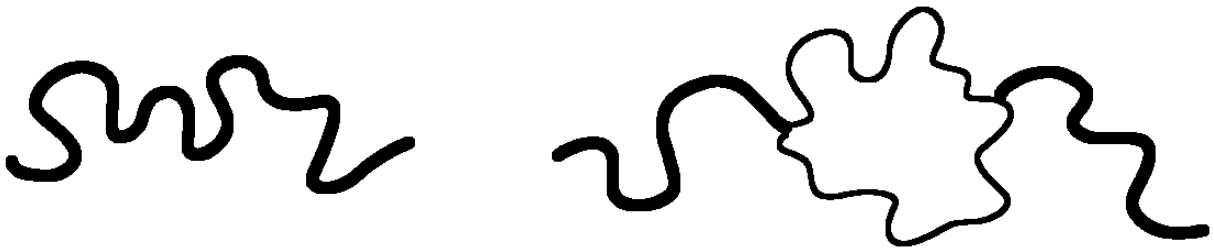

Figure 1.2. Model of DNA thermal denaturation we consider in this study. A double stranded macromolecule with end points $V\mathbf{1}$ is disattached ('unzipped') at points $V\mathbf{3}$. Resulting heterogeneous polymer network consists of two double strands $V\mathbf{1} - V\mathbf{3}$ (bound nucleobases, bold lines) and a denaturated single-stranded loop $V\mathbf{3} - V\mathbf{3}$ (unbound nucleobases, thin lines). Partition function of the loop attains a power-law scaling (1.34).

The Poland-Scheraga description, relies on a representation of the partition function $\mathcal{Z}$ of a polymer of N segments, each segment being in two possible states (bound and unbound monomers, see Fig. 1.2) in a form $\mathcal{Z} = x_1^N$, x_1 being maximal solution of the equation suggested in [78]. In turn, this allows to get the order parameter $\theta(T)$ (average number of ordered, bound pairs in a chain) and to observe different regimes for its temperature T dependence. These regimes are triggered by the loop closure exponent c for a single loop, defined as

$$\mathcal{Z}_{\text{loop}} \sim \mu^{\ell} \ell^{-c}, \tag{1.34}$$

where ℓ is loop length (number of segments) and μ is a non-universal factor. In particular, for low values of c, $\mathbf{0} \leq c \leq \mathbf{1}$, the order parameter is continuous

function of T smoothly changing between 0 and 1 when T decreases from ∞ to 0. For larger values of c the order parameter either continuously vanishes at $T = T_c$ for $\mathbf{1} < c \leq \mathbf{2}$ or disappears abruptly at $T = T_c$ for $c > \mathbf{2}$. The last two types of behaviour correspond to the second and first order phase transitions.

First attempts to define exponent c analytically let to $\mathbf{1} < c < \mathbf{2}$ and hence to the second order transition scenario. In particular, for a simplified model which considers a single denaturated loop and does not take into account interaction between bound and unbound segments (non-interacting RWs) one may obtain c by enumerating walks that return to the origin leading to $c = \mathbf{1}$, $c = \mathbf{3/2}$ for $d = \mathbf{2}$, $d = \mathbf{3}$, correspondingly [77]. A more general formula $c = d\nu$, with ν being polymer end-to-end distance scaling exponent was coined by Fisher [90]. In particular, it allows to take into account excluded volume effects for each of the segments. Its prediction is $c(d = \mathbf{2}) = \mathbf{3/2}$, $c(d = \mathbf{3}) \simeq \mathbf{1.764}$ and hence the transition still remains the second order. An interaction of a loop with the rest of the chain was taken into account in [85, 91] by making use of polymer network scaling description [94, 95, 114]. There, the configurational properties of a SAW polymer network with a single denaturated loop were recast in terms of the corresponding scaling exponents, cf. Fig. 1.2 for the homogeneous case. The phase transition was found to be of the first order for $d = \mathbf{2}$ and above, with $c(d = \mathbf{2}) = \mathbf{2 + 13/32} \simeq \mathbf{2.41}$, $c(d = \mathbf{3}) \simeq \mathbf{2.115}$. Numerical simulations at $d = \mathbf{3}$ futher supported the second order scenario with $c(d = \mathbf{3}) = \mathbf{2.10(4)}$ [93] and $c(d = \mathbf{3}) = \mathbf{2.18)6)}$ [92]. Effect of possible heterogeneity of a macromolecule was partially taken into account in [92] by assuming that entropic scaling exponents of the network may differ and introducing fit parameters to quantify such difference.

In our analysis we will be interested in the exponent c, Eq. (1.34) that governs scaling of a denaturated loop in the simplified picture of DNA unzipping considering that the macromolecule consists of chains of two different species, as shown in Fig. 1.2. The loop is formed by unbound nucleobases, let us take it to be of 'species 1' whereas the two chains $V\mathbf{1} - V\mathbf{3}$, $V\mathbf{3} - V\mathbf{1}$ consist of bound nucleobases, 'species 2'. In order to evaluate entropy of a single loop in a network in Fig. 1.2, we will

make use of scaling picture for copolymer networks, as suggested in [97, 98]. In particular, the partition function (number of configurations) of a copolymer nework $\mathcal{G}$ made of F_1 chains of species 1 and F_2 chains of species 2 scales with a mean size of a single polymer chain R as [97]:

$$\mathcal{Z}_{\mathcal{G}} \sim R^{\eta_{\mathcal{G}} - F_1\eta_{2,0} - F_2\eta_{0,2}}, \tag{1.35}$$

with

$$\eta_{\mathcal{G}} = -d\mathcal{L} + \sum_{f_1+f_2\geq 1} n_{f_1,f_2}\eta_{f_1,f_2}, \tag{1.36}$$

where d is space dimension, $\mathcal{L}$ is the number of loops in the network, n_{f_1,f_2} is number of vertices where f_1 chains of species 1 and f_2 chains of species 2 meet. Exponents $\eta_{f_1f_2}$ constitute a family of copolymer star exponents. Each of them describes scaling of a copolymer star of corresponding functionality, made of f_1 chains of species 1 and f_2 chains of species 2. Being universal, they depend only on space dimension d and the number of chains f_1, f_2, as well as three different types of fixed points (FPs) that govern scaling behavior [100]. These FPs correspond to the cases when (i) both species 1 and 2 are mutually interacting SAWs, the so-called symmetric fixed point S, (ii) species 1 and 2 are mutually interacting SAWs and RWs, correspondingly, unsymmetric fixed point U and (iii) both species 1 and 2 are RWs, however there is mutual avoidance interaction between species 1 and 2, fixed point G. By case (i) one recovers homogeneous polymer network, whereas cases (ii) and (iii) present non-trivial examples of copolymer scaling. Therefore the scaling properties of a heterogeneous polymer network made of interacting SAWs and RWs can be reformulated in terms scaling exponents of co-polymer stars made of two interacting sets of SAWs ($\eta^S_{f_1f_2}$), of RWs ($\eta^G_{f_1f_2}$) or of a set of SAWs that interacts with RWs ($\eta^U_{f_1f_2}$) [99]. Field-theoretical renormalization group calculations of the above copolymer star exponents resulted in $\varepsilon = 4 - d$ expansions which have been obtained successively within ε^3 [97] and ε^4 [86] accuracy.

Conclusions

In this chapter we discussed the principle of universality and scaling in critical phenomena. Among the cases that we consider in this thesis there is FSS above the upper critical dimension, where boundary conditions are a crucial choice. For example, for periodic boundary conditions, a new Q-FSS is observed at both critical temperature of the infinte system, and pseudocritical temperature of corresponding lattice size. Q-scaling suggests that near the critical point, correlation length experiences a drastic increase, which is not linear with respect to lattice size L, but is a power law instead. The new scaling exponent $\wp$ fixes broken hyperscaling relation, and agrees with the Monte-Carlo simulations for PBC. Another phenomenon that we pay close attention in this thesis is DNA thermal denaturation in terms of Poland-Scheraga model. This is a simplified model that discards the nuances of the chemical structure of DNA in a goal to focus on the interplay between energy and entropy. While being in a bound state is better energetically, there are more available configurations, when the chains are unzipped.

In the next chapters we will consider such unresponsed issues regarding universality in abovementioned phenomena: The understanding of finite-size scaling above the upper critical dimension, particularly with free boundary conditions at the pseudocritical point, remains unclear. Chapter 2 aims to shed light on this complex aspect of scaling using the extensive simulations. However, small lattice sizes present a challenge in observing meaningful finite-size scaling due to the overwhelming influence of strong boundary effects. This issue is a focal point in our exploration in Chapter 3, where we turn to two complementary techniques to find the FSS with higher accuracy. The aim is to find the critical exponents that will hint towards Q- or G-scaling. In the meantime, scaling exponents of copolymer networks, particularly in the context of the differences between the scaling of a denaturated loop and a bound chain in DNA thermal denaturation, have not been thoroughly considered. Chapter 4 seeks to fill this gap in understanding by accounting the possible heterogeneity in the polymer network that occurs during the DNA

denaturation. Additionally, we will seek the effects of impurities and irregularities in the environment, that have not been extensively applied to the study of complex polymers in solvent in Poland-Scheraga model before.

CHAPTER 2

FINITE-SIZE SCALING OF $5D$ ISING MODEL: NUMERICAL SIMULATIONS

In this and the forthcoming chapter we consider the Ising model above the upper critical dimension. Ising model is a ϕ^4 universality class model, which means that from the Ginzburg criterion, the upper critical dimension is $d_c = 4$. Field fluctuations can be neglected above d_c, therefore the mean field approximation delivers exact results for the exponents. The Ising model Hamiltonian reads:

$$\mathcal{H} = -\frac{J}{2}\sum_{<i,j>} S_i S_j - h\sum_{i}^{N} S_i. \tag{2.1}$$

Here, spins on each of the N sites take one of two possible states $S_i = \pm 1$. J is an interaction coefficient, usally set $J = 1$, h is the external magnetic field. Below, we will only consider the nearest neighbours interactions, but it is worth mentioning the previous works on the long-range Ising model (LRIM) like Ref. [46].

While in the thermodynamic limit the scaling exponents are indeed mean-field, the finite-size scaling (FSS) shows different results [36]. While for periodic boundary conditions (PBC) the Q-scaling is valid at both critical and pseudocritical points, for free boundary conditions (FBC) two scaling regimes apparently emerge [48].

Regular FSS of the observable O is of the form [23]:

$$O(t) \sim |t|^{\rho} \longrightarrow O(L) \sim L^{-\rho/\nu}. \tag{2.2}$$

This expression is derived from the correlation length scaling $\xi(t) \sim |t|^{-\nu}$ and the belief that correlation length is limited by the physical size of the system ($\xi \sim L$).

As already mentioned in the Literature Review, based on the argument that the correlation length is not bound by the system size in the vicinity of T_c, the new scaling exponent has been introduced [36]:

$$\xi \sim L^{\wp}, \quad \wp = \max(1, d/d_c). \tag{2.3}$$

Therefore, the new picture for the FSS (hereafter called Q-FSS) emerges:

$$O(L) \sim L^{-\rho\wp/\nu}. \tag{2.4}$$

In this chapter we will perform numerical simulations to test the above picture for FBC. Again, we expect (as Lundow & Markström have actually found in Ref. [39]) G scaling for FSS results at the critical point, and Q scaling at the pseudocritical point, as was found using the bulk boundary conditions in Ref. [38]. L & M, however, did not look at the pseudocritical points so we calibrate our efforts against theirs at the critical one only. The best we can do is $L = 50$ which compares with the impressive $L = 160$ of L & M. We also follow L & M when we look at FSS of the standard observables, namely magnetisation and isothermal susceptibility.

2.1. Methods: Wolff algorithm, resampling

For high dimensions number of particles N grows exponentially with the system size L, so the computing powers reach their limits quickly, but since the analytical solutions are not available for the Ising model above $d = 2$, the most practical way of investigating the finite-size scaling of magnetic systems is computer simulations. Usually, when speaking about computer simulations one begins wit the Metropolis algorithm, in which every step of the simulation the node may be flipped with some temperature-dependent probability, if the resulting configuration has lower energy than the initial configuration. This method is the simplest, but also can be incredibly slow, especially when our system sizes reach $N = L^d = 50^5 \simeq 3 \cdot 10^8$ sites. This is why we turn our attention to cluster update algorithms. The base premise of cluster update Monte-Carlo algorithms is that at each simulation step

we construct one (or several) cluster based on same-sign neighbouring spins, and then flip all the spins in the cluster(s). Here, we will focus on the Wolff algorithm, where just one cluster is built at every simulation step [54].

This is a cluster algorithm that updates the lattice by picking a random node and adding its neighbours to the cluster if they are of the same spin sign with probability

$$p = 1 - e^{-\beta \Delta E}, \tag{2.5}$$

where ΔE is a change of internal system energy if one spin is flipped [55–58]. In this way at least one node is flipped in every simulation step and at zero temperature the whole lattice is added to the cluster. More detailed explanation of Wolff algorithm is presented in Appendix C.

After this we turn to the big data analysis tricks. Since the dataset is large, but the adjacent configurations are connected. This might be a problem for statistics. We found that starting from an ordered state of the lattice (where all spins are pointing in the same direction) we complete the thermalisation process much faster than when starting with the disordered state of the lattice (where all spins are oriented randomly).

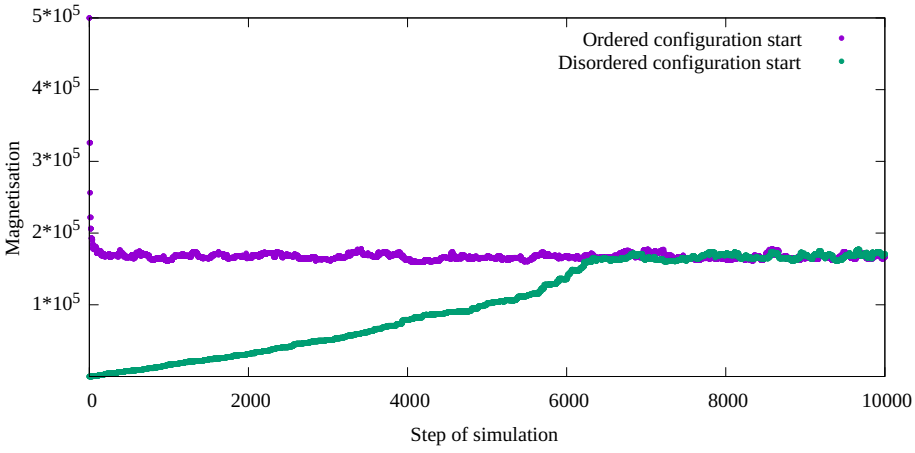

Figure 2.1. Thermalisation process in Wolff algorithm simulations of Ising model of $d = 5$ hypercubic lattice of size $L = 12$ at the same temperature $T = 8.37$. We observe that even though the mean magnetisation after thermalisation is closer to one of randomly disordered starting configuration, thermalisation itself finalises quicker when we choose the ordered starting configuration.

This effect is more stark for larger lattice sizes. The reason for this is clear — for cluster algorithms we need more adjacent spins of the same sign for the system to change quickly, and the disordered state does not have enough clusters to flip rapidly. The thermalisation comparison for lattice of size $L = 12$ is presented in the Figure 2.1. Therefore we start from ordered states throughout our simulations. For each temperature we performed 2×10^6 iterations, discarding first 10% of those as thermalisation.

Now, to calculate the mean values of observables from the set of simulations we need to make sure that each configuration is independent, and the dataset is reliable. In this work we rely on the jackknife method, which is used to estimate the variability and reduse the bias of a statistic [59]. In the jackknife method, the original dataset is systematically reduced by leaving out one observation at a time, creating multiple "subsets" or subsamples. The statistical analysis or calculation of interest is then performed on each of these subsets, resulting in a set of estimates. The errors for the magnetisation are provided in the Figure 2.2. There, we plot the jackknifing error that reads:

$$\delta m = \sqrt{\frac{n-1}{n} \sum_{i=1}^{n} (\langle m^{(i)} \rangle - \langle m \rangle)^2}, \tag{2.6}$$

where n is the number of measurements of state during the simulation, $\langle m \rangle$ is average magnetisation over all measured configurations, and $\langle m^{(i)} \rangle$ is the average of magnetisation over all but the ith configuration.

In addition to jackknifing, we will use the histogram reweighting technique to locate the exact temperature points of interest with higher accuracy [60]. The histogram reweighting technique enables one to extract data about the mean values of the observables at different temperatures and magnetic fields based on the energy distribution for the simulated lattice configurations for one temperature and magnetic field value. To this end, one considers for the Hamiltonian (2.1) probability

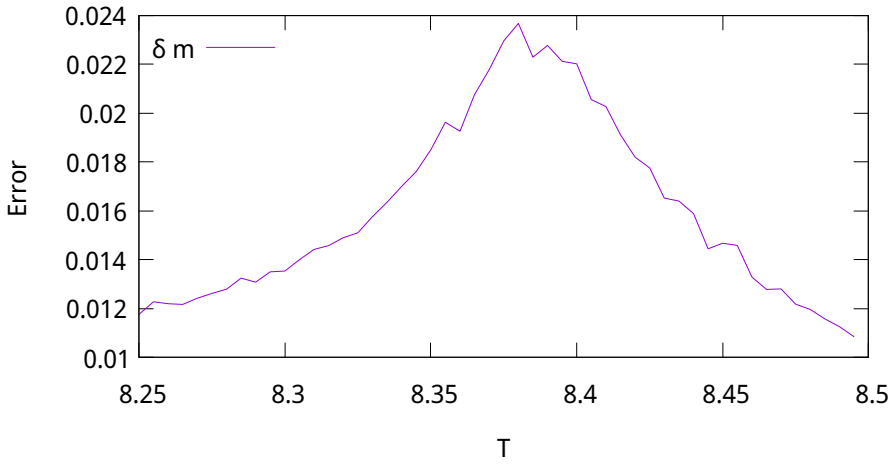

Figure 2.2. Magnetisation error, eq. 2.6 for the Wolff algorithm simulations of the Ising model for size $L = 12$ with jackknifing. Notice that the errors are larger near a pseudocritical point $T_L \simeq 8.38$.

distribution of $E = \sum s_i s_j$ and $M = \sum_i s_i$ in point $(\beta J, h)$:

$$P_{\beta,h}(E, M) = \frac{N(E, M)e^{\beta E + hM}}{z(\beta, h)}, \tag{2.7}$$

where $N(E, M)$ is number of configurations at point (E, M).

$$z(\beta, h) = \sum_{E,M} N(E, M)e^{\beta E + hM}. \tag{2.8}$$

Then an estimate probability distribution for different set of parameters (β', h') is

$$P_{\beta',h'}(E, M) = \frac{P_{\beta,h}(E, M)e^{(\beta'-\beta)E+(h'-h)M}}{\sum_{E,M} P_{\beta,h}(E, M)e^{(\beta'-\beta)E+(h'-h)M}}. \tag{2.9}$$

Here the denominator is an estimate for the partition function. As β' and h' are continuous, any functions of interest $f(E, M)$ can be calculated as continuous in those parameters:

$$\langle f(E, M)\rangle_{\beta',h'} = \sum_{E,M} f(E, M)P_{\beta',h'}(E, M). \tag{2.10}$$

In Refs. [39, 52, 53], authors conducted large-scale simulations of the $d = 5$ Ising model with FBCs . The magnetization at T_c, computed using space averaging over all sites, was clearly supportive of $m_L(T_c) \sim L^{-1.5}$. (We note that this result

was not determined through a free FSS fit to β/ν and instead expected values were imposed.) Table 1.2 in Chapter 1 suggests this is indicative of Gaussian (rather than Landau) FSS: $L^{-\beta/\nu} = L^{-3/2}$.

Simulations from Ref.[38] had previously yielded different results for the same quantity: $m_L(T_c) \sim L^{-1.7}$. This result doesn't support any of the theoretical suggestions of Table 1.2. Ref.[38] also looked at the pseudocritical point and found $m_L(T_L) \sim L^{-1.49}$. Contrary to the theoretical prediction, this aligns with G-scaling. At the time we suspected that these results — not supportive of any theory — were a product of the lattices used being not genuinely representative of five dimensions. In particular, sites at the lattice boundaries do not have the same number of neighbours as sites in the interior of the lattice. So, in Ref.[38], the authors took a step to minimize the role of lower-dimensional sub-manifolds in FBC systems. They computed the "core" magnetization, averaging only over the central $(L/2)^d$ sites. For the critical point, this yielded results of $m_L^{\text{core}}(T_c) \sim L^{-1.57}$, possibly in line with G-scaling at $d = 5$. For the pseudocritical point, the result was $m_L^{\text{core}}(T_L) \sim L^{-1.27}$, potentially aligned with Q-scaling.

There is a clear discrepancy between L & M results in Refs. [39, 52] at T_c and those of authors in [38] when all sites are used to perform the space average. The agreement is much better when only core sites are taken into account in the space average. This suggests that the previous results of Ref. [38] are strongly affected by crossovers due to the boundaries effects, while numerics in Refs. [39, 52] are more reliable because of the huge sizes reached.

Here we provide numerical simulations of the five-dimensional Ising model with free boundary conditions. We measure and analyse the scaling of magnetisation, isothermal susceptibility, both constituting a so-called magnetic sector (since they are obtained from the derivative of free energy over magnetic field), energy and heat capacity, thermal sector (since they are obtained from the derivative of

free energy over temperature), as:

$$m_L = L^{-d}\left\langle \sum_i^N s_i \right\rangle, \tag{2.11}$$

$$\chi_L = L^{-d}(\langle M^2 \rangle - \langle M \rangle^2), \tag{2.12}$$

$$e_L = L^{-d}\left\langle \sum_{<i,j>} s_i s_j \right\rangle, \tag{2.13}$$

$$c_L = \beta L^{-d}(\langle E^2 \rangle - \langle E \rangle^2). \tag{2.14}$$

In addition to these regular variables, we also will consider the FSS of the mixed free energy derivative, the magnetocaloric coefficient m_T that is often measured at the experiments. It reads:

$$m_T(L) = L^{-d}(\langle EM \rangle - \langle E \rangle \langle M \rangle). \tag{2.15}$$

In order to investigate the critical behaviour of the finite size $d = 5$ Ising model we performed Monte Carlo simulations using the Wolff algorithm. This is a cluster algorithm that updates the lattice by picking a random node and adding its neighbours to the cluster if they are of the same spin sign with probability $p = 1 - e^{-\beta \Delta E}$, where ΔE is a change of internal system energy if one spin is flipped [55–58]. In this way at least one node is flipped in every simulation step and at zero temperature the whole lattice is added to the cluster.

We set boundary conditions to be free, meaning that the sites on the edges of the lattice do not have a neighbour in one of the d directions. Instead they form a $(d-1)$-dimensional manifold.

2.2. Determination of pseudocritical temperature T_L

Besides at the critical temperature itself, we are interested in FSS at the pseudocritical temperature. This is shifted away from the actual critical point of the infinite system and the smaller the system size the more pronounced this effect is. Actually, for small lattices the system at the critical temperature is effectively

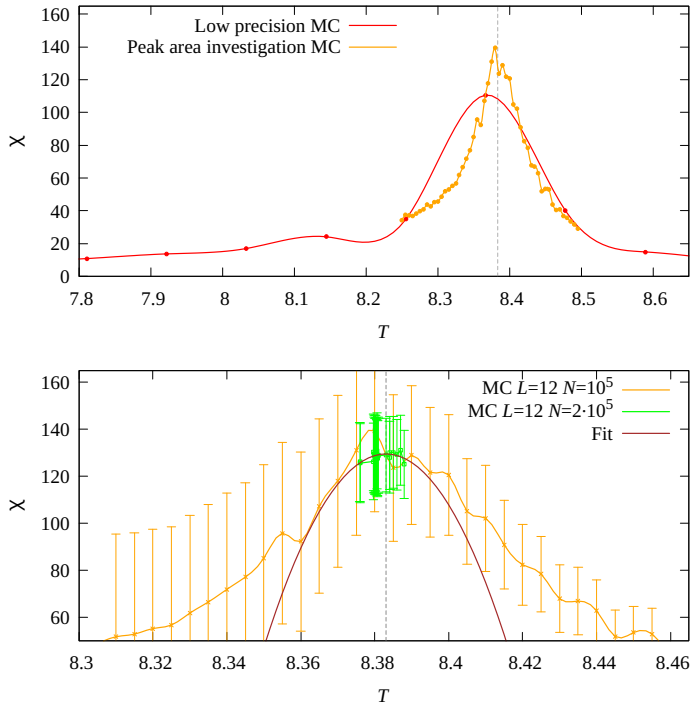

Figure 2.3. The process of estimating the pseudocritical temperature from the susceptibility for the $d = 5$ Ising model on a lattice of size $L = 12$. First (top) we scan greater interval of temperatures with relatively low precision. Then we perform this same procedure in more detail for an interval where the susceptibility is visibly higher. Finally (bottom) we simulate an interval of temperatures, where it seems that the peak should be located. with higher precision. We fit a polynomial through the highest points. This allows us to select an estimate for the pseudocritical point T_L (dashed vertical line). We perform final simulations at the resulting peak.

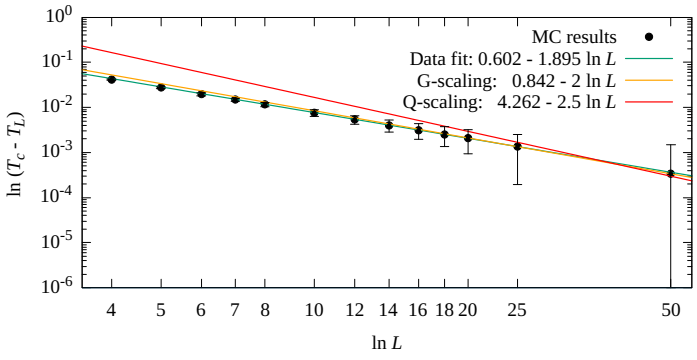

Figure 2.4. FSS data of the pseudocritical temperature (blue line). For the G-scaling predicted by theory for FBCs, t_L scales as L^{-2} (orange line). This is in marked contrast to $L^{-2.5}$ which comes from Q-scaling (red line) and is relevant for PBCs. Our fit gives $L^{-1.90\pm0.03}$, which is G-scaling within the error bars.

disordered. Our favoured determinant of the pseudocritical point is the susceptibility. The algorithm to locate the pseudocritical temperature T_L is illustrated in Fig. 2.3. The top part of the figure illustrates the rough values of the susceptibility for a wide range of temperature values. A peak is clearly visible and our task is to identify its location T_L with some precision. To identity this pseudocritical peak, then, we first scan a broad range of temperatures with low-precision simulations to find an approximate region that contains it for each lattice size. After that, one runs a set of high precision simulations narrowed around this temperature. The outcome is illustrated in the lower figure. Because of the fluctuations, the peak is difficult to identify manually. So we use a quadratic fit in an attempt to smoothen the curve so that a local maximum can be more readily identified. At this point, which we identify as T_L, we perform another high precision simulation and use the data from it for further analysis.

To investigate FSS of the pseudocritical point, we first require an estimate of the critical point itself. We use that ($T_c = 8.7784752$) coming from L & M (2014) [39]. This is the estimate of the critical point that we use throughout the paper as we also track the behaviour of various observables at the infinite system critical point T_c.

In Fig. 2.4 we present the FSS of the pseudocritical temperatures $t_L = T_c - T_L$. Mean-field or Gaussian FSS would predict $t_L \sim L^{-1/\nu} = L^{-2}$, where ν is the correlation-lenght critical exponent. In contrast, Q-scaling predicts $t_L \sim L^{-\mathfrak{9}/\nu} = L^{-2\mathfrak{9}} = L^{-5/2}$. The latter was proven for the PBC case, while the former was shown for FBCs in [61]. We observe $t_L \sim L^{-1.90\pm0.03}$ when we fit over the full range of data from $L = 4$ to $L = 50$. This value is much closer to the theoretically expected G-scaling, $t_L \sim L^{-2}$, and further away from the Q-scaling prediction $t_L \sim L^{-2.5}$. It is consistent with observations in the literature whereby shifting is bigger for FBCs than it is for PBCs. This result among other quantities results from this chapter is recorded in Table 2.1. As in the case of pseudocritical point, the table invites comparisons with available theoretical predictions.

2.3. Critical behaviour in magnetic sector

2.3.1. Finite-size scaling of the mean magnetisation m

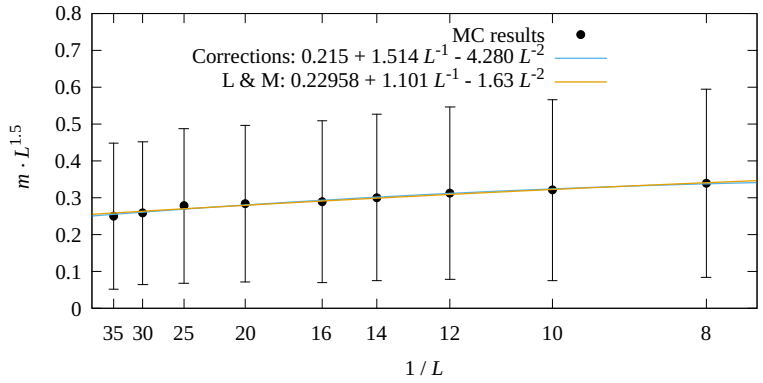

Figure 2.5. Leading behaviour and first corrections to the FSS for the magnetisation at the critical temperature T_c. We plot $m \cdot L^{1.5}$ against $1/L$.

Criticality: We next analyse the FSS of mean magnetisation m. Very detailed estimates for the FSS of the mean magnetisation at T_c were obtained by L & M in Ref. [39] with leading behaviours and corrections to scaling given by:

$$m_L(T_c) = 0.230L^{-3/2} + 1.101L^{-5/2} - 1.63L^{-7/2}. \tag{2.16}$$

We performed a similar analysis to compare our numerics with those of L & M. Although extracted using far smaller lattice sizes, our numerical results deliver similar outcomes:

$$m_L(T_c) = 0.215L^{-3/2} + 1.514L^{-5/2} - 4.280L^{-7/2}. \tag{2.17}$$

In Fig. 2.5 we plot corrections to scaling to illustrate the convincing nature of this fit. This suggests that our results are similar to those those of L & M and $m \sim L^{-3/2}$ as the Gaussian theory predicts.

Pseudocriticality: In Fig. 2.6 we show results of the simulations for the mean magnetisation m at the pseudocritical temperatures T_L for different values of L ranging from $L = 4$ to 50. As was previously suggested, we expect Q-scaling

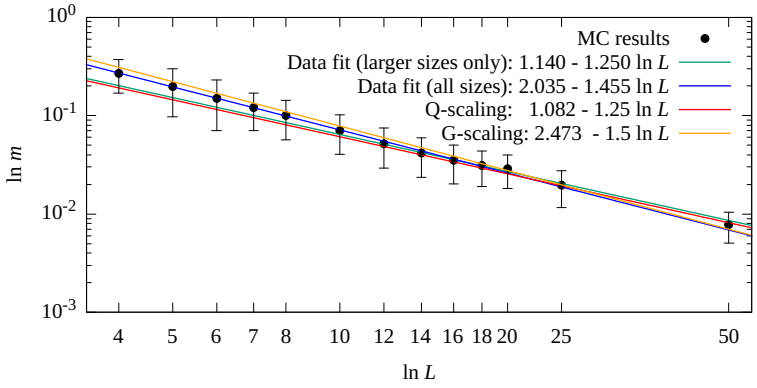

Figure 2.6. Scaling of magnetisation at the pseudocritical temperature T_L. The theoretical values are presented as orange (G-scaling), and red (Q-scaling) lines. We see that we can discard a few smallest lattice sizes to reach the expected scaling behaviour.

at T_L. At T_L we obtained $m \sim L^{-1.46\pm0.02}$ when the power law fit is performed over all lattice sizes. This is much closer to L & M's G-scaling $m \sim L^{-1.5}$ than to the theoretically expected Q-scaling $m \sim L^{-1.25}$. As explained in Ref. [38], our contention is that the boundary lattice sites in FBCs may be responsible for this discrepancy between the expectation and observed FSS; as the boundary effects are too strong to show a properly five-dimensional criticality. To illustrate this we discard the lowest sizes ($L = 4..12$) from the fit, and indeed the FSS reaches the scaling $m \sim L^{-1.25\pm0.09}$ (green line in Fig. 2.8, top). This suggests that for large enough lattice sizes (and discarding small lattices) the magnetisation for FBCs at pseudocriticality indeed falls within the Q-scaling regime.

2.3.2. Finite-size scaling of isothermal susceptibility χ

Criticality: Again, we first compare the results of our simulations at criticality with those coming from L & M in Ref. [39]. They assume a quadratic dependency of susceptibility on L and a fit delivers

$$\chi_L(T_c) = 0.817L^2 + 0.083L. \tag{2.18}$$

Our equivalent (for far smaller lattices) is

$$\chi_L(T_c) = 0.285L^2 + 0.030L. \tag{2.19}$$

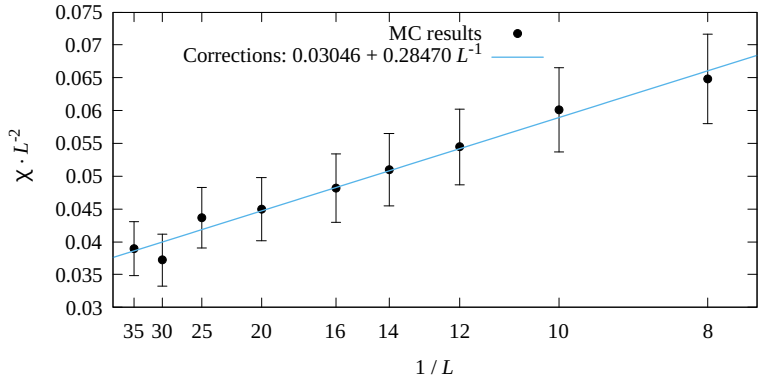

Figure 2.7. Leading behaviour and first corrections to the FSS for the susceptibility at the critical temperature T_c. For the susceptibility we plot $\chi \cdot L^{-2}$ against $1/L$.

The conclusion of Ref. [39] was in favour of standard FSS scaling for the isothermal susceptibility at the critical temperature $\chi_L(T_c) \sim L^2$, and we can see that, at first sight, that would seem to be the case.

However, as Table 2.1 illustrates, this could be standard MF scaling or G scaling. Our contention is that it is G and falls withing the theory of Q.

Pseudocriticality: Results for the FSS of isothermal susceptibility at the pseudocritical point are shown in Fig. 2.8. At T_L we obtained $\chi \sim L^{1.95\pm0.02}$ using all simulated lattices, in apparent agreement with G-scaling ($\chi \sim L^2$ as opposed to $\chi \sim L^{2.5}$ for Q-scaling). In our fit, data for $L = 4$ weights as much as $L = 50$, say. But clearly $L = 4$ is not genuinely representative of a five dimensional system. The fact that these data lie on such a line calls into suspicion $L = 50$ data as well. Thus we expect that the lattice sizes we reach in our simulations are possibly too small to converge to Q-scaling for susceptibility. Removing a few smaller sizes does not do a trick as it did for the magnetisation.

2.4. Critical behaviour in thermal sector

For thermal sector (internal energy and other free energy derivatives over temperature t) we observe some differences. Fluctuations are too big to consistently get accurate function behaviour, the pseudocritical temperature is difficult to find

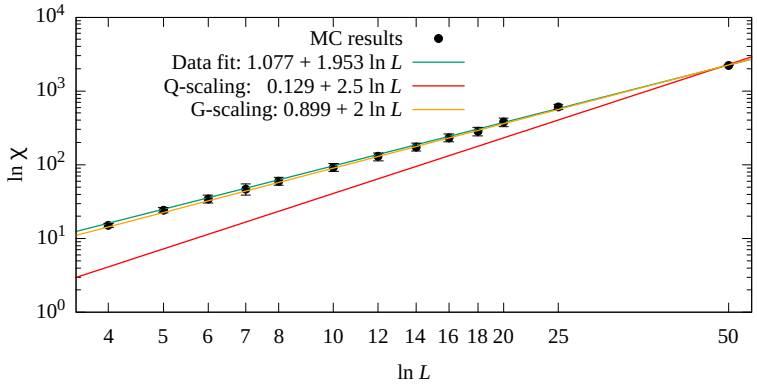

Figure 2.8. Scaling of the isothermal susceptibility at the pseudocritical temperature T_L. The theoretical values are presented as an orange line (G-scaling), and a red line (Q-scaling). While for the magnetisation we were able to discard a few smallest lattice sizes to reach the expected scaling behaviour, for susceptibility it is not the case and the lattice sizes are still to small to show Q-scaling.

because for heat capacity we are looking for the point of vanishing istead of the peak, thus Figure (2.9) is an attempt to find it for inverse heat capacity. Then also, the pseudocritical temperature derived from the magnetic susceptibility might not be the actual point of pseudocriticality for thermal sector. In addition to that, previous studies of thermal sector values at FBC, for example by L&M, show exotic behaviour that does not coincide with theory.

2.4.1. Finite-size scaling of internal energy e

Energy FSS gives in the vicinity of critical point:

$$e \sim L^{(\alpha-1)/\nu}. \tag{2.20}$$

Though, the scaling window of energy might be too narrow to observe Q- or even G-scaling at different temperatures.

Criticality: Simulated at $T_c = 8.778475$ we expect $e \sim L^{2-d}$ from G scaling ($e \sim L^{-3}$ for $d = 5$), but Lundow and Markström [39] got $e \sim L^{-1}$ as the leading order and the correction order of $L^{-3/2}$. Figure (2.10) shows results of our simulations: critical temperature T_c for our lattice sizes is effectively just a high

	t_L	m	χ	e	c	m_T
MFT	L^{-2}	L^{-1}	L^{2}	L^{-2}	$const$	L^{1}
GFP	L^{-2}	$L^{-1.5}$	L^{2}	L^{-3}	L^{-1}	$L^{0.5}$
Q-FSS	$L^{-2.5}$	$L^{-1.25}$	$L^{2.5}$	$L^{-2.5}$	$const$	$L^{1.25}$
[39] T_c		$L^{-1.5}$	L^{2}	L^{-1}	$L^{-1/3}$	
Our results T_L	$L^{-1.90\pm0.03}$	$L^{-\mathbf{1.25}\pm0.09}$	$L^{1.95\pm0.02}$	$L^{-1\pm0.1}$	$L^{-1/3\pm0.05}$	$L^{0.88\pm0.1}$
Our results T_c		$L^{-1.5}$	L^{2}	L^{-1}		

Table 2.1. FSS of the $d = 5$ Ising model at the critical point and at the pseudocritical point. In the upper section we present the theoretical values for the scaling laws, as well as the example from L & M. In the bottom section we present our results.

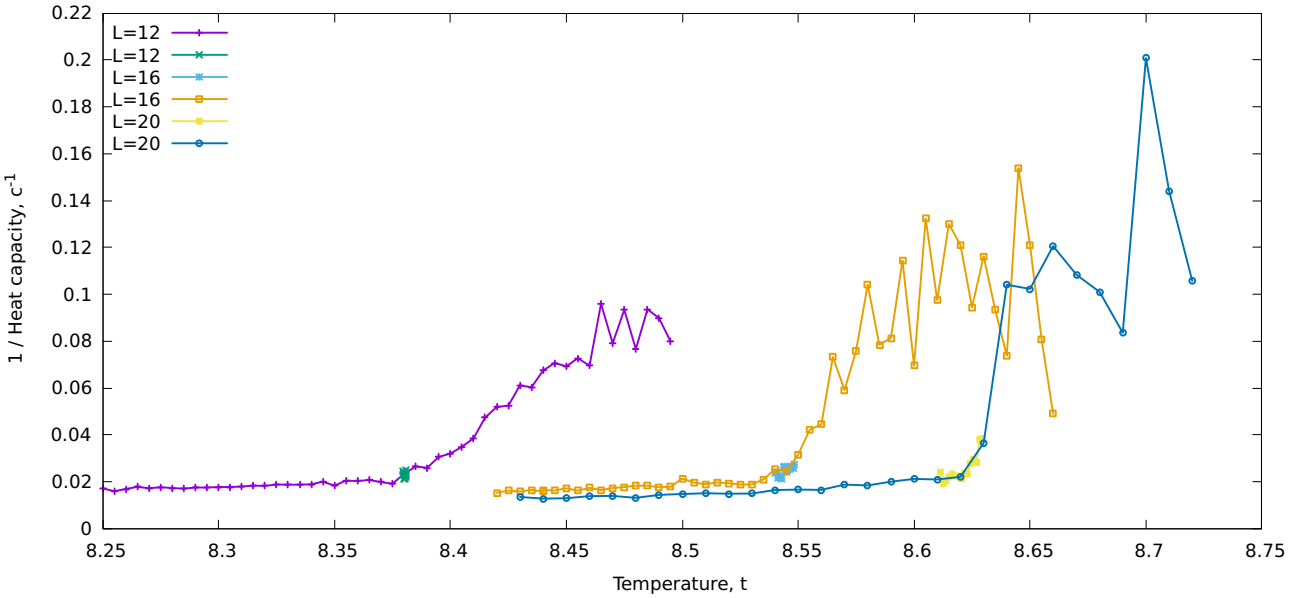

Figure 2.9. If one was to find the point at which the heat capacity reaches 0, it is reasonable to look at the maximum of inverted heat capacity instead. Although for our simulation results it is not apparent. The small sections of different colour for each lattice size include points where the pseudocritical temperature was investigated for susceptibility.

temperature point, since steps in both direction of it give little to no changes in scaling, this might also explain the deviant FSS of the energy.

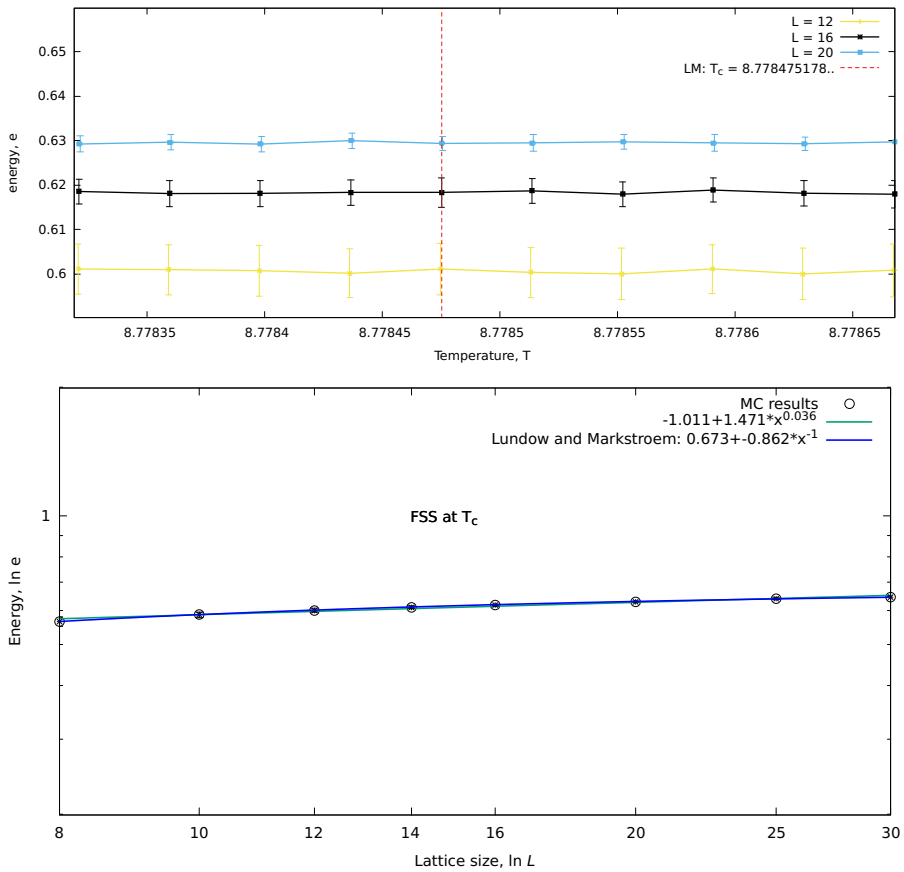

Figure 2.10. Energy in the vicinity of critical temperature (top) and the finite-size scaling (bottom) in comparison to Ref. [39].

Pseudocriticality: We expect $e \sim L^{2\varrho-d}$ from Q-scaling ($e \sim L^{-2.5}$ for $d = 5$). Energy around the psuocritical point T_L and its FSS are presented on Figure (2.11).

Our result is roughly $e \sim const$, far from any theoretical explanation.

2.4.2. Finite-size scaling of heat capacity c

Heat capacity FSS is expected to be:

$$c \sim L^{\alpha/\nu}. \tag{2.21}$$

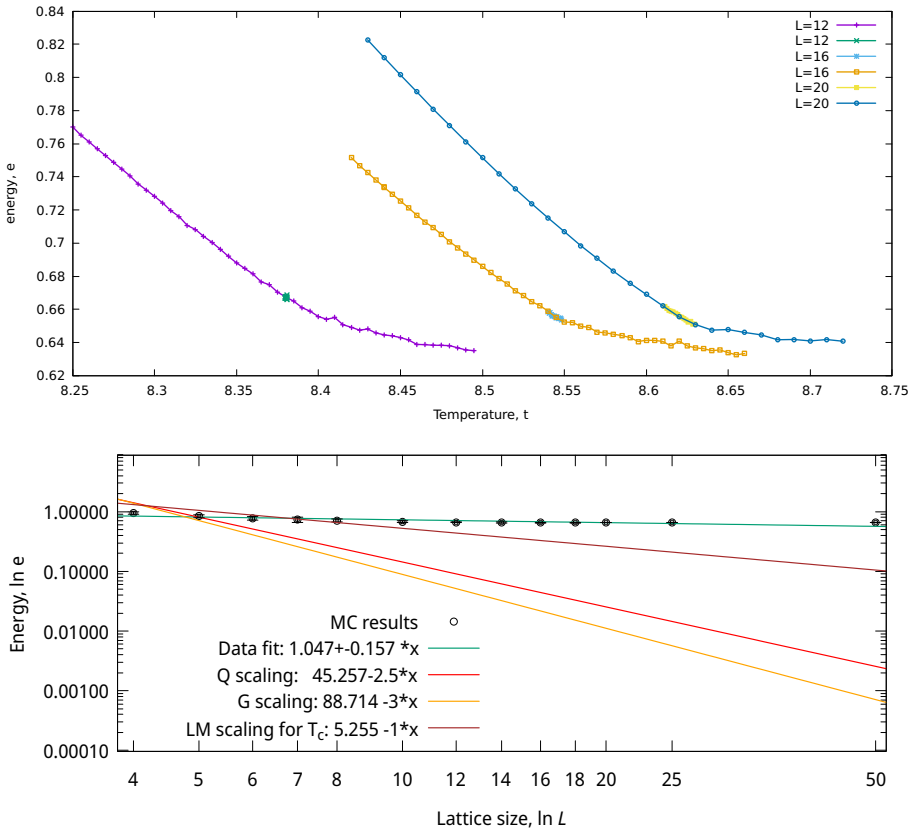

Figure 2.11. Energy in the vicinity of the pseudocritical temperature (top) and the finite-size scaling (bottom). The small sections of different colour for each lattice size at the top graph include points where the pseudocritical temperature was investigated.

Criticality: We expect $c \sim L^{4-d}$ from G scaling ($c \sim L^{-1}$ for $d = 5$), but Lundow and Markström got $c \sim L^{-1/3}$ as the leading order. Figure(2.12) is unclear, but coincides with findings of L&M.

Pseudocriticality: We expect $c \sim L^{4\varrho-d}$ from Q scaling ($c \sim const$ for 5D). Figure(2.13): We got: $c \sim L^{-1/2}$, which has no matches in the theory, but coincides within the error bars with LM's $-1/3$ (done for t_c) at these lattice sizes.

2.4.3. Magnetocaloric coefficient

$$m_T \sim L^{(1-\beta)/\nu} \tag{2.22}$$

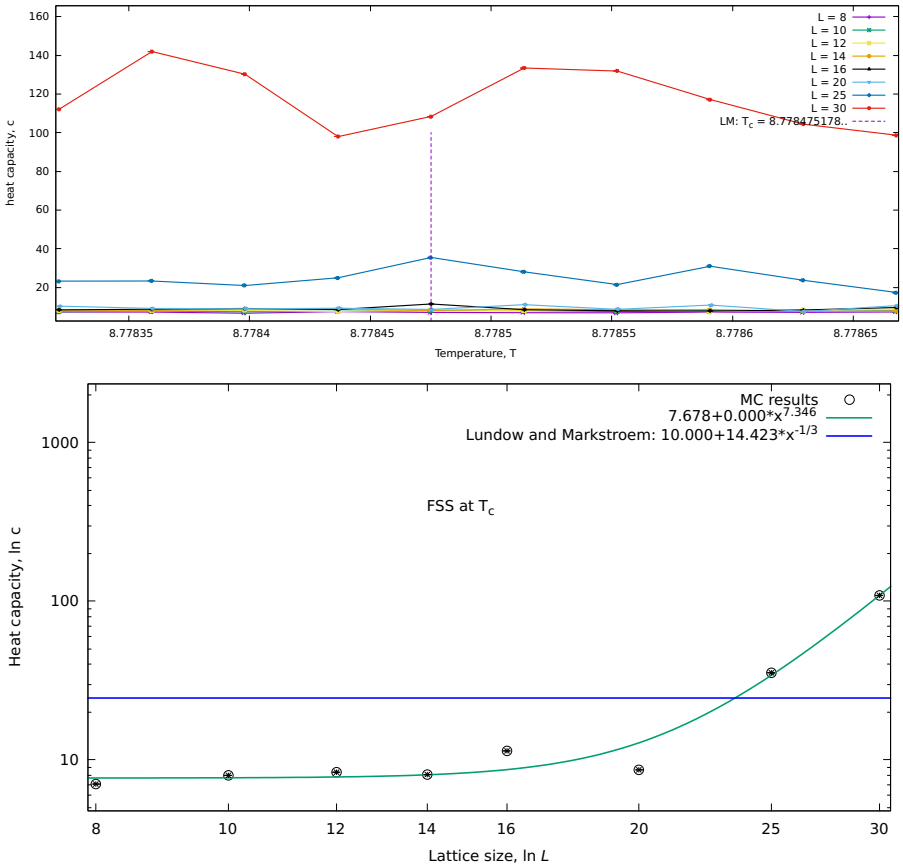

Figure 2.12. Heat capacity in the vicinity of critical temperature (top) and the finite-size scaling (bottom) in comparison to Ref. [39] .

Since we don't know yet what exactly to expect from the scaling of magnetocaloric coefficient, let us look on Figure (2.14): We got: $\mathcal{K}_L(T_c) \sim L^{-1.01}$ for FSS at the T_c, and $\mathcal{K}_L(T_L) \sim L^{0.558}$ for FSS at T_L.

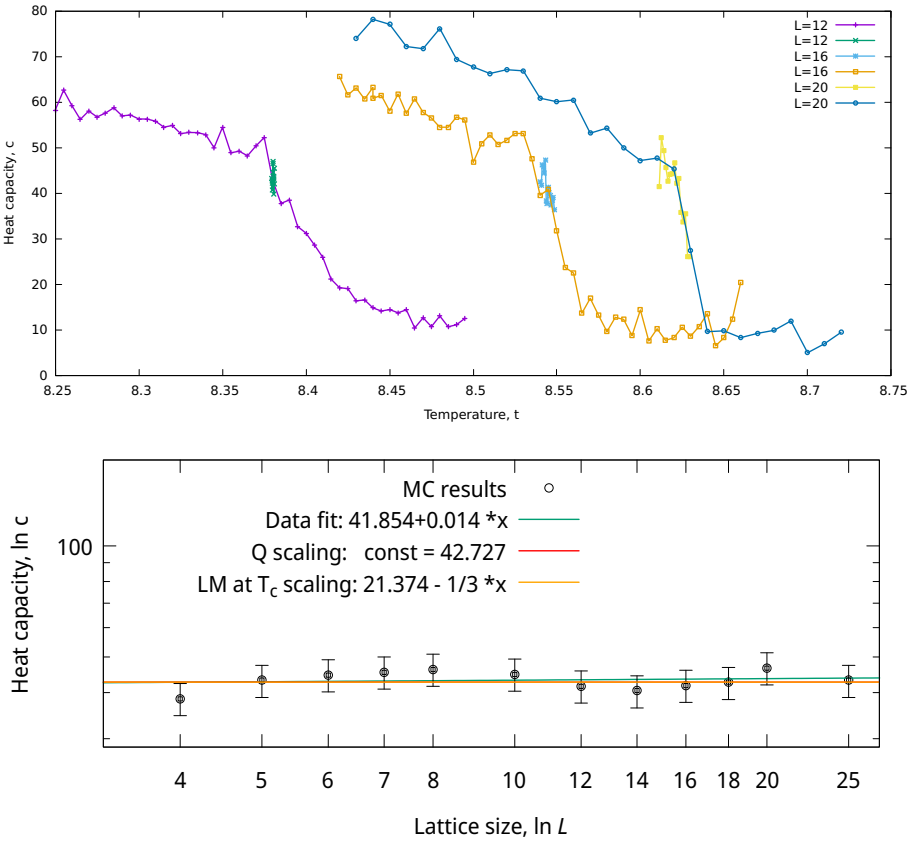

Figure 2.13. Heat capacity in the vicinity of the pseudocritical temperature (top) and the finite-size scaling (bottom) in comparison to [39] done at T_c. The small sections of different colour for each lattice size at the top graph include points where the pseudocritical temperature was found for susceptibility.

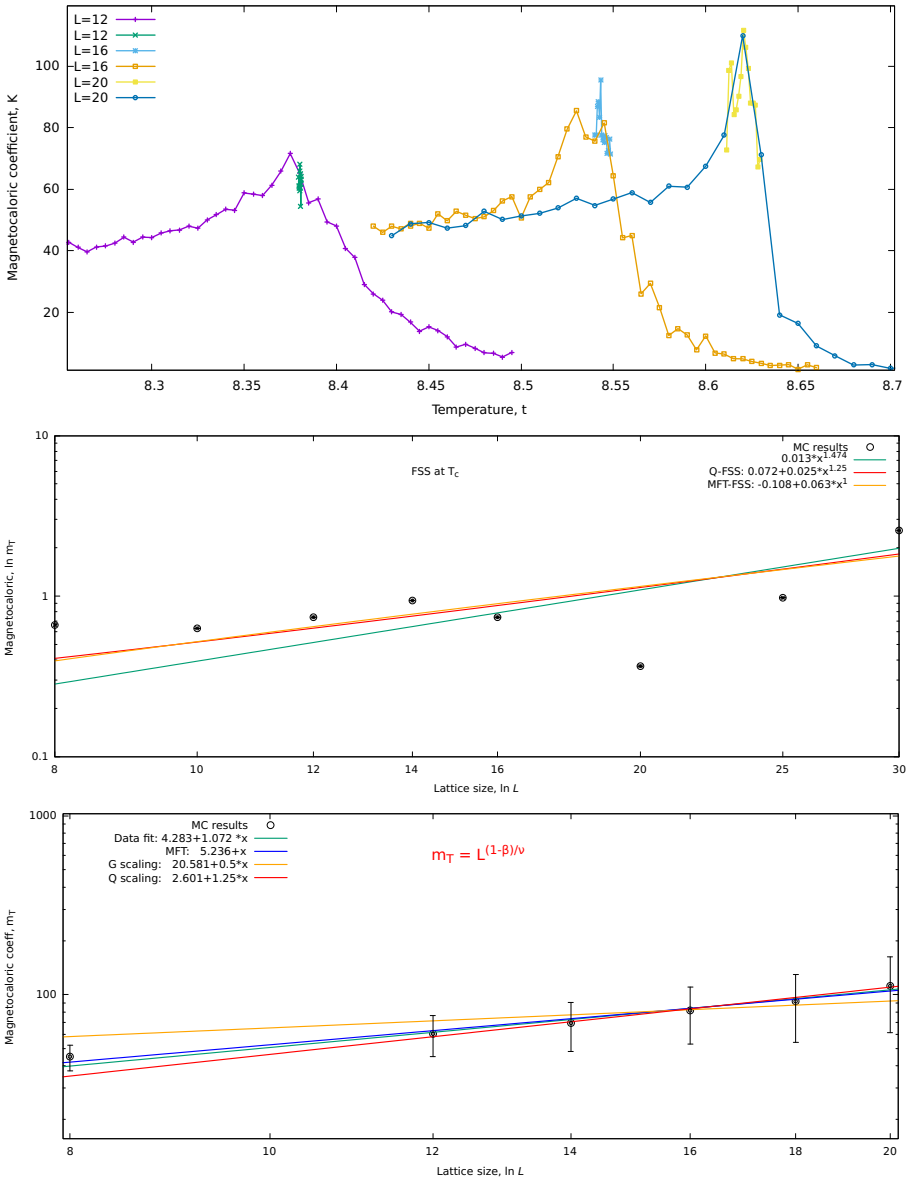

Figure 2.14. Magnetocaloric coefficient in the vicinity of pseudocritical temperature (top), its FSS at the T_c (middle), and its FSS at the T_L (bottom). The small sections of different colour for each lattice size include points where the pseudocritical temperature was found for susceptibility.

2.5. Conclusions

In this chapter we used Wolff algorithm to simulate $d = 5$ Ising model with free boundary conditions to get a scaling picture of the quantitities like magnetisation, isothermal susceptibility, energy, and heat capacity at zero magnetic field and critical and pseudocritical temperatures. In studying the Ising model above its critical dimension with numerical simulations, we focused on the finite-size scaling. We made a few conclusions:

Firstly, when the lattice size is small, the impact of the edges becomes too significant, making it difficult to see the expected changes at the pseudocritical temperature T_L. Essentially, the smaller the system, the more these edge effects overshadow the scaling picture, and the larger dimensionality we consider, the smaller lattice sizes are possible to compute.

Secondly, we noticed that for magnetisation, excluding the smallest lattice sizes helped seeing past the boundary efects and observe the scaling behaviour more accurately. However, for susceptibility, all our lattice sizes can only be considered "small". This means that the improvement in understanding magnetisation scaling doesn't apply universally to all properties. Though, magnetic sector, in general showed consistent results proving G-scaling at the critical temperature T_c, and Q-scaling for magnetisation, unlike the thermal sector, where the FSS could not be fit into any of the scaling regimes.

We conclude that figuring out the finite-size scaling above upper critical dimension d_c demands additional methodologies. The challenges posed by lattice sizes and the different behaviors of properties make it clear that we need more methods to fully understand how things change in this situation. As we keep exploring, using additional techniques will be crucial in untangling the complexities of the Ising model beyond its critical dimension. This will be the subject of the next Chapter.

CHAPTER 3

FINITE-SIZE SCALING OF $5D$ ISING MODEL: FOURIER MODES AND LEE-YANG ZEROS ANALYSIS

Since the direct look at the finite-size scaling above the upper critical dimension at free boundary conditions in previous Chapter is hindered by the surface effects, that are too large at our relatively small lattice sizes, other ways to improve the scaling accuracy can be applied. Previously mentioned Lundow and Markström had an access to a much greater computational facilities, thus performing the simulations for lattice sizes up to $L = 160$ in $d = 5$. Walter et al. in Ref. [38] made a trick of completely removing the boundary sites, so-called bulk boundary conditions. Both these methods required additional computing resources that were not available to us in this work, therefore in this Chapter we will turn to two other techniques that can help improve the accuracy of the FSS above the d_c. First, we will look at Fourier modes and partition function zeros (which L & M did not look at). It was shown earlier in Ref. [40] that only a part of Fourier modes contributes to the scaling, so discarding the rest might make the numeric scaling picture more accurate. Then, we will apply partition function zeros analysis. Zeros lie in the complex plane of parameters entering the partition function (i.e., external field or temperature). The notion was developed by Lee and Yang [49, 50], who studied the partition function as a polynomial in a parameter related to the external magnetic field. Following a similar idea, Fisher suggested the study of the zeros for the temperature complex plane. [20]. These ideas have been termed a "fundamental theory of phase transitions" [51].

3.1. Scaling of magnetisation Fourier modes

To start with the magnetisation Fourier modes let us show the one-dimensional case for simplicity first. For PBC we define:

$$S_n = L^{-1} \sum_{\hat{k}=0}^{L-1} \tilde{S}_k e^{-ikn}, \tag{3.1}$$

$$\tilde{S}_k = \sum_{n=0}^{L-1} S_n e^{ikn}, \tag{3.2}$$

where $k = 2\pi\hat{k}/L$, and $\hat{k} = 0, 1, \ldots, L-1$. To find the modes that contribute to the configurational magnetisation we consider:

$$M = \sum_{n=0}^{L-1} S_n \tag{3.3}$$

$$= L^{-1} \sum_{n=0}^{L-1} \sum_{\hat{k}=0}^{L-1} \tilde{S}_k e^{-ikn} = L^{-1} \sum_{\hat{k}=0}^{L-1} \tilde{S}_k \sum_{n=0}^{L-1} e^{-ikn} \tag{3.4}$$

$$= L^{-1} \sum_{\hat{k}=0}^{L-1} \tilde{S}_k \delta_{\hat{k},0} = \tilde{S}_0. \tag{3.5}$$

So the magnetisation at PBC is just the zero Fourier mode, and no non-zero modes contribute to M. Because magnetisation is a Q-FSS quantity above d_c, we refer to the zero mode as a Q-mode, and to all other modes as G-modes.

In a system with FBCs the Fourier modes are sine waves:

$$S_n = \frac{1}{L+1} \sum_{\hat{k}=1}^{L} \tilde{S}_k \sin \frac{\pi n \hat{k}}{L+1}, \tag{3.6}$$

$$\tilde{S}_k = \sum_{n=1}^{L} S_n \sin \frac{\pi n \hat{k}}{L+1}. \tag{3.7}$$

Notice, that we also imagine additional sites to the left and right labeled $n = 0$ and $n = L+1$, respectively, and set them to always be zero to satisfy the Dirichlet boundary conditions for the Fourier transform. This way the FBC are implemented because the S_1 and S_L are free, even though $S_0 = S_{L+1} = 0$. As for the PBC we

present magnetisation from the momentum modes:

$$M = \sum_{n=1}^{L} S_n \tag{3.8}$$

$$= \frac{1}{L+1} \sum_{n=1}^{L} \sum_{\hat{k}=1}^{L} \tilde{S}_k \sin \frac{\pi n \hat{k}}{L+1} = \frac{1}{L+1} \sum_{\hat{k}=1}^{L} \tilde{S}_k \sum_{n=1}^{L} \sin \frac{\pi n \hat{k}}{L+1} \tag{3.9}$$

$$= \frac{1}{L+1} \sum_{\hat{k}=1}^{L} \tilde{S}_k W_L(\hat{k}), \tag{3.10}$$

where mode weights

$$W_L(\hat{k}) = \sum_{n=1}^{L} \sin \frac{\pi n \hat{k}}{L+1}. \tag{3.11}$$

This sum can be rewritten as $\cos \frac{\pi(\hat{k}-1)}{2} \left(\sin \frac{\pi \hat{k}}{2} \cot \frac{\pi \hat{k}}{2(L+1)} - \cos \frac{\pi \hat{k}}{2} \right)$. If $\hat{k}$ is even, W_L is zero. If $\hat{k}$ is odd, the last term in parentheses vanishes and we find

$$M(k_{odd}) = \frac{1}{L+1} \sum_{\hat{k}_{odd}} \tilde{S}_k \cot \frac{\pi \hat{k}}{2(L+1)}. \tag{3.12}$$

Thus, for FBC all odd modes are Q-modes, and all even modes are G-modes. This also means that the contribution to magnetisation is stronger for lower modes, with $\hat{k} = 1$ as the strongest.

Now for the d-dimensional case the modes take the form

$$\psi_{\mathbf{k}} = \sqrt{2/L} \prod_{\alpha=1}^{d} \sin k_\alpha x_\alpha, \tag{3.13}$$

with wave vectors $k_\alpha = n_\alpha \pi/(L+1)$, $n_\alpha = 0, 1, \ldots, L$. Local quantities, like Ising spin $s_{\mathbf{x}_i}$, now read as

$$s_{\mathbf{x}_i} = \sum_{\mathbf{k}} \tilde{s}_{\mathbf{k}} \psi_{\mathbf{k}}. \tag{3.14}$$

However, in order to break the symmetry of the Ising model we should consider profile $\mu(\mathbf{x})$ of the spin $s_{\mathbf{x}}$ instead:

$$\mu(\mathbf{x}) = \left| \langle S(\mathbf{x}) \mathrm{sign}(M) \rangle_T \right|. \tag{3.15}$$

Here $\langle \dots \rangle_T$ denotes temperature average. Now Fourier transform and its inverse counterpart are:

$$\mu(\mathbf{x}) = \frac{1}{(L+1)^d} \sum_k \mu(\mathbf{k}) \prod_{\alpha=1}^{d} \sin(k_\alpha \cdot x_\alpha), \tag{3.16}$$

$$\mu(\mathbf{k}) = \sum_{x=1}^{N} \mu(\mathbf{x}) \prod_{\alpha=1}^{d} \sin(k_\alpha \cdot x_\alpha), \tag{3.17}$$

$\mathbf{k} = \pi/(L+1)\mathbf{K}_L$, where $x_\alpha \in [1, L]$ represents the Cartesian coordinates of a node, $\mathbf{K}_L$ consists of values in the range $(0, .., L-1)^d$.

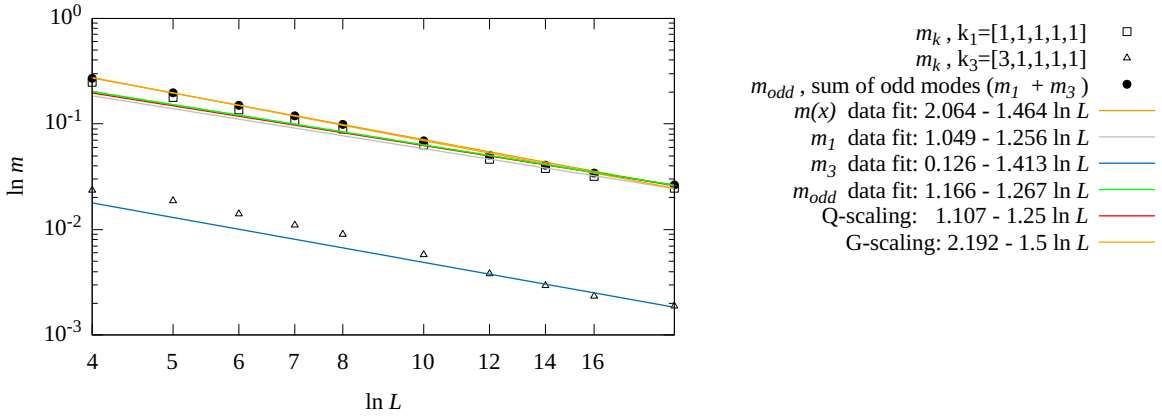

Figure 3.1. Fourier modes of the magnetisation FSS in the vicinity of pseudocritical point T_L. As expected, even k modes vanish, while odd modes provide accurate scaling.

The mean magnetization is

$$\begin{aligned} m &= \frac{1}{L^d} \sum_x \mu(\mathbf{x}) = \frac{1}{L^d} \frac{1}{(L+1)^d} \sum_x \sum_k \mu(\mathbf{k}) \prod_\alpha^d \sin(k_\alpha \cdot \mathbf{x}_\alpha) \\ &= \frac{1}{L^d} \frac{1}{(L+1)^d} \sum_k \left(\sum_x \mu(\mathbf{x}) \prod_\alpha^d \sin(k_\alpha \cdot \mathbf{x}_\alpha) \right) \cdot W_{\mathbf{k}} \ , \end{aligned} \tag{3.18}$$

where $W_{\mathbf{k}} = \sum_{\mathbf{x}} \prod_\alpha^d \sin(k_\alpha \cdot x_\alpha)$. For even modes $\mathbf{k}$ (i.e. modes for which at least one of the K_L's is even), the weights $W_{\mathbf{k}}$ are zero. These are called G-modes. Odd modes (i.e. modes for which all the K_L's are odd) are called Q-modes and should contribute to the scaling. The results provided in Fig. 3.1 show that for our range of lattice sizes it is still not enough for all sites of the system to represent a

five-dimensional lattice. We get $m(k=1) \sim L^{-1.26\pm0.05}$, which hints towards the Q-scaling, but for smaller lattice sizes again we see strong surface effects that shift scaling towards G-scaling. Without a definite answer we turn to another technique that is often used in the theory of criticality: partition function zeros.

3.2. Lee-Yang zeros determination

To summarise so far, although our results are consistent with those of L & M at T_c, we have had at best mixed results at T_L, which make it hard to disambiguate between Q suggested by RG theory and the G scaling preferred by numerics. Therefore we seek another way to detect whether we are in a regime with sufficiently high lattice sizes or not and we turn to partition function zeros. In our experience these deliver more reliable results than those coming from thermodynamic observables [136]. The latter are moments of the partition function or free energy. As such they are sensitive to amplitudes which themselves can be variable. E.g., if the amplitude of correction terms for susceptibility is sufficiently large at T_L, said correction terms can dominate and mask the leading FSS behaviour coming from power laws. In such circumstances it might take extraordinary large lattices for leading FSS behaviour to take effect. If this happens for FBCs and not for PBCs, it would lead to the behaviour we observed. Partition function zeros, on the other hand, are not subject to such amplitudes.

For any finite system, the partition function can be written as a polynomial in terms of fugacities and the partition function zeros are thus zeros in the complex plane of the appropriate variables. Analyzing phase transitions via the behaviour of the zeros when approaching the critical point was first suggested by Tsung-Dao Lee and Chen-Ning Yang for complex fields [49, 50] and later generalised for complex temperatures by Michael Fisher [20, 51]. In what follows below, we will study the properties of the Lee-Yang zeros. For most of the models though, the zeros and their critical properties can be only estimated by the extensive use of computer simulations [62]. Analytically, solving the partition function for zeros in the

complex plane is required. In particular, as the system size increases, Lee-Yang zeros exhibit a scaling behavior, accumulating near critical points in the thermodynamic limit. This scaling pattern allows for the extraction of critical exponents and classification of phase transitions into universality classes. Understanding the scaling properties of Lee-Yang zeros provides valuable insights into critical behavior and phase transitions, enabling the characterization of macroscopic properties and underlying physical phenomena.

Let us write down the definition of the partition function in the complex $h = h^R + ih^I$ plane at $\beta = \beta_c$ in more details:

$$Z(\beta_c, h^R + ih^I) = \sum_{\{s\}} e^{-\beta_c \sum_{i,j} S_i S_j + \beta_c h^R \sum_i S_i} \Big(\cos(\beta_c h^I \sum_i S_i) + i \sin(\beta_c h^I \sum_i S_i) \Big) , \tag{3.19}$$

where the first sum spans all spin configurations. This can be conveniently rewritten as:

$$Z(\beta_c, h^R + ih^I) = Z(\beta_c, h^R) \Big(\Big\langle \cos(\beta_c h^I \sum_i S_i) \Big\rangle_{\beta_c, h^R} + i \Big\langle \sin(\beta_c h^I \sum_i S_i) \Big\rangle_{\beta_c, h^R} \Big) , \tag{3.20}$$

here the averaging $\langle \dots \rangle_{\beta_c, h^R}$ is performed at the fixed values of temperature β_c and magnetic field h^R.

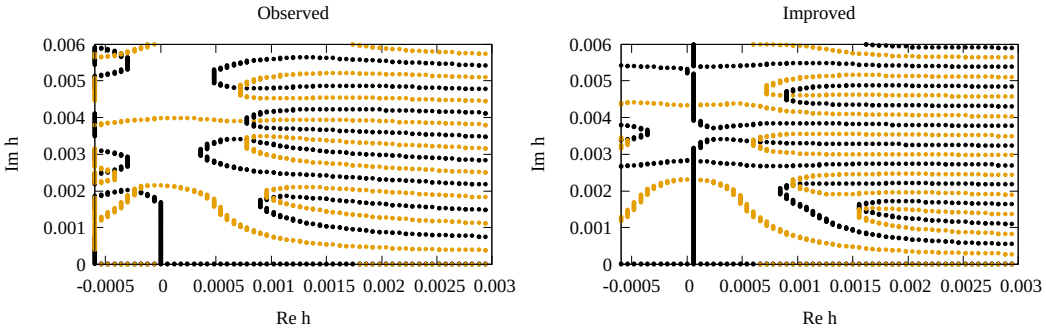

Figure 3.2. Using the symmetry of the Ising model, we can improve the amount of configurations and in this way also improve the positions of zeros on complex magnetic field plane. Left figure depicts the lines $ReZ = 0$ and $ImZ = 0$ for size $L = 20$ at $T = T_c$. Right figure is improved configuration number - the zeros are more accurate and visible.

With the data of numerical simulations to hand, to determine the points

where the partition function becomes zero, it is necessary for both the real and imaginary parts of the partition function to be zero, so we look at the values of trigonometric functions averages $\langle \mathbf{cos}(\beta_c h^I \sum_i S_i)\rangle_{\beta_c,h^R}$ and $\langle \mathbf{sin}(\beta_c h^I \sum_i S_i)\rangle_{\beta_c,h^R}$ by plotting the contours in the complex magnetic field plane along which these function separately vanish [63, 64], and then, more precise methods are implemented around the intersection of the said contours [65]. The simulations at the complex h values are not needed as we use the histogram reweighting technique around the real simulations at $h = 0$. Since the probability of states “up" and “down" are the same for the Ising model, we artificially improve our statistics by not only using the simulation data, but also applying random signs to the magnetisation of each state with the probability 50%. This way our statistics includes more possible states and improves drastically. The improved picture is shown on Figure 3.2.

Results presented in Fig. 3.3 at T_L show the position of several first Lee-Yang zeros for different lattice sizes. The zeros follow a unit circle theorem, which in our coordinates means that all zeros should lay on the imaginary axis. This is what we observe for few first zeros, though it is obscured later by the extrapolation from the simulation point. To further show this that our analysis of the first zeros is valid, we present a FSS of the first Lee-Yang zero in Figs.3.4, 3.5. The FSS of first Lee-Yang zero is governed by [66]:

$$h_1 \sim L^{-\frac{\Delta}{\nu}} = L^{-\frac{\beta+\gamma}{\nu}}. \tag{3.21}$$

The Lee-Yang analysis is contained essentially in 3.4, 3.5. Q and G scaling predict $h_1 \sim L^{3.75}$ and L^3, respectively.

Criticality: Fig.3.4 shows the FSS of the first Lee-Yang zero at T_c, where we get $h_1 \sim L^{-3.16\pm0.48}$, this might hint at G-scaling according to our other exponents at T_c.

Pseudocriticality: For the first zero h_1 we see that for T_L our fit when we discard the smallest lattice sizes, $h_1 \sim L^{-3.81\pm0.08}$, is well compared to Q-scaling

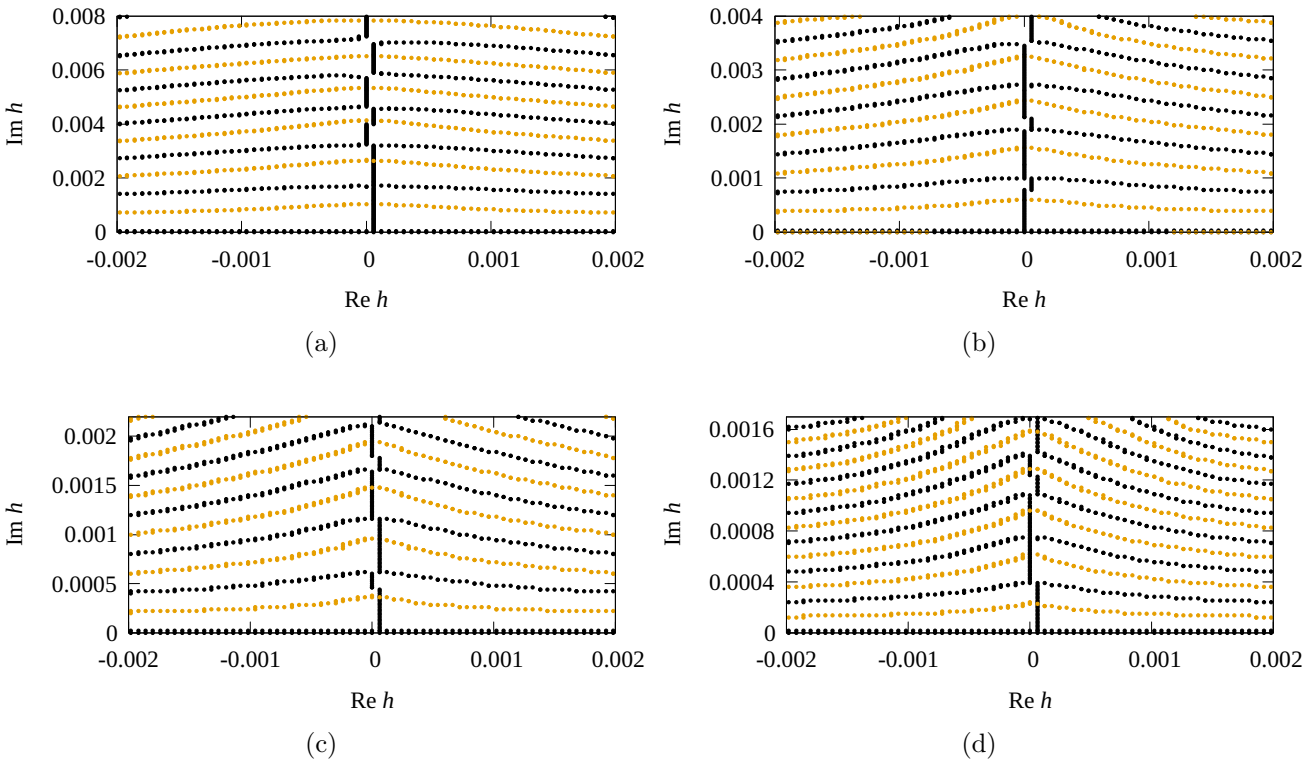

Figure 3.3. Lines of zeros $\mathbf{Im}\, Z(h^R, h^I) = 0$ (black curves) and $\mathbf{Re}\, Z(h^R, h^I) = 0$ (yellow curves) at the pseudocritical temperature T_L for lattice sizes $L = 12, 14, 16, 18$ (a,b,c,d respectively). Crossings of different colour lines give the position of Lee-Yang zeros. All zeros are located on the imaginary axis, in agreement with the unit circle theorem.

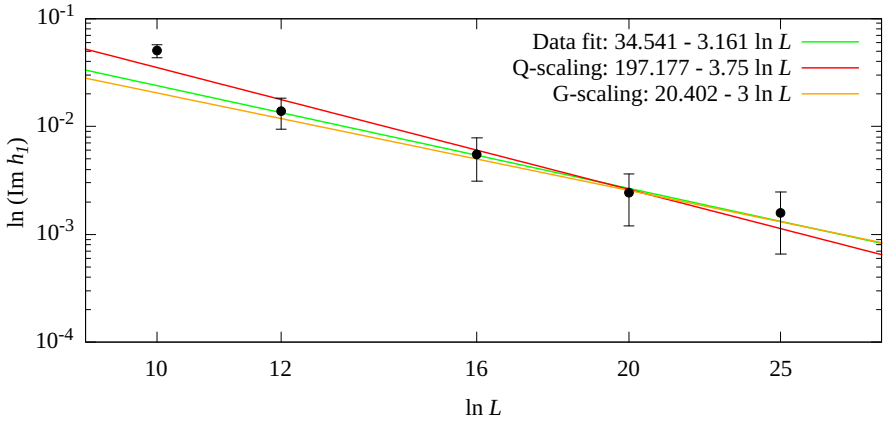

Figure 3.4. FSS of the first Lee-Yang zero for sizes $L = 10..25$ at T_c. Expected outcome: G-scaling.

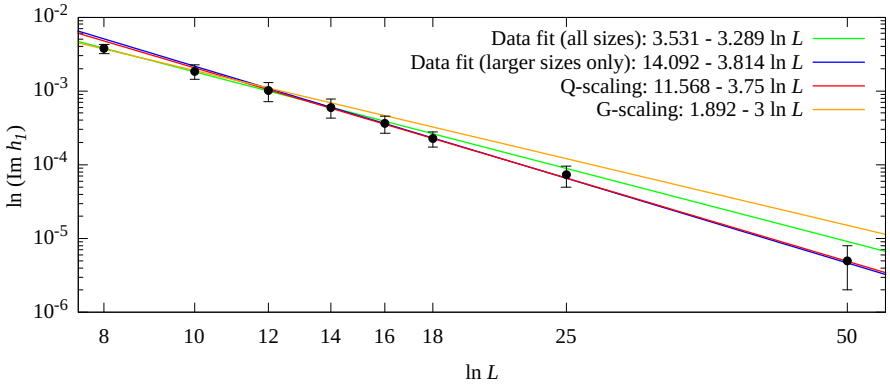

Figure 3.5. FSS of the first Lee-Yang zero for sizes $L = 10..25$ at T_L. Expected outcome: Q-scaling.

and far from G-scaling: $h_1^{(Q)} \sim L^{-3.75}$ versus $h_1^{(G)} \sim L^{-3}$, cf. Eq.(3.21).

3.3. Account of the partition function zeros for scaling at the pseudocritical point

Furthermore, from Eq.(1.24), we may write the susceptibility as

$$\chi \propto \frac{1}{L^d} \sum_j \frac{1}{(z - z_j(L))^2}\,, \tag{3.22}$$

where $z_j(L)$ is the jth zero for a system of size L. Assuming that the first zeros dominates this gives that

$$\chi \sim L^{-d} h_1^{-2} \sim L^{-2d\Delta/\nu}\,. \tag{3.23}$$

I.e., we can provide an estimate for the susceptibility in this way. We find the contribution of the first zero to the susceptibility, $L^{-d}h_1^{-2} \sim L^{2.62\pm0.10}$ which is far closer to Q ($\chi_L \sim L^{5/2}$) than to G ($\chi_L \sim L^2$). This means that, at least from the Lee-Yang-zeros analysis, even the susceptibility is supportive of Q for pesudocriticality and free boundaries.

3.4. Conclusions

In this chapter we have used two complementary methods to improve the FSS of the $d = 5$ Ising model with FBC above the upper critical dimension. These are

the Fourier modes analysis and Lee-Yang zeros analysis.

While for the PBC only the zero mode contributes to scaling, for the FBC all odd modes are so-called Q-modes and they collectively contribute to the FSS, and all even modes vanish. Results for this method are presented in Fig. 3.1. We see that the magnetisation Fourier modes repeat the behaviour of magnetisation in Chapter 2, and confirm Q-scaling, but do not improve the scaling picture drastically.

In the meantime, partition function zeros showed good results even by themself, as the FSS of the first Lee-Yang zero h_1 is presented in Figures 3.4, 3.5. We observe $h_1 \sim L^{-3.16\pm0.48}$ at T_c, that hints towards G-scaling ($h_1 \sim L^{-3}$), and $h_1 \sim L^{-3.75}$ at T_L, which hints towards Q-scaling.

Moreover, when examining the isothermal susceptibility in terms of Lee-Yang zeros, a scaling behavior was observed at the pseudocrtitcal point T_L with better accuracy. Notably, this scaling is found to be much closer to Q-scaling than to G-scaling. This indicates that the scaling behaviour at FBC exhibits in a manner that is more consistent with our scaling expectations (Q-scaling) than with the conflicting conclusions in the literature, providing valuable insights into the dynamics of this property.

Lastly, the partition function zeros analysis emerged as a powerful tool to enhance the accuracy of scaling assessments above the upper critical dimension. Remarkably, this approach demonstrated its effectiveness without necessitating the use of exceptionally large lattice sizes or the isolation of the lattice core. The partition function zeros analysis thus stands out as a valuable method for refining the understanding of scaling behaviors in the Ising model beyond its upper critical dimension.

CHAPTER 4

CO-POLYMER NETWORK SCALING EXPONENTS AND POLAND-SCHERAGA MODEL OF DNA DENATURATION

In this chapter we will consider scaling in soft matter physics, particularly in polymers. It has been shown that the scaling behaviour and scaling exponents that govern conformational properties of long flexible polymer chains in a good solvent are related to the scaling exponents in magnetism (the Ising model in Chapters 2,3), see Eq.(1.28), (1.29). Our primary focus in this chapter is the phenomenon of DNA thermal denaturation in description of the Poland-Scheraga (PS) model [76, 77], briefly discussed below. The results of this chapter have been published in Refs. [2, 3].

In its native state DNA has a form of a helix that consists of two strands bound together by hydrogen bonds. During biological processes involving DNA (such as duplication or transcription) unbinding occurs, phenomenon known also as denaturation, helix-to-coil transition or DNA unzipping [71]. An analogue to DNA unwinding in a cell can be observed also *in vitro*, in solutions of purified DNA. Already in the middle 50-ies of the last century it has been observed that heating of DNA solutions above room temperature results in cooperative transition of the bound helix-structures strands to single strands. Although the mechanism of such unwinding clearly differs from the biological protein-mediated process, ongoing experimental studies of DNA alone are important steps toward understanding much more complex phenomenon that occurs *in vivo* in a cell [73, 74]. The mechanism of such transition may be an external pulling force applied to one of DNA strands (me-

chanical unzipping) [75], changes in the pH of the DNA contained solvent (chemical unzipping) or its heating (thermal unzipping) [71]. The scaling laws that govern this last phenomenon are the subject of analysis in this chapter.

One of important experimental observations of the DNA melting curves, where the fraction of the bound pairs $\theta(T)$ is measured as a function of temperature T is their abrupt behaviour [71, 82]. With an increase of T, $\theta(T)$ manifests a jump at certain transition temperature clearly signalling that the DNA thermal denaturation is a first order transition. Numerous theoretical approaches to represent the process of DNA thermal denaturation in a two-state Ising-like manner were developed. Here, we concentrate on the PS type description, where the transition is governed by an interplay of two factors: chain binding energy and configurational entropy [79]. In turn, the entropy of a polymer in a good solvent attains a scaling form (1.32) and this is how the scaling exponents that govern configurational properties of polymer macromolecules of different topology come into play in descriptions of DNA thermal denaturation.

Similar as the Ising model suggested to describe ferromagnetism fails if one models a ferromagnet as a one-dimensionsal chain, the PS model suggested to describe the 1st order transition of DNA thermal denaturation fails (predicting the 2nd order scenario) if one models DNA strands as non-interacting random walks (RWs) [76, 77, 90]. With a span of time (see a short overview in Section 1.3) it became clear that an account of in- and inter-strand interactions plays crucial role and leads to correct picture of the transition. In particular the role of interactions between denaturated DNA loop and bound chain has been analyzed both numerically [85] and analytically [92, 112]. Corresponding analytical calculations have been performed by field-theoretic approach in $d = 4 - \varepsilon$ dimensions with ε^3 accuracy [86]. Besides, it was suggested [91] that chain heterogeneity may impact the order of the transition too.

So far, the origin of such heterogeneity has been attributed to effective scaling behaviour differing from that of a self-avoiding walk (SAW). However, it is well known that depending on temperature, the asymptotic scaling behaviour of a

flexible macromolecule belongs either to RW ($T = T_\theta$) or to SAW ($T > T_\theta$) universality class (T_θ denoting the θ-point) [100, 101]. Therefore, it is tempting to recast the heterogeneity in scaling behaviour of a single- and double-stranded chains by studying asymptotic scaling properties of mutually interacting SAWs and RWs.

The structure of the forthcoming Chapter is as follows: First, we will discuss the scaling relations for the loop exponent c in the PS model with the account of possible heterogeneity. Secondly, we will apply resummation technique to calculate the exponents at the space dimensionality $d = 3$ from the asymptotic ε-expansions. Then, we will show how the crowded environment effects the order of phase transition. Finally, we will validate our results by comparing them to exact solutions for the exponents at $d = 2$.

4.1. Scaling relations and account of DNA chain heterogeneity

Depending on temperature, the asymptotic scaling behaviour of a long flexible polymer macromolecule in a good solvent belongs either to random walk (RW), $T = T_\theta$, or to self-avoiding walk (SAW), $T > T_\theta$ universality classes (T_θ denoting the θ-point) [100]. Therefore, the only difference that may be observed in asymptotic scaling of chains of different species (in our case these are the double- and single-stranded chains) is due to the difference in asymptotic scaling properties of mutually interacting SAWs and RWs. Based on this fact we have applied polymer field theory [113, 114] to derive scaling relations that express the loop exponent c in terms of the familiar copolymer star exponents $\eta_{f_1 f_2}$. The latter govern scaling of the star-like polymer structures that are created by linking together the end points of polymer chains of two different species at a common core, as shown in Fig. 1.2. When such a copolymer star is immersed in a good solvent its asymptotic properties are universal in the limit of long chains. In particular, the partition function (the number of configurations) of a copolymer star made of two sets of f_1 and f_2 mutually avoiding

RWs scales with its size R as [99, 116]:

$$Z^{G}_{f_1 f_2} \sim R^{\eta^{G}_{f_1 f_2}} . \tag{4.1}$$

In turn, the partition function of a copolymer star made of mutually avoiding sets of f_1 SAWs and f_2 RWs scales as:

$$Z^{U}_{f_1 f_2} \sim R^{\eta^{U}_{f_1 f_2} - f_1 \eta^{U}_{20}} . \tag{4.2}$$

The third case which is of interest here is the star of two sets of f_1 and f_2 SAWs. For its partition function one gets:

$$Z^{S}_{f_1 f_2} \sim R^{\eta^{S}_{f_1, f_2} - (f_1 + f_2)\eta^{S}_{20}} . \tag{4.3}$$

Indices G, U, S in the above formulas refer to the fixed points (FPs) of the renormalization group transformation that govern scaling of corresponding mutually avoiding structures: Gaussian FP for RWs, Unsymmetric FP for RW and SAW, and Symmetric FP for SAWs, see [116] for more details. Exponents $\eta^{S}_{f_1,f_2}$ are related to $\eta^{U}_{f_1,f_2}$ and to the homogeneous star exponents η_f [114] via: $\eta^{S}_{f_1,f_2} = \eta^{U}_{f_1+f_2,0} = \eta_{f_1+f_2}$.

According to the above, one can distinguish four different cases that take into account heterogeneity of the network shown in Fig. 1.2 and consider mutual avoidance between all SAWs and RWs. In each of this cases, applying Eq. (1.36) we arrive at the following expressions for $\eta_{\mathcal{G}}$:

(i) *SAW-SAW-SAW:* both chains $V_1 - V_3$ and $V_3 - V_3$ are SAWs,

$$\eta_{\mathcal{G}} = -d + 2\eta^{S}_{12}, \tag{4.4}$$

(ii) *SAW-RW-SAW:* chains $V_1 - V_3$ are SAWs, chains $V_3 - V_3$ are RWs;

$$\eta_{\mathcal{G}} = -d + 2\eta^{U}_{12}, \tag{4.5}$$

(iii) *RW-SAW-RW:* chains $V_1 - V_3$ are RWs, chains $V_3 - V_3$ are SAWs;

$$\eta_{\mathcal{G}} = -d + 2\eta^{U}_{21}, \tag{4.6}$$

(iv) *RW-RW-RW:* all chains $V_1 - V_3$ and $V_3 - V_3$ are RWs;

$$\eta_{\mathcal{G}} = -d + 2\eta_{12}^{G}. \tag{4.7}$$

In the 'symmetric' case (i) we recover usual homogeneous polymer picture by taking into account that $\eta_{12}^{S} = \eta_3$, η_3 being scaling exponent of the homogeneous three-leg SAW star [94, 95].

With the above expressions for the heterogeneous co-polymer network exponents $\eta_{\mathcal{G}}$ at hand, it is straightforward to proceed deriving loop closure exponents for each of the cases (i)-(iv). To this end, following [85, 91–93] we generalize expression (1.35) to the case when the network is formed by chains of different sizes: R for the side chains $V1 - V3$ and r for the loop $V3 - V3$. Then the expression for the partition function reads:

$$\mathcal{Z}_{\mathcal{G}} \sim R^{\eta_{\mathcal{G}} - F_1 \eta_{20}^{U}} f(r/R). \tag{4.8}$$

Here $f(x)$ is the scaling function, F_1 is the number of SAWs in the network and we have taken into account that the exponent $\eta_{02}^{U} = 0$ for RWs [98]. Furthermore, considering the limit $r/R \to 0$ we apply the short-chain expansion [97] and make use of the observation that for vanishing loop size the partition function (4.8) should reduce to that of a single (either SAW or RW) chain, $\mathcal{Z}_{\text{chain}} \sim R^{\eta_{\text{chain}}}$ with $\eta_{\text{chain}} = \eta_{02}^{U} = 0$ for RW and $\eta_{\text{chain}} = \eta_{20}^{U}$ for SAW [98]. This implies the power-law asymptotics for the scaling function:

$$f(x) \sim x^{y}, \quad \textbf{with} \quad y = \eta_{\mathcal{G}} - F_1 \eta_{20}^{U} - \eta_{\text{chain}}\,. \tag{4.9}$$

Indeed, with (4.9) the partition function factorizes as

$$\mathcal{Z}_{\mathcal{G}} \sim R^{\eta_{\text{chain}}} \times r^{y} \sim \mathcal{Z}_{\text{chain}} \mathcal{Z}_{\text{loop}}\,. \tag{4.10}$$

Comparing Eqs. (1.34) and (4.9) one arrives at the following expression for the loop closure exponent c:

$$c = \nu_{\text{loop}} [\eta_{\text{chain}} - \eta_{\mathcal{G}} + F_1 \eta_{20}^{U}]\,, \tag{4.11}$$

where $\nu_{\rm loop}$ is the end-to-end distance scaling exponent of the loop forming chain, $\mathcal{Z}_{\rm loop} \sim r^y \sim \ell^{\nu_{\rm loop} y}$.

Combining formula (4.11) with the corresponding expressions for $\eta_{\mathcal{G}}$ of four different heterogeneous networks formed by mutually interacting SAWs and RWs, Eqs. (4.4)–(4.7) we arrive at the following loop closure exponents in each of these networks, in the following denoted as c_1–c_4:

$$\textit{SAW-SAW-SAW:} \quad c_1 = \nu_{\rm SAW}(3\eta^S_{20} + d - 2\eta^S_{12})\,, \tag{4.12}$$

$$\textit{SAW-RW-SAW:} \quad c_2 = \nu_{\rm RW}(\eta^S_{20} + d - 2\eta^U_{12})\,, \tag{4.13}$$

$$\textit{RW-SAW-RW:} \quad c_3 = \nu_{\rm SAW}(2\eta^S_{20} + d - 2\eta^U_{21})\,. \tag{4.14}$$

$$\textit{RW-RW-RW:} \quad c_4 = \nu_{\rm RW}(d - 2\eta^G_{21})\,, \tag{4.15}$$

where $\nu_{\rm RW} = 1/2$ and $\nu_{\rm SAW}$ are the end-to-end mean distance exponents for RW and SAW, correspondingly and d is space dimension. The exponents $\eta_{f_1 f_2}$ have been calculated within field-theoretical renormalization group approach [99, 116] and are currently know in the fourth order of the $\varepsilon = 4 - d$ expansion [86]. By (1.34), each of the above expressions govern the loop closure in the heterogeneous network and therefore defines the order of the phase transition of DNA thermal denaturation in the frames of the Poland-Scheraga model. In the following section we will evaluate these expressions for the case $d = 3$.

4.2. ε-expansion and its resummation

Scaling relations (4.12)–(4.15) express exponents c_i in terms of the familiar co-polymer star exponents $\eta_{f_1 f_2}$ [97]. The latter have been calculated by means of field-theoretic renormalization group approach are currently available in $\varepsilon = 4 - d$-expansion up to order ε^4 [86]. Below, we list them together [87]:

$$\begin{aligned}\eta^S_{20}(\varepsilon) = &-\varepsilon/4 - 9\varepsilon^2/128 + \varepsilon^3(264\zeta(3) - 49)/2048 \\ &+ \varepsilon^4(704\pi^4 - 297600\zeta(5) + 38160\zeta(3) + 235)/655360,\end{aligned} \tag{4.16}$$

$$\eta^S_{12}(\varepsilon) = -3\varepsilon/4 - 3\varepsilon^2/128 + 3\varepsilon^3(40\zeta(3) + 23)/2048 \tag{4.17}$$

$$+\varepsilon^4(64\pi^4-32640\zeta(5)-6480\zeta(3)+3333)/131072,$$

$$\eta_{12}^U(\varepsilon)=-3\varepsilon/4+\varepsilon^2(42\zeta(3)-13)/128+\varepsilon^3(384\zeta(3)-5)/2048 \tag{4.18}$$
$$+\varepsilon^4(1024\pi^4-528000\zeta(5)+14880\zeta(3)+7655)/655360,$$

$$\eta_{21}^U(\varepsilon)=-\varepsilon+\varepsilon^2(42\zeta(3)+1)/64+17\varepsilon^3/1024 \tag{4.19}$$
$$-\varepsilon^4(1056\zeta(3)-721)/65536,$$

$$\eta_{21}^G(\varepsilon)=-\varepsilon, \tag{4.20}$$

$$\nu_{\mathrm{SAW}}(\varepsilon)=1/2+\varepsilon/16+15\varepsilon^2/512+\varepsilon^3(135/8192-(33/1024)\zeta(3)) \tag{4.21}$$
$$+\varepsilon^4(3799/524288-(873/32768)\zeta(3)-(11/40960)\pi^4+(465/4096)\zeta(5))\,.$$

Where $\zeta(x)$ is Riemann zeta-function. Note that the formula for the exponent η_{21}^G contains only linear in ε term and is exact.

Substituting 4.16-4.21 into 4.12-4.15 one readily gets the corresponding expansions for exponents c_i:

$$c_1=2+1/8\,\varepsilon+\frac{5}{256}\,\varepsilon^2+\left(-\frac{87}{4096}+\frac{3}{512}\,\zeta\left(3\right)\right)\varepsilon^3+$$
$$\left(-\frac{3547}{262144}+\frac{903}{16384}\,\zeta\left(3\right)+\frac{1}{20480}\,\pi^4-\frac{1815}{2048}\,\zeta\left(5\right)\right)\varepsilon^4, \tag{4.22}$$

$$\begin{aligned}c_2 \;=\; & 2+1/8\,\varepsilon+\left(\frac{17}{256}-\frac{21}{64}\,\zeta\left(3\right)\right)\varepsilon^2+\\ & \left(-\frac{63}{512}\,\zeta\left(3\right)-\frac{39}{4096}\right)\varepsilon^3+\left(-\frac{3015}{262144}+\right.\\ & \left.\frac{105}{16384}\,\zeta\left(3\right)+\frac{1185}{2048}\,\zeta\left(5\right)-\frac{21}{20480}\,\pi^4\right)\varepsilon^4,\end{aligned} \tag{4.23}$$

$$c_3 \;=\; 2+3/4\,\varepsilon+\left(\frac{21}{128}-\frac{21}{32}\,\zeta\left(3\right)\right)\varepsilon^2+$$

$$\left(\frac{157}{2048}-\frac{27}{128}\zeta\left(3\right)\right)\varepsilon^3+\left(\frac{4125}{131072}-\frac{165}{1024}\zeta\left(3\right)-\frac{11}{10240}\pi^4-\frac{465}{1024}\zeta\left(5\right)\right)\varepsilon^4, \tag{4.24}$$

$$c_4 = 2 + 1/2\,\varepsilon\,, \tag{4.25}$$

where $\zeta(x)$ is Riemann ζ-function. Note that because of $\eta_{21}^G(d=3)=\eta_{12}^G(d=3)=-1$ [97] the corresponding analytic expression for c_4 is exact and contains only a linear term.

The FT ε-expansions mentioned above yield a very obscure property - in most cases they diverge asymptotically. For one to avoid such inconveniences some kind of resummation has to be done. There are different approaches to the problem, here we use the conformal mapping trick, introduced in [103]. The algorithm goes as follows:

For the function in form of a series expansion up to L order of perturbation theory:

$$\upsilon = \sum_{n=0}^{L} C_n x^n, \tag{4.26}$$

it is known that for $n \to \infty$ one obtains the following behaviour for coefficients C_n:

$$C_n \sim n!(-a)^n$$

Let us consider the Borel-image of (4.26) which is used to mitigate the factorial-like behaviour of the coefficients

$$B(xt) = \sum_{n=0}^{L} \frac{C_n (xt)^n}{n!} \upsilon = \int_0^\infty dt \cdot e^{-t} B(xt) \tag{4.27}$$

Assuming that every singularity in $B(xt)$ lies on the negative semiaxis, the biggest singularity is located at $1/a$, and that the function $B(xt)$ is analytical in the complex plane excluding the part of real axis $(-\infty; -\frac{1}{a})$, it is widely known to use a conformal mapping trick cutting the plane and transforming it onto a disk of

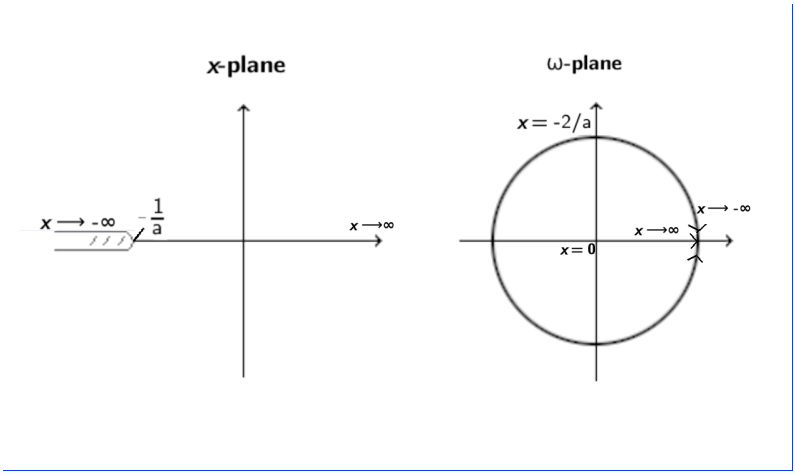

Figure 4.1. Visual presentation of conformal mapping (4.28)

radius 1 (Figure 4.1):

$$xt = \frac{4}{a}\frac{\omega}{(1-\omega)^2}. \tag{4.28}$$

The full procedure can be generalized by introducing two additional fit parameters b and α. Substituting the factorial $n!$ by the Euler gamma-function $\Gamma(n+b+1)$ (and inserting an additional factor t^b into the integral (4.27) takes into account the finite size of ε-expansions we have. Fit parameter α is included after conformal mapping transformation by multiplication of the expression by $\frac{(1-\omega)^\alpha}{(1-\omega)^\alpha}$ and expanding the numerator into series in ω. Here, the numerator cancels the divergence from the denominator in (4.28) and is included in $\tilde{C}_n$. Final expression for the resummed υ reads:

$$V(\omega) = \int_0^\infty dt \cdot t^b e^{-t} \sum_{n=0}^{L} \left(\frac{4}{a}\right)^n \frac{\tilde{C}_n \omega^n(t)}{\Gamma(n+b+1)(1-\omega(t)^\alpha)}, \tag{4.29}$$

However, physical value υ should not be dependent on parameters α and b. Therefore Principle of minimal sensitivity is used [106][107]:

$$\frac{\partial V^{(L)}(b,\alpha)}{\partial b}|_{b_{opt}^{(L)},\alpha_{opt}^{(L)}} = \frac{\partial V^{(L)}(b,\alpha)}{\partial \alpha}|_{b_{opt}^{(L)},\alpha_{opt}^{(L)}} = 0 \tag{4.30}$$

Set of optimal points $(b,\alpha)^L$ is obtained for every L. Out of these points we have to choose ones that converge in the most efficient way, introducing the Principle of fastest apparent convergence [106][107], by minimizing values:

$$V^{(L+1)}(b^{(L+1)},\alpha^{(L+1)}) - V^{(L)}(b^{(L)},\alpha^{(L)}) \tag{4.31}$$

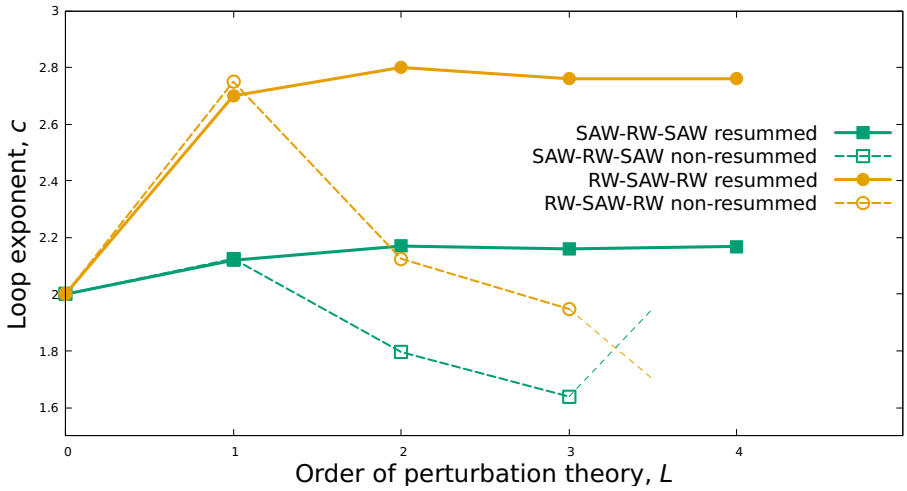

Figure 4.2. Visual presentation of conformal mapping resummation technique. Direct sum of the ε-expansions (dashed lines) diverges, while the resummed values (solid lines) quickly come to their asymptotics.

	I	*II*	*III*	*IV*
ν_{SAW}	0.54(3)	0.56(2)	0.582(8)	0.585(3)
η_{20}	-0.25(6)	-0.292(4)	-0.289 (5)	-0.276(3)
η_3	-0.75(4)	-0.77(2)	-0.75(1)	-0.743(5)
η_{12}^U	-0.75(8)	-0.82(5)	-0.77(3)	-0.795(5)
η_{21}^U	-1.(2)	-0.9(8)	-0.95(8)	-0.98(3)

Table 4.1. Critical exponents ν and $\eta_{f_1 f_2}$, resummed in different orders of perturbation theory at $d = 3$ ε-expansions using the conformal mapping method.

The effectiveness of this resummation technique can be seen in Figure 4.2. It displays the divergent series with dashed lines and their resummed counterparts with solid lines. Even though the first order of the ε-expansion seems to be in line with the resummation, further perturbation orders diverge drastically, and without the resummation it would be impossible to confidently find the values of the exponents. The results of resummation for the exponents (4.16-4.21) are presented in Table 4.1.

Using the formulas from the above we have calculated the exponents c_i up to the fourth order (Table 4.2).

The value of the exponent c_1 is in a good agreement with typical MC estimates $c_1 = 2.10(4)$ [93], $c_1 = 2.18(6)$ [92]. Up to our knowledge, no MC simulations for

	I	*II*	*III*	*IV*
c_1 (SAW-SAW-SAW)	2.04 (5)	2.05 (2)	2.13 (1)	2.147 (4)
c_2 (SAW-RW-SAW)	2.12 (9)	2.17 (5)	2.16 (3)	2.169 (5)
c_3 (RW-SAW-RW)	2.7 (2)	2.78 (1)	2.77 (2)	2.588 (9)
c_4 (RW-RW-RW)	2.5	2.5	2.5	2.5

Table 4.2. Loop exponent c calculated for different conformations of model network system in different orders of perturbation theory at $d = 3$.

the loop-chain compositions that are governed by the exponents c_2–c_4 are available. Clearly, $c > 2$ in all configurations, which confirms the first order transition.

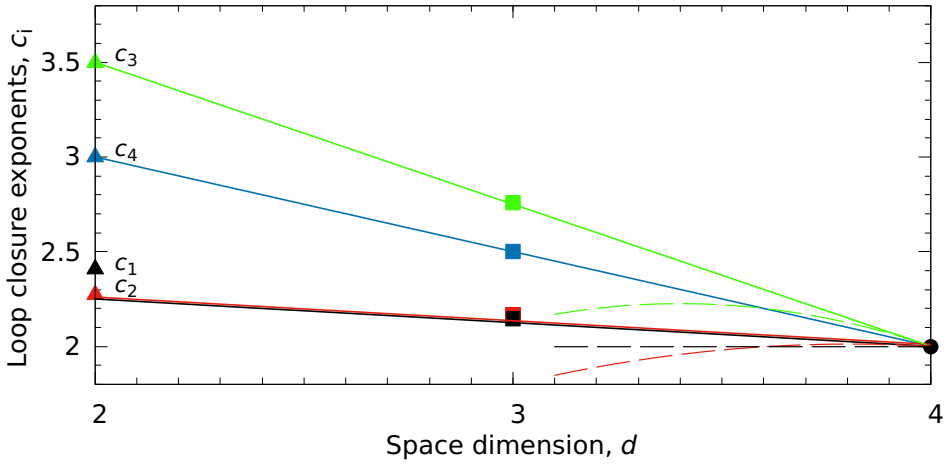

Figure 4.3. (*Colour online*) Loop closure exponents c_i at different space dimension d. Triangles show exact results at $d = 2$ (4.41) and squares show most accurate results obtained by resummation at $d = 3$ [2]. The lines show analytic continuation to non-integer d via ε-expansion in the first and second orders, thick solid and thin dashed lines, correspondingly. Note that in the case of mutually avoiding RWs (blue line) loop closure exponents $c_4(\varepsilon)$ is exact and linear in ε.

4.3. Effect of the environment

In two former sections, 4.1 and 4.2, we discussed an impact of the solvent quality on the order of the DNA thermal denaturation transition. Another factor that may modify scaling exponents of long flexible polymer macromolecules is the presence of impurities – impenetrable regions in a solvent that restrict the number of

polymer configurations, see e.g. [119] and references therein. Statistics of polymers in disordered medium is of interest for number of reasons, in the context of our study it is important to mention its relevance for treating macromolecules in a cell, composed of many different kinds of biochemical species [120–122].

There exist different analytic frameworks to model an impact of disordered medium on scaling properties of (interacting) SAWs and RWs. To give a few examples, the latter are studied on a percolation cluster [123] or at presence of quenched defects [124, 126–128, 131]. Whereas the uncorrelated defects do not influence polymer scaling [124], the so-called 'extended' or long-range correlated structural disorder has been shown to be relevant. A model of long-range correlated disorder has been suggested in Ref. [126] and further exploited in studies of polymers [128, 131]. Within this model, one considers defects, characterized by the density-density pair correlation function $g(r)$ decaying at large distance r according to a power law

$$g(r) \sim r^{-a}\,. \tag{4.32}$$

For integer values of a such defects have a direct interpretation: the case $a = d$ corresponds to point-like defects, while $a = d-1$ ($a = d-2$) correspond to straight lines (planes) of defects of random orientation. Sometimes non-integer values of a are interpreted in terms of fractal structures, see also Refs. [132], where the relation of fractal dimension to the analytically continued non-integer dimension is discussed in more details. Detailed analysis of an impact of the long-range correlated disorder (4.32) on possible changes in the exponents (4.12-4.15) and hence on the DNA thermal denaturation is beyond the scope of this study. However, we will use some of the previously obtained results in order to understand and qualitatively describe this possible impact.

It is easy to see that the presence of long-range correlated impurities may or may not be relevant and change the polymer scaling exponents depending of the value of a. Indeed, large-distance asymptotics of the pair correlation function (4.32) corresponds to the power-law behaviour of its Fourier-image at small wave

vector k in the form k^{a-d}. Therefore, by simple power counting one arrives at the conclusion that such term becomes relevant at small k for $a < d$. Applying field-theoretic renormalization group technique, the corresponding polymer model has been analysed and the scaling exponents were calculated in the two-loop approximation at fixed $d = 3$ and different values of the correlation parameter a as well as in a one-loop order by the double expansion in $\varepsilon = 4 - d$ and $\delta = 4 - a$ [128]. The derivation given below is based on these double ε, δ expansion. In particular, it has been shown that for certain region of parameters $\varepsilon/2 < \delta < \varepsilon$ the scaling properties of a single flexible polymer chain in porous environment with a long-range correlated structure are governed by a new, 'long-range' fixed point L. The mean square end-to-end distance exponent $\nu_{\rm SAW}$ in the first order of ε, δ expansion reads [128]:

$$\nu^{L}_{\rm SAW} = 1/2 + \delta/8 + \dots \,. \tag{4.33}$$

In turn, the $\eta_{f_1 f_2}$ exponents for co-polymer stars in porous environment with long-range correlated structure are given by Eq. (39) from Ref. [131]:

$$\eta^{S_L}_{f_1 f_2} = \frac{-(f_1+f_2)(f_1+f_2-1)\delta}{4}\,, \tag{4.34}$$

$$\eta^{U_L}_{f_1 f_2} = \frac{-f_1(f_1+3f_2-1)\delta}{4}\,, \tag{4.35}$$

$$\eta^{G_L}_{f_1 f_2} = -f_1 f_2 \delta\,. \tag{4.36}$$

In Eqs. (4.34)–(4.36), the first exponent $\eta^{S_L}_{f_1 f_2}$ corresponds to the star of $f_1 + f_2$ SAWs, the second exponent $\eta^{U_L}_{f_1 f_2}$ describes the star of mutually avoiding sets of f_1 SAWs and f_2 RWs, and the third exponent $\eta^{G_L}_{f_1 f_2}$ describes the star of two mutually avoiding sets of f_1 and f_2 RWs.

Two cautions are at place here. First, the 'long-range' fixed point S_L is accessible in the region where the above mentioned power counting shows that the disorder is irrelevant. Second, the fixed points U_L and G_L can be reached only for specific initial conditions. Similar situation is encountered also when the ε, δ expansion is applied to study models of m-vector magnets with long-range correlated quenched disorder [126]. However, an account of higher order contributions

restores physical region of stability of the 'long-range' fixed point confirming qualitatively correct result of the first-order analysis, see e.g. [108] and references therein. Therefore, with an aim of getting qualitative description of an impact of extended long-range correlated impurities on the DNA thermal denaturation transition, we proceed with formulas (4.33)–(4.36) substituting them into the scaling relations 4.12-4.15 and arrive at the following first-order values for the c_i exponents:

$$c_1^L = c_2^L = 2 - \varepsilon/2 + 5\delta/4\,, \tag{4.37}$$

$$c_3^L = c_4^L = 2 - \varepsilon/2 + 2\delta\,. \tag{4.38}$$

As it follows from Eq. (4.32), the smaller the a, the stronger correlations in porous structure that restricts the volume available for the macromolecule. Indeed, the density-density correlation function $g(r)$ decays slower with a decrease of a, attaining the fat-tail features. The positive sign at the linear in δ terms in Eqs. (4.37), (4.38) brings about an increase in the exponents c_i with an increase of $\delta = 4 - a$. This allows to conclude, that an increase in density correlations of the porous structure leads to strengthening of the DNA thermal denaturation transition. Moreover, comparing Eqs. (4.37) and (4.38) one concludes that $c_3^L, c_4^4 > c_1^L, c_2^L$, similar as it was observed for the DNA denaturation in a pure solvent without porous medium. The difference between the exponents increases with an increase of δ: $c_{3,4}^L - c_{1,2}^L = 3\delta/4$. Of course, with all cautions mentioned above, these results have to be considered as a qualitative predictions, rather as a quantitative description of DNA denaturation in crowded environment. Moreover, obtained above relations $c_1^L = c_2^L$ and $c_3^L = c_4^L$ may be (and perhaps indeed are) violated in the second order of the perturbation theory. However, it is worth mentioning that the scaling arguments supported by the renormalization group calculations predict effect of strengthening the order of the denaturation transition when it occurs in presence of extended structures that restrict swelling of the polymer coil.

4.4. Comparison with exact results at $d = 2$

As has been discussed above, the ε-expansions for the c_i may serve as a basis for reliable numerical estimates at $d = 3$ provided appropriate resummation technique is applied. With the perturbative expansions and their numerical estimates at hand, it is instructive to corroborate the results by comparing them with data for other space dimensions, if available. One obvious result is obtained for $d = 4$: there, as it is easy to check via Eqs. (4.12-4.15), all exponents are equal: $c_i(d = 4) = 2$. Besides, there is a tempting opportunity to get exact values for the exponents at $d = 2$. Indeed, to this end one can make use of the exact results for the scaling exponents of $d = 2$ copolymer stars of mutually avoiding bunches of SAW and RW [96, 112]. There, the relations between exponents in fluctuating geometry (quantum gravity) and flat $d = 2$ geometry have been used to extract the exact values of the exponents. In notations of the previous section, the exponents read (Eqs. (100), (101) of Ref. [99]):

$$\eta^G_{f_1 f_2} = \frac{1}{48}\left\{4 - \left[\sqrt{24 f_1 + 1} + \sqrt{24 f_2 + 1} - 2\right]^2\right\}, \tag{4.39}$$

$$\eta^U_{f_1 f_2} = \frac{1}{48}\left\{4 + 5 f_1 - \left[3 f_1 + \sqrt{24 f_2 + 1} - 1\right]^2\right\}. \tag{4.40}$$

Substituting these formulas into Eqs. 4.12-4.15 and taking into account that $\nu_{\mathrm{SAW}}(d = 2) = 3/4$ [113], one gets the following exact values of the exponents c_i at $d = 2$:

$$c_1 = \frac{77}{32} \simeq 2.406, \quad c_2 = \frac{109}{48} \simeq 2.271, \tag{4.41}$$

$$c_3 = \frac{7}{2}, \quad c_4 = 3\,.$$

These values are shown by triangles in Fig. 4.3. The obtained result for the exponent c_3 recovers the value predicted at $d = 2$ by the exact formula that follows from Eq. (4.14) and is valid also for other values of d: $c_3 = 2 + \varepsilon/2$.

Comparing the values of the loop closure exponents c_i at $d = 2$ and at $d = 3$ one can arrive at certain conclusions about an impact of chain heterogeneity on

the strength of the DNA thermal denaturation transition. The first observation is that passing from the homogeneous SAW composition within the Poland-Scheraga model (as described by the exponent c_1) usually leads to strengthening of the 1st order transition. When the SAW side chains are substituted by RWs, the strength of the transition increases: $c_3 > c_1$, $c_4 > c_2$. In turn, when the side chains remain unchanged, the change of the SAW loop to the RW one decreases the strength of the 1st order transition: $c_3 > c_4$ and $c_1 > c_2$. The last effect is more pronounced for the RW side chains and at space dimension $d = 2$. In general, the following rule holds: $c_2 < c_1 < c_4 < c_3$ (with $c_2 \sim c_1$ at $d = 3$).

Another striking feature that follows from the comparison of the exact and perturbative results shown in Fig. 4.3 is rather unusual behaviour of the ε-expansion curves. Indeed, the first order ε-expansion for the exponents c_i (solid lines in the plot) nicely corresponds to the resummed ε^4-data at $d = 3$ and to the exact values at $d = 2$. Such behaviour is obvious for the exponent c_3, where the first order ε-expansion provides an exact number. However, for the other exponents, an account of the higher orders of the perturbative expansion needs careful application of the resummation technique. Being evaluated naïvely by simple adding higher order contribution, the ε-expansion holds only very close to the upper critical dimension $d = 4$, as shown in the figure by the thin dashed lines for the case of ε^2-data. Therefore, the first order ε-expansion provides the so-called optimal truncation [118] for the $c_i(\varepsilon)$ series.

Conclusions

In this chapter we have considered the scaling exponents of a complex copolymer network that occurs in the thermal denaturation of DNA within the Poland-Scheraga model. We have derived new scaling relations for the loop closure exponent c_i that controls the order of the phase transition from ordered to disordered phase with the account of possible heterogeneity between the denaturated loop and bound chains. The value of the loop closure exponent c discriminates between different

ways the thermal denaturation of the DNA occurs: for $c_i > 2$, the denaturated loop emerges abruptly, in the first order phase transition manner, for $1 \leq c \leq 2$, the transition is continuous, and for $c < 1$, no transition happens. Numerous attempts of theoretical description and numerical simulation of this phenomenon finally led to the coherent picture, observed also in the *in vitro* experiments and simulations [71, 111, 112, 135]: the transition is of the first order and $c_i > 2$. Besides, the factors that may have an impact on the strength, and, eventually, even on the order, of this transition are discussed in the literature [82]. Influence of possible heterogeneity in entropic scaling exponents of bound and denaturated DNA strands on the loop closure exponent c is manifest by an interplay of two factors. On the one hand, the number of configurations of a denaturated loop is influenced by the loop self-avoidance interactions (the number is larger for the RW loop and smaller of the SAW one). On the other hand, the number of loop configurations is restricted by the side chains. Calculations presented here give a reliable way to judge about the values of exponents c_i for different heterogeneity conditions and hence to judge about the order of DNA thermal denaturation transition. Our analysis is grounded on the field theory of co-polymer networks. By scaling relations we connect loop closure exponents c_i to scaling exponents $\eta_{f_1 f_2}$ that govern entropic properties of co-polymer stars made by mutually interacting sets of SAWs and RWs. Using powerful resummation technique, we resum ε^4 expansions for these exponents and evaluate them at space dimension $d = 3$. As one can see, the effects of heterogeneity significantly influence the strength of the first order transition (the exponent c increases in comparison to the usual homogeneous SAW case). We support this observation providing exact results at $d = 2$. Moreover, we show that the effect of strengthening is further enhanced by the so-called crowded environment with the long-range correlated inhomogeneities.

CONCLUSIONS

In the context of modern studies of phase transitions and critical phenomena, universality is rarely questioned. However, for some less studied problems, especially at the finite sizes, many subtle issues arose. The combined insights from this dissertation enriches our understanding of complex systems, providing a nuanced perspective on finite-size scaling, Ising model, and the variety of scaling laws in complex polymer networks. We see that indeed the whole is greater then the sum of its parts, as the wide topic of this research only broadens our understanding of complexity in criticality. The following extensive conclusion summarizes the key findings from each chapter:

In Chapter 2, we explored the $d = 5$ Ising model above the upper critical dimension $d_c = 4$ using thorough computer simulations to understand critical phenomena better. The focus on how the observables such as magnetisation and susceptibility change with the size of the simulated lattice reveals the challenges posed by finite-size scaling. We found that for free boundary conditions the surface effects become too large at small lattice sizes, making it harder to see the overall scaling pattern. However, when we ignore the smallest lattice sizes, it helps us better understand how magnetization scales, highlighting the complexities of finite-size scaling. Importantly, the chapter concluded with a call for additional methodologies to navigate the challenges posed by the upper critical dimension, emphasizing the need for a diversified toolkit to fully comprehend the evolving landscape of scaling above d_c.

Chapter 3 suggests new ways of exploring scaling challenges above the upper critical dimension in the Ising model, introducing novel approaches such as Fourier modes analysis and the partition function zeros analysis. The meticulous

examination of scaling behaviors in the $d = 5$ Ising model illuminated the successful confirmation of Q-scaling for magnetisation at the pseudocritical point, offering valuable insights into the scaling dynamics of this specific dimension. The isothermal susceptibility, defined in terms of Lee-Yang zeros, revealed a scaling behavior closer to Q-scaling than to G-scaling, introducing a better accuracy for understanding the susceptibility scaling dynamics in numerical studies. The observation that the partition function zeros analysis is a powerful tool that doesn't require really large lattice sizes or isolating the lattice core, shows that this new method works well, and it is already being used in new research [136]. Together, these findings contribute to a refined understanding of scaling behaviours in the Ising model above the upper critical dimension, showcasing the utility of innovative methodologies in addressing complex challenges.

Chapter 4 further expanded our topics, delving into the scaling laws of complex co-polymer networks, such as the intricate thermal denaturation of DNA in Poland-Scheraga model and the crucial role played by the loop closure exponent c. Discriminating between various denaturation scenarios, the chapter highlighted the coherent picture observed in both theoretical descriptions and *in vitro* experiments, firmly establishing the denaturation transition as of the first order ($c_i > 2$). The nuanced exploration of the impact of heterogeneity on c sheds light on the interplay of loop self-avoiding interactions and side chains, influencing the strength and order of the denaturation transition. Grounded in the field theory of co-polymer networks, the analysis provided robust theoretical underpinnings, connecting loop closure exponents c_i to co-polymer star exponents $\eta_{f_1 f_2}$ and offering valuable insights into the effects of heterogeneity on the first-order transition. The findings further emphasized the enhancement of the strengthening effect in a crowded environment with long-range correlated inhomogeneities, showcasing the intricate interplay of environmental factors in influencing DNA denaturation.

In sum, this dissertation presents a multifaceted look at universality. The insights from this work underscores the importance of a diversified toolkit and innovative methodologies in addressing the complexities of critical phenomena. As

we discover all this new knowledge, the dissertation helps guide future studies and pushes our understanding of scaling and universality principles to new places.

BIBLIOGRAPHY

1. Honchar, Yu.; Berche, B.; Holovatch, Yu.; Kenna, R. When Correlations Exceed System Size: Finite-Size Scaling in Free Boundary Conditions above the Upper Critical Dimension. Preprint ArXiv: arXiv:2311.11721, 2023. DOI: 10.48550/arXiv.2311.11721.
2. Honchar, Yu.; von Ferber, C.; Holovatch, Yu. Variety of Scaling Laws for DNA Thermal Denaturation. *Physica A* **2021**, *573*, 125917. DOI:10.1016/j.physa.2021.125917
3. Holovatch, Yu.; von Ferber, C.; Honchar, Yu. DNA Thermal Denaturation by Polymer Field Theory Approach: Effects of the Environment. *Condens. Matter Phys.* **2021**, *24*, 33603. DOI:10.5488/CMP.24.33603
4. Гончар Ю. Закони скейлінгу в термічній денатурації ДНК. *19-та Всеукраїнська школа-семінар та Конкурс молодих вчених зі статистичної фізики та теорії конденсованої речовини.* Збірка тез. с. 22. Львів, 13-14 червня 2019.
5. Honchar, Yu.; von Ferber, C.; Holovatch, Yu. Resummation of ε-Expansion for Co-Polymer Star Exponents Reveals the Order of the Phase Transition in Thermal Denaturation of DNA.*5-th Conference on Statistical Physics: Modern Trends and Applications.* Book of abstracts. p. 113. Lviv, 3-6 липня 2019.
6. Гончар Ю.; Головач Ю.; фон Фербер К. Ефекти середовища у термічній Денатурації ДНК. *XXI Всеукраїнська школа-семінар та Конкурс молодих вчених зі статистичної фізики та теорії конденсованої речовини.* Збірка тез. с. 23. Львів, Україна, 11-12 жовтня, 2021.
7. Гончар Ю. Скейлінґ для моделі Ізінґа на п'ятивимірній ґратці з вільними граничними умовами. *XXII Всеукраїнська Школа-семінар зі*

статистичної фізики і теорії конденсованої речовини. Збірка тез. с. 21. Львів, 24-25 листопада 2022.

8. Гончар Ю. Модель Ізінґа над верхньою критичною вимірністю. *XXIII Всеукраїнська Школа-семінар зі статистичної фізики і теорії конденсованої речовини.* Збірка тез. с. 20. Львів, 26-27 жовтня 2023.
9. Honchar, Yu.; von Ferber, C.; Holovatch, Yu. On the Order of DNA Thermal Denaturation Phase Transition. *"Різдвяні дискусії 2020"*. ЛНУ ім. І.Франка. J. Phys. Stud., 24(1), 1998:4-5, Львів, 11-12 січня 2020.
10. Honchar, Yu.; von Ferber, C.; Holovatch, Yu. DNA Thermal Denaturation Viewed as a Phase Transition: Scaling Laws and Beyond. *Різдвяні дискусії 2022*. ЛНУ ім. І.Франка. J. Phys. Stud. 26. 1998-1. Львів, 11-12 січня 2022.
11. Honchar, Yu.; Berche, B.; Holovatch, Yu.; Kenna, R. Finite-Size Scaling for the Ising Model above the Upper Critical Dimension. *"Різдвяні дискусії 2022/2023"*. ЛНУ ім. І.Франка. J. Phys. Stud. 27. 1998-3. Львів, 22-23 грудня 2022.
12. Honchar, Yu. DNA Thermal Denaturation by Polymer Field Theory Approach. *46th Middle European Cooperation in Statistical Physics MECO 41*. Book of Abstracts. p. 71. Riga, Latvia, May 11-13, 2021.
13. Honchar, Yu.; Berche, B.; Holovatch, Yu.; Kenna, R. Numerical Exploration of Finite-Size Scaling above the Upper Critical Dimension. *48th Middle European Cooperation in Statistical Physics MECO 48*. Book of Abstracts. p. 58 Stará Lesná, Slovakia. May 22-26, 2023.
14. Honchar, Yu.; Berche, B.; Holovatch, Yu.; Kenna, R. Finite-Size Scaling for 5D Ising Model with Free Boundary Conditions. *DPG-Verhandlungen, Condensed Matter Section 2023*, MA 23.47. Dresden. March 26-31, 2023.
15. Honchar, Yu.; von Ferber, C.; Holovatch, Yu. Variety of Scaling Laws for DNA Thermal Denaturation. Preprint ArXiv: 2103.08725, 2021. DOI:10.48550/arXiv.2103.08725
16. Holovatch, Yu.; von Ferber, C.; Honchar, Yu. DNA Thermal Denaturation by Polymer Field Theory Approach: Effects of the Environment. Preprint ArXiv:

2107.11812, 2021. DOI:10.48550/arXiv.2107.11812

17. Chaikin, P. M.; Lubensky, T. C. *Principles of Condensed Matter Physics*; Cambridge University Press: Cambridge, UK, 2000.
18. Holovatch, Y. (Ed.) *Order, Disorder, and Criticality: Advanced Problems of Phase Transition Theory*; Vols. 1–7; World Scientific: Singapore, 2004–2023.
19. Holovatch, Yu.; Honchar, Yu.; Krasnytska, M. Фізика і фізики в НТШ у Львові. *J. Phys. St.* **2018**, *22* (4), 4003 (31 pages). DOI:10.30970/jps.22.4003
20. Fisher, M. E. The Nature of Critical Points. In *Lectures in Theoretical Physics*, Britten, W. E., Ed.; University of Colorado Press: Boulder, Colorado, 1965; Vol. 7C, pp 1–159.
21. Josephson, B. Inequality for the Specific Heat: I. Derivation. *Proc. Phys. Soc.* **1967**, *92*, 269. DOI:10.1088/0370-1328/92/2/301.
22. Rushbrooke, G. S. On the Thermodynamics of the Critical Region for the Ising Problem. *J. Chem. Phys.* **1963**, *39*, 842. DOI:10.1063/1.1734338.
23. Widom, B. Surface Tension and Molecular Correlations near the Critical Point. *J. Chem. Phys.* **1965**, *43*, 3892. DOI:10.1063/1.1696617. Widom, B. Equation of State in the Neighborhood of the Critical Point. *J. Chem. Phys.* **1965**, *43*, 3898. DOI:10.1063/1.1696618.
24. Fisher, M. E. Correlation Functions and the Critical Region of Simple Fluids. *J. Math. Phys.* **1964**, *5*, 944. DOI:10.1063/1.1704197.
25. Landau, L. D. On the Theory of Phase Transitions. *Zh. Eksp. Teor. Fiz.* **1937**, *7*, 19–32.
26. Wilson, K. G. Renormalization Group and Critical Phenomena. I. Renormalization Group and the Kadanoff Scaling Picture. *Phys. Rev. B* **1971**, *4*, 3174. DOI:10.1103/PhysRevB.4.3174.
27. Patashinskii, A. Z.; Pokrovsky, V. L. Behavior of Ordered Systems near the Transition Point. *Sov. Phys. JETP* **1966**, *23*, 292.
28. Kadanoff, L. P. Scaling Laws for Ising Models near T_c. *Physics Physique Fizika* **1966**, *2*, 263. DOI:10.1103/PhysicsPhysiqueFizika.2.263.

29. Amit, D. J. The Ginzburg Criterion-Rationalized. *J. Phys. C: Solid State Phys.* **1974**, *7*, 3369. DOI:10.1088/0022-3719/7/18/020.
30. Amit, D. J.; Martin-Mayor, V. *Field Theory, the Renormalization Group, and Critical Phenomena*; 3rd ed.; World Scientific: Singapore, 2005. DOI:10.1142/5715.
31. Janke, W.; Kenna, R. Finite-Size Scaling and Corrections in the Ising Model with Brascamp-Kunz Boundary Conditions. *Phys. Rev. B* **2002**, *65* (6), 064110. DOI:10.1103/PhysRevB.65.064110.
32. Berche, B.; Ellis, T.; Holovatch, Yu.; Kenna, R. Phase Transitions above the Upper Critical Dimension. *SciPost Phys. Lect. Notes* **2022**, *60*. DOI:10.21468/SciPostPhysLectNotes.60.
33. Privman, V.; Fisher, M. E. Finite-Size Scaling of the Correlation Length above the Upper Critical Dimension in the Five-Dimensional Ising Model. *J. Stat. Phys.* **1983**, *33*, 385. DOI:10.1007/BF01009803
34. Binder, K.; Nauenberg, M.; Privman, V.; Young, A. P. Finite-Size Tests of Hyperscaling. *Phys. Rev. B* **1985**, *31*, 1498. DOI:10.1103/PhysRevB.31.1498
35. Luijten, E.; Blöte, H. W. J. Finite-Size Scaling and Universality above the Upper Critical Dimensionality. *Phys. Rev. Lett.* **1996**, *76*, 1557. DOI:10.1103/PhysRevLett.76.1557 Luijten, E.; Blöte, H. W. J. Finite-Size Scaling and Universality above the Upper Critical Dimensionality. *Phys. Rev. Lett.* **1996**, *76*, 3662. DOI:10.1103/PhysRevLett.76.3662
36. Berche, B.; Chatelain, C.; Dhall, C.; Kenna, R.; Low, R.; Walter, J.-C. Extended Scaling in High Dimensions. *J. Stat. Mech.: Theory Exp.* **2008**, P11010. DOI:10.1088/1742-5468/2008/11/P11010
37. Ellis, T.; Kenna, R.; Berche, B. The Fifty-Year Quest for Universality in Percolation Theory in High Dimensions. *Condens. Matter Phys.* **2023**, *26* (3), 33606. DOI:10.5488/CMP.26.33606
38. Berche, B.; Kenna, R.; Walter, J.-C. Hyperscaling above the Upper Critical Dimension. *Nucl. Phys. B* **2012**, *865* (1), 115. DOI:10.1016/j.nuclphysb.2012.07.021

39. Lundow, P. H.; Markström, K. Finite Size Scaling of the 5d Ising Model with Free Boundary Conditions. *Nucl. Phys. B* **2014**, *889*, 249. DOI:10.1016/j.nuclphysb.2014.10.011
40. Flores-Sola, E. J.; Berche, B.; Kenna, R.; Weigel, M. Role of Fourier Modes in Finite-Size Scaling above the Upper Critical Dimension. *Phys. Rev. Lett.* **2016**, *116*, 115701. DOI:10.1103/PhysRevLett.116.115701
41. Kenna, R.; Berche, B. A New Critical Exponent 'Coppa' and Its Logarithmic Counterpart 'Hat Coppa'. *Condens. Matter Phys.* **2013**, *16* (2), 23601. DOI:10.5488/CMP.16.23601
42. Kenna, R.; Berche, B. Universal Finite-Size Scaling for Percolation Theory in High Dimensions. *J. Phys. A: Math. Theor.* **2017**, *50* (23), 235001. DOI:10.1088/1751-8121/aa6bd5
43. Berche, B.; Henkel, M.; Kenna, R. Critical Phenomena: 150 Years Since Cagniard de la Tour. *Journal of Physical Studies* **2009**, *13*, 3201, arXiv:0905.1886. DOI:10.1590/S1806-11172009000200015
44. Brezin, E.; Zinn-Justin, J. Finite Size Effects in Phase Transitions. *Nucl. Phys. B* **1985**, *257*, 867. DOI:10.1016/0550-3213(85)90379-7
45. Jones, J. L.; Young, A. P. Finite-Size Scaling of the Correlation Length above the Upper Critical Dimension in the Five-Dimensional Ising Model. *Phys. Rev. B* **2005**, *71*, 174438. DOI:10.1103/PhysRevB.71.174438
46. Flores-Sola, E.; Berche, B.; Kenna, R.; Weigel, M. Finite-Size Scaling above the Upper Critical Dimension in Ising Models with Long-Range Interactions. *Eur. Phys. J. B* **2015**, *88*, 28. DOI:10.1140/epjb/e2014-50683-1
47. Kenna, R.; Berche, B. Fisher's Scaling Relation above the Upper Critical Dimension. *Eur. Phys. Lett.* **2014**, *105*, 26005. DOI:10.1209/0295-5075/105/26005
48. Kenna, R.; Berche, B. Scaling and Finite-Size Scaling above the Upper Critical Dimension. In *Order, Disorder, and Criticality: Advanced Problems of Phase Transition Theory* Vol. 4; Holovatch, Y., Ed.; World Scientific: Singapore, 2015; pp 1-54.

49. Yang, C. N.; Lee, T. D. Statistical Theory of Equations of State and Phase Transitions. I. Theory of Condensation. *Phys. Rev.* **1952**, *87*, 404. DOI:10.1103/PhysRev.87.404
50. Lee, T. D.; Yang, C. N. Statistical Theory of Equations of State and Phase Transitions. II. Lattice Gas and Ising Model. *Phys. Rev.* **1952**, *87* (3), 410. DOI:10.1103/PhysRev.87.410
51. Wu, F. Y. Professor C. N. Yang and Statistical Mechanics. *Int. J. Mod. Phys. B* **2008**, *22* (12), 1899. DOI:10.1142/S0217979208039198
52. Lundow, P. H.; Markström, K. Non-Vanishing Boundary Effects and Quasi-First-Order Phase Transitions in High Dimensional Ising Models. *Nucl. Phys. B* **2011**, *845*, 120–139. DOI:10.1016/j.nuclphysb.2010.12.002
53. Lundow, P. Boundary Effects on Finite-Size Scaling for the 5-Dimensional Ising Model. *Nucl. Phys. B* **2021**, *967*, 115422. DOI:10.1016/j.nuclphysb.2021.115422
54. Wolff, U. Collective Monte Carlo Updating for Spin Systems. *Phys. Rev. Lett.* **1989**, *62*, 361. DOI:10.1103/PhysRevLett.62.361
55. Kasteleyn, P. W.; Fortuin, C. M. Phase Transitions in Lattice Systems with Random Local Properties. *J. Phys. Soc. Jpn. Suppl.* **1969**, *26*, 11.
56. Fortuin, C. M.; Kasteleyn, P. W. On the Random-Cluster Model: I. Introduction and Relation to Other Models. *Physica* **1972**, *57* (4), 536. DOI:10.1016/0031-8914(72)90045-6
57. Ferrenberg, A. M.; Swendsen, R. H. New Monte Carlo Technique for Studying Phase Transitions. *Phys. Rev. Lett.* **1988**, *61*, 2635. DOI:10.1103/PhysRevLett.61.2635
58. Ferrenberg, A. M.; Swendsen, R. H. Optimized Monte Carlo Data Analysis. *Phys. Rev. Lett.* **1989**, *63*, 1195. DOI:10.1103/PhysRevLett.63.1195
59. Wu, C.F.J. Jackknife, Bootstrap and Other Resampling Methods in Regression Analysis. *The Annals of Statistic* **1986**, *14* (4), 1261-1295. DOI:10.1214/aos/1176350142
60. Ferrenberg, A.; Landau, D.; Swendsen, R. Statistical Errors in Histogram

Reweighting. *Phys. Rev. E* **1994**, *51*, 5092. DOI:10.1103/PhysRevE.51.5092

61. Rudnick, J.; Gaspari, G.; Privman, V. Effect of Boundary Conditions on the Critical Behavior of a Finite High-Dimensional Ising Model. *Phys. Rev. B* **1985**, *32*, 7594. DOI:10.1103/PhysRevB.32.7594
62. Bena, I.; Droz, M.; Lipowski, A. Statistical Mechanics of Equilibrium and Nonequilibrium Phase Transitions: The Yang–Lee Formalism. *Int. J. Mod. Phys. B* **2005**, *19* (29), 4269. DOI:10.1142/S0217979205032759
63. Krasnytska, M.; Berche, B.; Holovatch, Y.; Kenna, R. Partition Function Zeros for the Ising Model on Complete Graphs and on Annealed Scale-Free Networks. *J. Phys. A: Math. Theor.* **2016**, *49* (13), 135001. DOI:10.1088/1751-8113/49/13/135001
64. Krasnytska, M.; Berche, B.; Holovatch, Yu.; Kenna, R. Violation of Lee-Yang Circle Theorem for Ising Phase Transitions on Complex Networks. *Europhys. Lett.* **2015**, *111*, 60009. DOI:10.1209/0295-5075/111/60009
65. Press, W. H.; *et al. Numerical Recipes 3rd Edition: The Art of Scientific Computing*; Cambridge University Press: Cambridge, UK, 2007.
66. Itzykson, C.; Pearson, R.; Zuber, J. Distribution of Zeros in Ising and Gauge Models. *Nuclear Physics B* **1983**, *220* (4), 415. DOI:10.1016/0550-3213(83)90499-6
67. Staudinger, H. *Die Hochmolekularen Organischen Verbindungen*; Springer: Berlin, Germany, 1932.
68. Stanley, H. E. *Introduction to Phase Transitions and Critical Phenomena*; Clarendon Press: Oxford, UK, 1971.
69. De Gennes, P.-G. *Scaling Concepts in Polymer Physics*; Cornell University Press: Ithaca, NY, 1979.
70. Des Cloizeaux, J. The Lagrangian Theory of Polymer Solutions at Intermediate Concentrations. *J. Physique* **1975**, *36*, 281. DOI:10.1051/jphys:01975003604028100.
71. Wartell, R. M.; Benight, A. S. Thermal Denaturation of DNA Molecules: A Comparison of Theory With Experiment. *Phys. Reports* **1985**, *126* (2), 67.

DOI:10.1016/0370-1573(85)90060-2

72. Binder, K.; Paul, W. Monte Carlo Simulations of Polymer Dynamics: Recent Advances. *J. Pol. Sci. B* **1997**, *35* (1), 1–31. DOI:10.1002/(SICI)1099-0488(19970115)35:1<1::AID-POLB1>3.0.CO;2-%23
73. Blake, R. D.; *et al.* Statistical Mechanical Simulation of Polymeric DNA Melting with MELT-SIM. *Bioinformatics* **1999**, *15*, 370-375. DOI:10.1093/bioinformatics/15.5.370.
74. Blossey, R.; Carlon, E. Reparametrizing Loop Entropy Weights: Effect on DNA Melting Curves. *Phys. Rev. E* **2003**, *68*, 061911. DOI:10.1103/PhysRevE.68.061911
75. Volkov, S.; Solov'yov, A. The Mechanism of DNA Mechanical Unzipping. *Eur. Phys. J. D* **2009**, *54*, 657–666. DOI:10.1140/epjd/e2009-00194-5
76. Poland, D.; Sheraga, H. A. Phase Transitions in One Dimension and the Helix—Coil Transition in Polyamino Acids. *J. Chem. Phys.* **1966**, *45*, 1456. DOI:10.1063/1.1727785
77. Poland, D.; Sheraga, H. A. Occurrence of a Phase Transition in Nucleic Acid Models. *J. Chem. Phys.* **1966**, *45*, 1464. DOI:10.1063/1.1727786
78. Lifson, S. Intramolecular Energy Functions for Conformation and Vibrational Analysis. *J. Chem. Phys.* **1964**, *40*, 3705. DOI:10.1051/jcp/1968650040
79. Poland, D.; Scheraga, H. A. *Theory of Helix-Coil Transitions in Biopolymers: Statistical Mechanical Theory of Order-Disorder Transitions in Biological Macromolecules*; Academic Press: New York, NY, 1970.
80. Wiegel, F.; Boersma, J. The Green Function for the Half-Plane Barrier: Derivation from Polymer Entanglement Probabilities. *Physica A* **1983**, *122* (1–2), 325-333. DOI:10.1016/0378-4371(83)90096-1.
81. Richard, C.; Guttmann, A. Poland-Scheraga Models and the DNA Denaturation Transition. *J. Stat. Phys.* **2004**, *115* (3-4), 925-947. DOI:10.1023/B:JOSS.0000022370.48118.8b.
82. Reiter-Schad, M.; Werner, E.; Tegenfeldt, J.; Mehlig, B.; Ambjörnsson, T. How Nanochannel Confinement Affects the DNA Melting Transition within the

Poland-Scheraga Model. *J. Chem. Phys.* **2015**, *143*, 115101. DOI:10.1063/1.4930220.

83. Berger, Q.; Giacomin, G.; Khatib, M. Disorder and Denaturation Transition in the Generalized Poland-Scheraga Model. *Ann. Henri Lebesgue* **2020**, *3*, 299-339. DOI:10.5802/ahl.34.hal-03911982
84. Legrand, A. Influence of Disorder on DNA Denaturation: The Disordered Generalized Poland-Scheraga Model. *Electron. J. Probab.* **2021**, *26*, Article No. 10, 1-43. DOI:10.1214/20-EJP563.
85. Kafri, Y.; Mukamel, D.; Peliti, L. Why is the DNA Denaturation Transition First Order? *Phys. Rev. Lett.* **2000**, *85*, 4988. DOI:10.1103/PhysRevLett.85.4988
86. Schulte-Frohlinde, V.; Holovatch, Yu.; von Ferber, C.; Blumen, A. Scaling of Star Polymers: High Order Results. *Phys. Lett. A* **2004**, *328*, 335. DOI:10.1016/j.physleta.2004.06.063
87. Kleinert, H.; Schulte-Frohlinde, V. *Critical Properties of ϕ^4-Theories*; World Scientific: Singapore, 2001.
88. Thomas, R. Research on the denaturation of desoxyribonucleic acids. *Biochim. Biophys. Acta* **1954**, *14*, 231. DOI:10.1016/0006-3002(54)90163-8
89. Rice, S. A.; Doty, P. The Thermal Denaturation of Desoxyribose Nucleic Acid. *J. Am. Chem. Soc.* **1957**, *79*, 3937. DOI:10.1021/ja01572a001
90. Fisher, M. Effect of Excluded Volume on Phase Transitions in Biopolymers. *J. Chem. Phys.* **1966**, *45*, 1469. DOI:10.1063/1.1727787
91. Kafri, Y.; Mukamel, D.; Peliti, L. Melting and Unzipping of DNA. *Eur. Phys. J. B* **2002**, *27*, 135. DOI:10.1140/epjb/e20020138
92. Baiesi, M.; Carlon, E.; Stella, A. L. A Simple Model of DNA Denaturation and Mutually Avoiding Walks Statistics. *Phys. Rev. E* **2002**, *66*, 021804. DOI:10.1140/epjb/e2002-00270-2
93. Carlon, E.; Orlandini, E.; Stella, A. L. Roles of Stiffness and Excluded Volume in DNA Denaturation. *Phys. Rev. Lett.* **2002**, *88*, 198101. DOI:10.1103/PhysRevLett.88.198101

94. Duplantier, B. Polymer Network of Fixed Topology: Renormalization, Exact Critical Exponent γ in Two Dimensions, and $d = 4 - \varepsilon$. *Phys. Rev. Lett.* **1986**, *57* (18), 2332-2332. DOI:10.1103/PhysRevLett.57.2332
95. Schäfer, L. Chain-Length Distribution in a Model of Equilibrium Polymerization. *Phys. Rev. B* **1992**, *46*, 6061. DOI:10.1103/PhysRevB.46.6061
96. Duplantier, B. Two-Dimensional Copolymers and Exact Conformal Multifractality. *Phys. Rev. Lett.* **1999**, *82*, 880. DOI:10.1103/PhysRevLett.82.880
97. von Ferber, C.; Holovatch, Yu. Copolymer Networks and Stars: Scaling Exponents. *Phys. Rev. E* **1997**, *56*, 6370. DOI:10.1103/PhysRevE.56.6370. von Ferber, C.; Holovatch, Yu. Copolymer Networks: Multifractal Dimension Spectra in Polymer Field Theory. *Europhys. Lett.* **1997**, *39*, 31. DOI:10.1209/epl/i1997-00309-6
98. von Ferber, C.; Holovatch, Yu. Multifractality of Brownian Motion Near Absorbing Polymers. *Phys. Rev. E* **1999**, *59*, 6914. DOI:10.1103/PhysRevE.59.6914
99. von Ferber, C. Scaling of Miktoarm Star Polymers. In *Order, Disorder and Criticality. Advanced Problems of Phase Transition Theory*; Holovatch, Y., Ed.; World Scientific: Singapore, 2004; pp 201–251. DOI:10.1142/5376
100. Schäfer, L.; Kapeller, C. A Renormalization Group Analysis of Ternary Polymer Solutions. *J. Phys. (Paris)* **1985**, *46*, 1853. DOI:10.1051/jphys:0198500460110185300. Colloid Polym. Sci. **1990**, *268*, 995
101. Schäfer, L.; Lehr, U.; Kapeller, C. Higher Order Calculations of the Renormalization Group Flow for Multicomponent Polymer Solutions. *J. Phys. I* **1991**, *1*, 211. DOI:10.1051/jp1:1991125
102. Le Guillou, J. C.; Zinn-Justin, J. Critical Exponents From Field Theory. *Phys. Rev. B* **1980**, *21*, 3976. DOI:10.1103/PhysRevB.21.3976
103. Zinn-Justin, J. *Quantum Field Theory and Critical Phenomena*, 3rd ed.; Oxford University Press: New York, NY, 1989.
104. Flory, P. J. The Configuration of Real Polymer Chains. *J. Chem. Phys.* **1949**, *17*, 303–310. DOI:10.1063/1.1747243

105. Flory, P. J. Theory of Elastic Mechanisms in Fibrous Proteins. *J. Am. Chem. Soc.* **1956**, *78*, 5222. DOI:10.1021/ja01601a025

106. Delamotte, B.; Holovatch, Yu.; Ivaneyko, D.; Mouhanna, D.; Tissier, M. Fixed Points in Frustrated Magnets Revisited. *J. Stat. Mech.* **2008**, 03014. DOI:10.1088/1742-5468/2008/03/P03014

107. Delamotte, B.; Dudka, M.; Holovatch, Yu.; Mouhanna, D. Analysis of the 3d Massive Renormalization Group Perturbative Expansions: A Delicate Case. *Condens. Matter Phys.* **2010**, *13*, 43703. DOI:10.5488/CMP.13.43703

108. Holovatch, Yu.; Blavats'ka, V.; Dudka, M.; von Ferber, C.; Folk, R.; Yavors'kii, T. Weak Quenched Disorder and Criticality: Resummation of Asymptotic(?) Series. *Int. J. Mod. Phys. B* **2002**, *16*, 4027. DOI:10.1142/S0217979202014760

109. Folk, R.; Holovatch, Yu.; Yavors'kii, T. Critical Exponents of a Three-Dimensional Weakly Diluted Quenched Ising Model. *Phys.-Usp.* **2003**, *46*, 169 [*Usp. Fiz. Nauk* **2003**, *173*, 175]. DOI:10.1070/PU2003v046n02ABEH001077

110. Itzykson, C.; Drouffe, J.-M. *Statistical Field Theory*; Cambridge University Press: Cambridge, UK, 1989.

111. Causo, M. S.; Coluzzi, B.; Grassberger, P. Simple Model for the DNA Denaturation Transition. *Phys. Rev. E* **2000**, *62*, 3958. DOI:10.1103/PhysRevE.62.3958

112. Carlon, E.; Baiesi, M. Unbinding of mutually avoiding random walks and two-dimensional quantum gravity. *Phys. Rev. E* **2004**, *70*, 066118. DOI:10.1103/PhysRevE.70.066118

113. des Cloizeaux, J.; Jannink, G. *Polymers in Solution: Their Modelling and Structure*; Oxford University Press: New York, NY, 1991.

114. Duplantier, B. Statistical Mechanics of Polymer Networks of Any Topology. *J. Stat. Phys.* **1989**, *54*, 581. DOI:10.1007/BF01019770

115. Schäfer, L.; von Ferber, C.; Lehr, U.; Duplantier, B. Renormalization of Polymer Networks and Stars. *Nucl. Phys. B* **1992**, *374*, 473. DOI:10.1016/0550-3213(92)90397-T

116. von Ferber, C.; Holovatch, Yu. Copolymer Networks and Stars: Scaling Exponents. *Phys. Rev. E* **1997**, *56*, 6370. DOI:10.1103/PhysRevE.56.6370
117. von Ferber, C.; Holovatch, Yu. Copolymer Networks: Multifractal Dimension Spectra in Polymer Field Theory. *Europhys. Lett.* **1997**, *39*, 31. DOI:10.1209/epl/i1997-00309-6
118. Hardy, G. *Divergent Series*; Oxford University Press: Oxford, UK, 1949.
119. Chakrabarti, B. K., Ed. *Statistics of Linear Polymers in Disordered Media*; Elsevier: Amsterdam, The Netherlands, 2005. DOI:10.1016/B978-0-444-51709-8.X5000-2
120. Goodesel, D. S. Inside a Living Cell. *Trends Biochem. Sci.* **1991**, *16*, 203. DOI:10.1016/0968-0004(91)90083-8
121. Minton, A. The Influence of Macromolecular Crowding and Macromolecular Confinement on Biochemical Reactions in Physiological Media. *J. Biol. Chem.* **2001**, *276*, 10577. DOI:10.1074/jbc.R100005200
122. Blavatska, V.; von Ferber, C.; Holovatch, Yu. Disorder Effects on the Static Scattering Function of Star Branched Polymers. *Condens. Matter Phys.* **2012**, *15*, 33603. DOI:10.5488/CMP.15.33603
123. Meir, Y.; Harris, A. B. Self-avoiding Walks on Diluted Networks. *Phys. Rev. Lett.* **1989**, *63*, 2819. DOI:10.1103/PhysRevLett.63.2819
124. Kim, Y. Renormalisation-group Study of Self-avoiding Walks on the Random Lattice. *J. Phys. C: Solid State Phys.* **1983**, *16*, 1345. DOI:10.1088/0022-3719/16/8/005
125. Harris, A. B. Self-avoiding Walks on Random Lattices. *Z. Phys. B: Condens. Matter* **1983**, *49*, 347. DOI:10.1007/BF01301596
126. Weinrib, A.; Halperin, B. I. Critical Phenomena in Systems With Long-Range-Correlated Quenched Disorder. *Phys. Rev. B* **1983**, *27*, 413. DOI:10.1103/PhysRevB.27.413
127. Blavatska, V.; Haydukivska, K. Polymers in Anisotropic Environment with Extended Defects. *Eur. Phys. J. Spec. Top.* **2013**, *216*, 191. DOI:10.1140/epjst/e2013-01742-2

128. Blavatska, V.; von Ferber, C.; Holovatch, Yu. Polymers in Long-Range-Correlated Disorder. *Phys. Rev. E* **2001**, *64*, 041102. DOI:10.1103/PhysRevE.64.041102

129. Blavatska, V.; von Ferber, C.; Holovatch, Yu. Polymers In Media With Long-Range-Correlated Quenched Disorder. *J. Mol. Liq.* **2001**, *92*, 77. DOI:10.1016/S0167-7322(01)00179-9

130. Blavatska, V.; von Ferber, C.; Holovatch, Yu. Entropy-induced Separation of Star Polymers in Porous Media. *Phys. Rev. E* **2006**, *74*, 031801. DOI:10.1103/PhysRevE.74.031801

131. Blavatska, V.; von Ferber, C.; Holovatch, Yu. Star Copolymers in Porous Environments: Scaling and Its Manifestations. *Phys. Rev. E* **2011**, *83*, 011803. DOI:10.1103/PhysRevE.83.011803

132. Wu, Y. K.; Hu, B. Phase Transitions on Complex Sierpinski Carpets. *Phys. Rev. A* **1987**, *35*, 1404. DOI:10.1103/PhysRevA.35.1404

133. Holovatch, Yu.; Shpot, M. *J. Stat. Phys.* **1992**, *66*, 867. DOI:10.1007/BF01055706

134. Holovatch, Yu.; Yavorskii, T. Critical Exponents of the Diluted Ising Model between Dimensions 2 and 4. *J. Stat. Phys.* **1998**, *92*, 785. DOI:10.1023/A:1023032307964

135. Blake, R. D.; Bizzaro, J. W.; Blake, J. D.; Day, G. R.; Delcourt, S. G.; Knowles, J.; Marx, K. A.; SantaLucia, J. Jr. Statistical mechanical simulation of polymeric DNA melting with MELTSIM. *Bioinformatics* **1999**, *15*, 370. DOI:10.1093/bioinformatics/15.5.370

136. Moueddenne L.; Fytas N.; Holovatch Yu.; Kenna R.; Berche B. *Accepted to IOP (Journal of Statistical Mechanics: Theory and Experiment (JSTAT))*

APPENDIX A

LIST OF PUBLICATIONS

1. *Honchar Yu., von Ferber C., Holovatch Yu.* Variety of scaling laws for DNA thermal denaturation. // *Physica A: Statistical Mechanics and its Applications.* — 2021. — Vol. 573. — P. 125917. Scopus (Q1), DOI: 10.1016/j.physa.2021.125917

2. *Holovatch Yu., von Ferber C., Honchar Yu.* DNA thermal denaturation by polymer field theory approach: effects of the environment. // *Condensed Matter Physics.* — 2021. — Vol. 24. — P. 33603. Scopus (Q3), DOI: 10.5488/CMP.24.33603

3. *Honchar Yu., Berche B., Holovatch Yu., Kenna R.* When correlations exceed system size: finite-size scaling in free boundary conditions above the upper critical dimension. // preprint ArXiv:. — 2023. — arXiv:2311.11721. (*to appear in Condens.Matter Phys 2024, 1*) DOI:10.48550/arXiv.2311.11721

4. *Honchar Yu., von Ferber C., Holovatch Yu.*, Variety of scaling laws for DNA thermal denaturation. // preprint ArXiv:. — 2021. — arXiv:2103.08725. DOI:10.48550/arXiv.2103.08725

5. *Holovatch Yu., von Ferber C., Honchar Yu.* DNA thermal denaturation by polymer field theory approach: effects of the environment.// preprint ArXiv:. — 2021. — arXiv:2107.11812. DOI:10.48550/arXiv.2107.11812

6. *Гончар Ю.* Закони скейлінгу в термічній денатурації ДНК. *19-та Всеукраїнська школа-семінар та Конкурс молодих вчених зі статистичної фізики та теорії конденсованої речовини.* Збірка тез. с.

22. Львів, 13-14 червня 2019.

7. *Honchar Yu., von Ferber C., Holovatch Yu.* Resummation of ε-expansion for co-polymer star exponents reveals the order of the phase transition in thermal denaturation of DNA. *5-th Conference on Statistical Physics: Modern Trends and Applications.* Book of abstracts. p. 113. Lviv, 3-6 липня 2019.

8. *Honchar Yu., von Ferber C., Holovatch Yu.* On the Order of DNA Thermal Denaturation Phase Transition. *"Різдвяні дискусії 2020"*. ЛНУ ім. І.Франка. J. Phys. Stud. 24(1), p. 1998:4-5, Львів, 11-12 січня 2020.

9. *Гончар Ю., Головач Ю., фон Фербер К.* Ефекти середовища у термічній Денатурації ДНК. *XXI Всеукраїнська школа-семінар та Конкурс молодих вчених зі статистичної фізики та теорії конденсованої речовини.* Збірка тез. с. 23. Львів, Україна, 11-12 жовтня, 2021.

10. *Honchar Yu.* DNA thermal denaturation by polymer field theory approach. *46th Middle European Cooperation in Statistical Physics MECO 41.* Book of Abstracts. p. 71. Riga, Latvia, May 11-13, 2021.

11. *Honchar Yu., C. Von Ferber C., Holovatch Yu.* DNA thermal denaturation viewed as a phase transition: scaling laws and beyond. *Різдвяні дискусії 2022.* ЛНУ ім. І.Франка. J. Phys. Stud. 26. p. 1998-1. Львів, 11-12 січня 2022.

12. *Гончар Ю.* Скейлінґ для моделі Ізінґа на п'ятивимірній ґратці з вільними граничними умовами. *XXII Всеукраїнська Школа-семінар зі статистичної фізики і теорії конденсованої речовини.* Збірка тез. с. 21. Львів, 24-25 листопада 2022.

13. *Honchar Yu., Berche B., Holovatch Yu., Kenna R.* Finite-size scaling for the Ising model above the upper critical dimension. *"Різдвяні дискусії 2022/2023"*. ЛНУ ім. І.Франка. J. Phys. Stud. 27. p. 1998-3. Львів, 22-23 грудня 2022

14. *Honchar Yu., Berche B., Holovatch Yu., Kenna R.* Finite-size scaling for 5D

Ising model with free boundary conditions. *DPG-Verhandlungen, Condensed Matter Section 2023*, MA 23.47. Dresden. March 26-31, 2023.

15. *Honchar Yu., Berche B., Holovatch Yu., Kenna R.* Numerical exploration of finite-size scaling above the upper critical dimension. *48th Middle European Cooperation in Statistical Physics MECO 48.* Book of Abstracts. p. 58 Stará Lesná, Slovakia. May 22-26, 2023.

16. *Гончар Ю.* Модель Ізінґа над верхньою критичною вимірністю. *XXIII Всеукраїнська Школа-семінар зі статистичної фізики і теорії конденсованої речовини.* Збірка тез. с. 20. Львів, 26-27 жовтня 2023.

APPENDIX B

APPROBATION OF OBTAINED RESULTS

Key results of this research were presented at the conferences: 5-th Conference on Statistical Physics: Modern Trends and Applications, Lviv (July 3-6 2019) [5], School of statistical physics and condensed matter physics for young scientists, Institute for Condensed Matter Physics of the National Academy of Sciences of Ukraine, Lviv (June 13-14, 2019, October 11-12, 2021, November 24-25, 2022, October 26-27, 2023)[4, 6–8], Christmas Discussions, Ivan Franko University of Lviv (January 11-12, 2020, January 11-12, 2021, December 22-23, 2022) [9–11], The Conferences of the Middle European Cooperation in Statistical Physics (MECO) (Riga, May 11-13, 2021, Stara Lesna, May 22-26, 2023) [12, 13], Deutsche Physikalische Gesellschaft 2023 Spring Meeting, Dresden (March 26-31, 2023) [14], as well as seminars of the ICMP, seminars "Statistical physics of complex systems" at the Laboratory of statistical physics of complex systems at ICMP, post-graduate seminars in Fluids and complex systems centre at Coventry University.

APPENDIX C

WOLFF ALGORITHM

In this Appendix we sketch the key steps of the Wolff algorithm [54] used in Chapter 2, 3 to simulate $d = 5$ Ising model near the critical point.

- Initiate $N = L^d$ nodes: create a lattice such that for each node i according to dimensionality and boundary conditions each number i has a corresponding list of its neighbours $nbr^{(i)}$, of size $nbrCountForNode^{(i)}$

  For FBC: neighbours of the node i are nodes $i+L^j$ and $i-L^j$, $j \in [0, D-1]$, except when node i is located at any margin and neighbours on the side of the margin get skipped.

- Create an initial configuration of spins S_i - either random (each node is assigned -1 or 1 randomly) or ordered (each node is spin up).

- One Monte-Carlo iteration:

  Pick random node i, add it to the cluster

  For each node j in a list $nbr^{(i)}$ check if $S_j = S_i$

  If the condition is met, add node j to the cluster with probability $p = 1 - e^{-\beta \Delta E}$, β is the inverse temperature

  repeat the search of neighbour nodes for the newly added node j (skip new nodes that have been checked already as neighbours of previous members of the cluster)

  Flip all spins in the cluster $S_{cluster} = -S_{cluster}$

- After the thermalization (I use 10% of total Number of iterations)

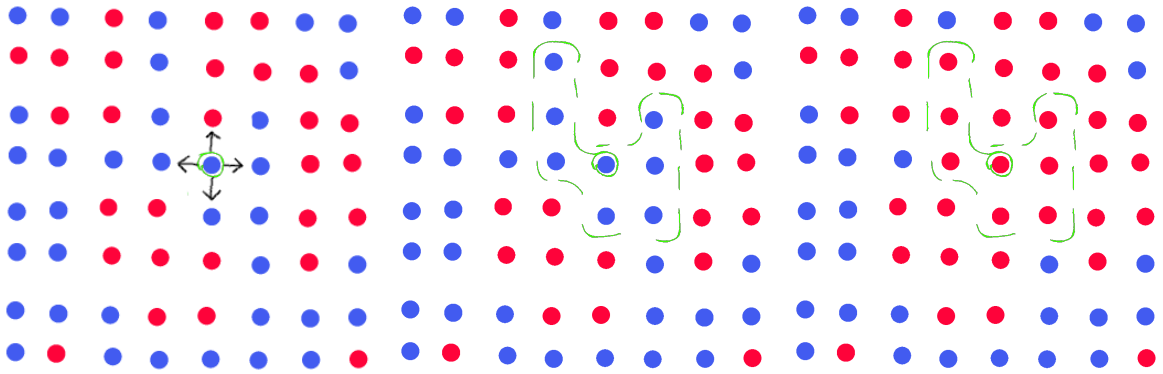

(a) (b) (c)

Figure C.1. The Wolff algorithm goes as follows: first, (a) we randomly pick one spin s_i and check all of his neighbours if any have the same sign. For all with the same sign, add them to the cluster with probability p, and (b) look for all of their neighbours that haven't been checked yet, until the cluster can no longer be built bigger. Finally, (c) flip all of the spins in the cluster and forget about the cluster. Repeat from (a).

Calculate the magnetization of this configuration $M = \sum S_i$, store $|M/N| = m = \frac{1}{N}\left|\sum S_i\right|$

Calculate and store the energy of this configuration $e = \frac{1}{N}\left|\sum_{i,j} S_i S_j\right|$

On each node i add the profile of the spin $\mu_i += S_i * sign(M)$

- After last iteration

  Calculate and store the profile of the spin on each of the nodes: $\mu_i / N_{iterations}$